DISSERTATIONS IN
HEALTH SCIENCES

Nick Hayward

Magnetic Resonance Imaging of the Hemodynamic and Cerebrovascular Sequelae of Traumatic Brain Injury, Ischemic Stroke, and Status Epilepticus in Rats

Publications of the University of Eastern Finland
Dissertations in Health Sciences

UNIVERSITY OF
EASTERN FINLAND

NICK HAYWARD

Magnetic resonance imaging of the hemodynamic and cerebrovascular sequelae of traumatic brain injury, ischemic stroke, and status epilepticus in rats

To be presented by permission of the Faculty of Health Sciences, University of Eastern Finland for public examination in Mediteknia Auditorium (MET), Kuopio, University of Eastern Finland,
on Saturday 27th November 2010 at 12 noon

Publications of the University of Eastern Finland
Dissertations in Health Sciences
34

Biomedical NMR and Epilepsy Research Groups
A. I. Virtanen Institute, Department of Neurobiology
Faculty of Health Sciences, University of Eastern Finland
Kuopio
2010

Kopijyvä Oy
Kuopio, 2010

Distribution:
Eastern Finland University Library/Sales of publications
P. O. Box 1627, FI-70211 Kuopio, Finland
http://www.uef.fi/kirjasto

ISBN: 978-952-61-0261-0 (print)
ISBN: 978-952-61-0262-7 (pdf)
ISSN: 1798-5706 (print)
ISSN: 1798-5714 (pdf)
ISSNL: 1798-5706

Author's address: A. I. Virtanen Insitute for Molecular Sciences
P. O. Box 1627
FI-70211 Kuopio
Finland
E-mail: nick.hayward@uef.fi

Supervisors: Prof Olli Gröhn, PhD
Professor of Biomedical NMR
Department of Neurobiology
A. I. Virtanen Institute for Molecular Sciences
University of Eastern Finland
Kuopio, Finland

Prof Asla Pitkanen, MD PhD
Professor of Neurobiology
Department of Neurobiology
A. I. Virtanen Institute for Molecular Sciences
University of Eastern Finland
Kuopio, Finland

Reviewers: Dr Rick Dijkhuizen, PhD
University Medical Center Utrecht
Heidelberglaan 100
Utrecht, The Netherlands

Prof Astrid Nehlig, PhD
INSERM U 666
Strasbourg, France

Opponent: Dr Rod Scott, MB ChB PhD MRCP MRCPCH
Institute of Child Health
University College London
London, United Kingdom

Hayward, Nick. Magnetic resonance imaging of the hemodynamic and cerebrovascular sequelae of traumatic brain injury, ischemic stroke, and status epilepticus in rats. Publications of the University of Eastern Finland. Dissertations in Health Sciences 34. 2010. 83 p.

ABSTRACT

Magnetic resonance imaging (MRI) provides *in vivo* visualization of soft tissues. For this thesis, long-term cerebrovascular changes after traumatic brain injury, ischemic stroke, and status epilepticus were studied using MRI of rat models for each disease. The research provided new understandings of the pathological processes that occur after central nervous system (CNS) injury.

Traumatic brain injury (TBI) is a leading cause of mortality and morbidity worldwide. However, relatively few TBI studies have considered cerebrovascular factors linked to secondary brain damage. In the first study, we hypothesized that hemodynamic responses to TBI in rodents match those of TBI patients. The study used MRI to quantify absolute regional cerebral blood flow (CBF) and relative regional cerebral blood volume (CBV) over 14 days after TBI in rats. In addition, corresponding regional blood vessel density was examined by immunohistochemistry. There were several new findings, including the first demonstration of three distinct phases of ipsilateral changes in regional CBF after TBI in rats, which matched those of patients shown in prior clinical studies. Acute hypoperfusion was followed by sub-acute CBF recovery and then delayed, secondary hypoperfusion. These fluctuations were associated with a loss and recovery of blood vessels in some regions, including the perilesional cortex.

In the second study, we hypothesized that neurovascularization is important for long-term functional recovery after TBI. Chronic vascular responses were studied 8 months after TBI in rats by MRI. Also, functional recovery and seizure susceptibility were measured over the study period. There were many noteworthy findings, including the discovery that hemodynamic and vascular abnormalities are different between the perilesional cortex, hippocampus, and thalamus. In all rats with TBI, the thalamus was chronically hyperperfused and showed markedly increased blood vessel density. In addition, thalamic hypervascularization correlated with increased seizure susceptibility.

Ischemic stroke is a leading cause of death and adult onset disability in developed countries (Thom et al. 2006, Donnan et al. 2008). In the third study, we hypothesized that long-term hemodynamic and cerebrovascular disruption occurs in the thalamus after cerebral ischemia. We used MRI to quantify regional absolute CBF

over 3 months after transient middle cerebral artery occlusion (MCAO) in rats. Also, sensorimotor functions were examined in the same animals over the study duration. We also studied thalamic angiogenesis by RECA-1 immunohistochemistry at 3 months after MCAO, in combination with the expression of angiogenesis related cadherin adhesion proteins. To our knowledge, we are the first to report initial bilateral hypoperfusion in the thalamus after cerebral ischemia, which is followed by long-term ipsilateral hyperperfusion. As in the ipsilateral thalamus after TBI, chronic hyperperfusion was likely due to a parallel increase in blood vessel density due to angiogenesis. Angiogenesis may be supported by upregulated sub-acute expression of developmental vascular adhesion factors. Functionally, hyperperfusion and angiogenesis in the thalamus correlated with improved forelimb use after ischemia.

Around 0.8% of the global population has a form of epilepsy (Porter 1993). Status epilepticus (SE) is one possible trigger for epilepsy development (epileptogenesis). In the fourth study, we investigated the cerebrovascular consequences of pilocarpine-induced SE over 2 weeks in rats. We found amygdaloid hyperperfusion up to 14 days after SE, which was associated with increased blood vessel density. This is the first report of long-term hemodynamic and cerebrovascular changes in the amygdala after SE in rats.

Our novel cerebrovascular understandings of CNS injury provide small steps towards our future goals in the field of neurobiological MRI. Specifically, we aim to better understand CNS injury progression by finding biomarkers or surrogate MRI markers that will help predict disease progression and treatment responses. A more detailed understanding of brain pathologies will hopefully lead to successful new treatments for secondary damage after brain injury.

National Library of Medicine Classifications: WN 185, WL 354, WL 355, WL 385.

Medical Subject Headings: Brain, magnetic resonance imaging, neurobiology, animal models, cerebrovascular response, cerebral blood flow, cerebral blood volume, blood vessel, traumatic brain injury, ischemic stroke, epilepsy, status epilepticus, thalamus, cortex, hippocampus, amygdala.

For Richard, Julia, Jo, and Steve

"This disease styled sacred comes from the same causes as others, from the things that come to and go from the body, from cold, sun, and from the changing restlessness of winds… there is no need to put the disease in a special class and to consider it more divine than the others; they are all divine and all human. Each has a nature and power of its own; none is hopeless or incapable of treatment."

A Hippocratic doctor's view of epilepsy
Hippocrates of Cos (c. 460–c. 370 BC*)*

ACKNOWLEDGEMENTS

This research was conducted with the Biomedical NMR Group and Epilepsy Research Group at the A. I. Virtanen Institute for Molecular Sciences, and in collaboration with the Department of Neurology, University of Eastern Finland during years 2006-2010.

I am sincerely thankful to my principal supervisor, Professor Olli Gröhn, for his generous professional and personal guidance, resourcefulness, and understanding nature throughout my time in Finland. His calm and welcoming attitude has provided me with a very comfortable and productive few years here. I equally appreciate the plentiful support of my co-supervisor, Professor Asla Pitkänen, whose great enthusiasm and ambition have helped me to reach new heights in science. It has been a privilege to work alongside you both, simply because I searched the globe to find such personable mentors with your impressive expertise.

I am always delighted to look back on the wealth of discussions and guidance so enthusiastically provided by my personal tutor, Dr Riikka Immonen. Riikka's positivity and experience in our work have greatly accelerated my progression and she has often helped to boost my motivation along the way. Recently, I have also had the pleasure of collaborating closely with Dr Jukka Jolkkonen and his colleagues, and I thank him for a thorough introduction to stroke research. I also much appreciate the hard work of Professor Hilkka Soininen and Dr Mark Lythgoe in providing me with the original opportunity for such valuable PhD studies here in Finland.

I will forever be grateful to my colleagues in Kuopio, not only for their scientific guidance and research contributions, but also for their extensive personal and professional support. Especially upon arriving in Finland, many individuals helped me make a smooth transition and even provided plenty of laughs along the way. In particular, I appreciate the great efforts of Paukku Korhonen, Teemu Laitinen, Joanna Huttunen, Heikki Nieminen, Mikko Nissi, Otto Manninen, Antti Airaksinen, Juhis Niskanen, Maarit Pulkkinen, Johanna Närväinen, Pasi Tuunanen, Timo Liimatainen, and Kimmo Jokivarsi for creating a supportive and successful environment for our studies and more. I will miss all of you and much look forward to the antics of our future encounters.

Word has spread that I am about to begin fast track medicine studies at Imperial College, London. This remarkable opportunity has only become a reality thanks to a few exceptionally accommodating individuals at Kuopio University Hospital, who have provided me with a wide window into the clinical side of my preclinical research. Most especially, I am enormously grateful to Professor Juha Jääskeläinen and the Department of Neurosurgery, where many individuals have diligently demonstrated their skills and bountifully shared their knowledge with me – a clinical novice. Of special note, I say one big 'Efharisto poli' to Dr Petros Karamanakos, who so warmly

and selflessly provided me with so much education and friendship over two years worth of on call duties and more. I am also very thankful for all the teachings and kindness shared by Dr Arto Immonen, Dr Timo Koivisto (also for frequently but unknowingly loaning me his shoes for the operating room – a comfortable fit), Dr Antti Ronkainen, Professor Jaakko Rinne, Dr Ville Leinonen, Dr Sakari Savolainen, and many of their colleagues. I am also appreciative of Professor Esa Mervaala, Professor Ritva Vanninen, Professor Hannu Manninen and their departments for improving my clinical education so enjoyably.

Residing overseas can make it difficult to stay in touch with all the loyal family and friends in the UK. Naturally though, I will never forget the years of extensive care, provision and self sacrifice made by my parents, Julia and Richard, to whom this thesis is dedicated. I also dedicate this thesis to two exceptional individuals who generously and selflessly gave my education so much extra attention at pivotal moments in my life. My fond memories of Dr Jo Short and Steve Callacher will live on after their recent passing during the creation of this research.

I thank the reviewers of this thesis, Dr Rick Dijkhuizen and Professor Astrid Nehlig, for sharing their own insights and expertise to help improve my understanding of the topics within. I thank Dr Rod Scott for welcoming our invitation to oppose this thesis and I look forward to learning more from him in the future.

This research was funded by the BiND Program with an EU Marie Curie Early Stage Trainee Research Fellowship MEST-CT-2005-019217, The Health Research Council of The Academy of Finland, The Sigrid Juselius Fundation, The Nordic Centre of Excellence in Neurodegeneration, and the Finnish Funding Agency for Technology and Innovation grant 70048/09.

Kuopio, 1st August 2010

Nick M E A Hayward BA (Hons) MA (Cantab) MNatSci

LIST OF ORIGINAL PUBLICATIONS

This thesis is based on the following original publications that are referred to by their Roman numerals:

I. Hayward NM, Tuunanen P, Immonen R, Ndode-Ekane XE, Pitkänen A, Gröhn O: Magnetic resonance imaging of regional hemodynamic and cerebrovascular recovery after lateral fluid-percussion brain injury in rats. Journal of Cerebral Blood Flow & Metabolism, advance online publication, 19th May 2010; doi:10.1038/jcbfm.2010.67.

II. Hayward NM, Immonen R, Tuunanen P, Ndode-Ekane XE, Gröhn O, Pitkänen A: Association of chronic vascular changes with functional outcome after TBI in rats. Journal of Neurotrauma, advance online publication, 18th October 2010; doi:10.1089/neu.2010.1448.

III. Hayward NM, Yanev P, Haapasalo A, Miettinen R, Hiltunen M, Gröhn O, Jolkkonen J: Chronic hyperperfusion and angiogenesis follow sub-acute hypoperfusion in the thalamus of rats subjected to focal cerebral ischemia. Journal of Cerebral Blood Flow and Metabolism 2010, accepted for publication.

IV. Hayward NM, Ndode-Ekane XE, Kutchiashvili N, Gröhn O, Pitkänen A: Elevated cerebral blood flow and vascular density in the amygdala after status epilepticus in rats. Neuroscience Letters 2010: 48: 39–42.

The publishers of these original articles have kindly granted permission for them to be reprinted in this Doctoral thesis.

CONTENTS

1 INTRODUCTION 1

1.1 Nuclear magnetic resonance principles 1
1.1.1 Nuclear spin 1
1.1.2 Relaxation 4
1.1.3 Signal and image contrast generation 8

1.2 Magnetic resonance imaging of hemodynamic and vascular activity: Cerebral blood flow and cerebral blood volume 10
1.2.1 Arterial spin labeling for absolute quantification of cerebral blood flow 11
1.2.2 Dynamic susceptibility contrast methods for relative quantification of cerebral blood volume and cerebral blood flow 14
1.2.3 Other modalities for cerebral perfusion measurement 17

1.3 The value of preclinical magnetic resonance imaging and its clinical translation 19

2 REVIEW OF THE LITERATURE 20

2.1 Experimental traumatic brain injury 20
2.1.1 Traumatic brain injury 20
2.1.2 Magnetic resonance imaging of experimental traumatic brain injury in rodents 22
2.1.3 Hemodynamic and cerebrovascular responses to traumatic brain injury 22
2.1.4 Magnetic resonance imaging studies of the hemodynamic and cerebrovascular responses to traumatic brain injury 24

2.2 Ischemic stroke and experimental focal ischemia 25
2.2.1 Ischemic stroke 25
2.2.2 Magnetic resonance imaging development for clinical and experimental ischemia 26
2.2.3 Hemodynamic and cerebrovascular responses to ischemic stroke 28
2.2.4 Magnetic resonance imaging studies of the long-term hemodynamic and cerebrovascular response to focal ischemia in rodents 29

2.3 Status epilepticus and experimental epilepsy 30
2.3.1 Epilepsy and status epilepticus 30
2.3.2 Magnetic resonance imaging studies of the hemodynamic and cerebrovascular responses to epileptogenesis 31

3 HYPOTHESES AND AIMS 32

4 MATERIALS AND METHODS 33

4.1 Animal models 33
*4.1.1 Lateral fluid-percussion induced traumatic brain injury (**I**, **II**)* 33
*4.1.2 Focal ischemia by transient middle cerebral artery occlusion (**III**)* 34
*4.1.3 Pilocarpine induced status epilepticus (**IV**)* 35

4.2 Magnetic resonance imaging 35
4.2.1 Anesthesia 35
4.2.2 Anatomical imaging 36
4.2.3 Cerebral blood flow 36
4.2.4 Cerebral blood volume 37
4.2.5 MRI data analyses 37

4.3 Behaviourology 38
4.3.1 Composite neuroscore after traumatic brain injury 38
4.3.2 Morris water maze after traumatic brain injury 38
4.3.3 Behavioral outcome measures after focal ischemia 39

4.4 Chronic seizure susceptibility after traumatic brain injury 40
4.4.1 Video-EEG recording 40
4.4.2 Pentylenetetrazol test 41

4.5 Histological approaches 41
4.5.1 Tissue fixation and processing 41
4.5.2 Nissl staining 42
4.5.3 RECA-1 immunohistochemistry after traumatic brain injury or status epilepticus 42
4.5.4 RECA-1 immunohistochemistry after focal ischemia 43
4.5.5 Quantifying blood-brain barrier leakage after focal ischemia 45

4.6 Molecular biology techniques 45

4.7 Statistics 46

5 RESULTS 48

5.1 Prolonged hemodynamic disruption after traumatic brain injury 48

5.2 Vascular reorganization after traumatic brain injury 49

5.3 Long-term functional consequences of traumatic brain injury 50

5.4 Prolonged cerebral blood flow disruption after cerebral ischemia 52

5.5 Vascular reorganization after cerebral ischemia 53

5.6 Long-term functional consequences of cerebral ischemia 54

5.7 Prolonged hyperperfusion and increased blood vessel density after status epilepticus 54

6 DISCUSSION AND CONCLUSIONS 56

6.1 Cerebrovascular responses to traumatic brain injury 56
6.1.1 Severe traumatic brain injury disrupts acute contralateral cerebral blood flow 56
6.1.2 Acute and sub-acute hemodynamic changes in ipsilateral regions match those of patients 57
6.1.3 Vascular reorganization only partly explains hemodynamic changes 58
6.1.4 Chronic cerebrovascular responses to traumatic brain injury are region specific 58
6.1.5 Traumatic brain injury and epileptogenesis 59

6.2 Cerebrovascular responses to cerebral ischemia 61
6.2.1 Thalamic hypoperfusion and delayed hyperperfusion after cerebral ischemia 61
6.2.2 Thalamic hyperperfusion is likely due to angiogenesis 62

6.3 The cerebrovascular sequalae of traumatic brain injury and ischemic stroke may share common neurobiological mechanisms 63
6.3.1 Early shared mechanisms 63
6.3.2 Chronic shared mechanisms of thalamic cerebrovascular responses 66

6.4 Cerebrovascular responses to status epilepticus 67

6.5 Methodological considerations 68
6.5.1 Magnetic resonance imaging suits hemodynamic studies of brain disorders 68
6.5.2 Anesthesia 69
6.5.3 Functional recovery after TBI and cerebral ischemia 69

6.6 Future directions 70

7 REFERENCES 73

APPENDIX: ORIGINAL PUBLICATIONS (I-IV)

ABBREVIATIONS

AIF	Arterial input function
ANCOVA	Analysis of covariance
ANOVA	Analysis of variance
APP	Amyloid precursor protein
asf	Area sampling fraction
ASL	Arterial spin labeling
Aβ	Amyloid beta
BBB	Blood-brain barrier
CBF	Cerebral blood flow
CBV	Cerebral blood volume
CCI	Controlled cortical impact
CNS	Central nervous system
CPP	Cerebral perfusion pressure
CSF	Cerebrospinal fluid
CT	Computed tomography
DAB	Diaminobenzadine
DSC	Dynamic susceptibility contrast
DWI	Diffusion weighted imaging
ED	Epileptiform discharge
EDCF	Endothelium-derived contracting factor
EEG	Electroencephalography
FID	Free induction decay
fMRI	Functional magnetic resonance imaging
ICP	Intracranial pressure
IgG	Immunoglobulin G
KPBS	Potassium phosphate buffered saline
LFPI	Lateral fluid-percussion injury
MCA	Middle cerebral artery
MCAO	Middle cerebral artery occlusion
MION	Monocrystalline iron oxide nanoparticles
MR	Magnetic resonance
MRI	Magnetic resonance imaging
MTT	Mean transit time
NeuN	Neuron-specific nuclear protein
NGS	Normal goat serum
NHS	Normal horse serum
Ni-DAB	Ni-enhanced diaminobenzidine
NMR	Nuclear magnetic resonance
NO	Nitric oxide
PAGE	Polyacrylamide gel electrophoresis
PBS	Phosphate buffered saline

PCDH1	Protocadherin-1
PCDH17	Protocadherin-17
PCT	Perfusion computed tomography
PECAM-1	Platelet-endothelial adhesion molecule 1
PET	Positron emission tomography
PTZ	1,5-pentamethylenetetrazole (pentylenetetrazol)
PWI	Perfusion weighted imaging
RECA-1	Rat endothelial cell antigen-1
RF	Radiofrequency
ROI	Region of interest
RT ECL	Reverse transcription electrochemiluminescence
rtPA	Recombinant tissue plasminogen activator
SD	Standard deviation
SE	Status epilepticus
SEM	Standard error of the mean
SPECT	Single photon emission computed tomography
ss-CE	Steady-state contrast enhanced
ssf	Section sampling fraction
SWI	Susceptibility weighted imaging
TBI	Traumatic brain injury
TBS	Tris-buffered saline
TBST	Tris-buffered saline with 0.1% Tween
TBS-T	Triton X-100
TE	Time to echo
tsf	Tissue sampling fraction
VE-cadherin	Vascular endothelial cadherin
VEGF	Vascular endothelial growth factor
XeCT	Xenon-enhanced computed tomography

1 INTRODUCTION

Magnetic resonance imaging (MRI) is a versatile tool for *in vivo* and *ex vivo* visualization of soft tissues. The combination of MRI and animal disease models provides us with the opportunity to research the neurobiology of neurological disorders and central nervous system (CNS) injury, in order to achieve clinically valuable insights and translational technologies. In this thesis, the long-term hemodynamic and cerebrovascular events that occur after traumatic brain injury, ischemic stroke, and status epilepticus in rats were researched through *in vivo* MRI.

Unlike computed tomography (CT), ultrasound, or autoradiography, MRI is based upon the principles of electromagnetism and relies on a physical phenomenon of atomic nuclei called nuclear magnetic resonance (NMR).

1.1 Nuclear magnetic resonance principles

1.1.1 Nuclear spin

Certain atomic nuclei possess the property of spin. Spin can be visualized as a nucleus' rotation about its central axis, much like the way our planet rotates, although nuclear spin occurs more rapidly. The spin of an atomic nucleus is defined by its total angular momentum, which is the sum of the angular momenta of its constituent protons and neutrons. Nuclei are quantum mechanical systems whereby a nucleus' spin angular momentum, *S*, is quantized into discrete values determined by its spin quantum number, *I*. The magnitude of *S* for a given nucleus can be described as follows:

$$S = \hbar[I(I+1)]^{1/2}$$

where $\hbar = \frac{h}{2\pi}$ and h is Planck's constant. The mathematical laws governing spin allow *I* to take a value as follows:

1. If the number of neutrons and the number of protons are both even, then *I* = 0.
2. If the number of neutrons plus the number of protons is odd, then *I* takes a half integer value (1/2, 3/2, 5/2, etc).

3. If the number of neutrons and the number of protons are both odd, then *I* has an integer value (1, 2, 3, etc).

As *S* is a vector quantity, it carries both magnitude and direction. Its direction is dependent on the magnetic quantum number for the nucleus, *m*, and the magnitude of *S* can be described as follows:

$$S = m\hbar$$

where

$$m = I, I-1, \ldots, -I+1, -I$$

or a total of 2*I* + 1 quantized values under experimental conditions, which provide a projection of the direction of the spin angular momentum. This is an oversimplification in that an infinite number of directions can exist as described by the theory of quantum superposition. However, the nuclear spin dynamics for NMR theory are neatly described by the 2*I* + 1 relationship. When a nucleus is placed in an applied magnetic field (B_0) during an NMR experiment, it takes up 2*I* + 1 possible energy states due to the interaction between the nuclear angular momentum and B_0, because spinning nuclei carry their own magnetic field. All of these laws are important because nuclei with a spin quantum number *I* = 0 will therefore not interact with B_0 and not be NMR active.

Now if one considers a hydrogen nucleus, ^{1}H, our laws dictate that this unpaired proton has a spin quantum number *I* = 1/2. Solving our equations gives a spin angular momentum *S* = ±1/2ħ and the magnetic quantum number *m* = ±1/2 for the hydrogen nucleus. The two values for *m*, +1/2 and -1/2, can be visualized as the two directions given to the spin angular momentum *S* in space, which are more easily denoted as 'parallel' and 'antiparallel' or as +*z* and –*z* on a three-way Cartesian axes set. As there are 2*I* + 1 possible energy states, it follows that there are two for the ^{1}H nucleus. In the absence of an applied magnetic field, these states would be at the same energy level. However, an applied B_0 interacts with the spin angular momentum to create torque, resulting in a separation between the two energy levels as follows:

$$Torque\ (T) = \mu \times B_0$$

where μ is the nuclear angular moment of the spinning nucleus and depends on the characteristic gyromagnetic ratio constant for that nucleus, γ:

$$\mu = \gamma S$$

and therefore, under B_0, the energy states are separated as follows:

$$\Delta E = \gamma \hbar B_0$$

The separate energy states of a nucleus provide the basis of NMR experiments. A spinning nucleus can be excited from the lower energy state to the higher energy state by applying an oscillating magnetic field to the system, B_1, as an electromagnetic wave. The energy of the applied wave must match the energy difference between the two states under B_0 as follows:

$$\Delta E = h v_0$$

where v_0 is the frequency of quantized electromagnetic radiation. The energy difference due to B_0 in NMR experiments must be matched by oscillating electromagnetic waves that are typically in the radiofrequency (RF) range, hence B_1 is applied through RF wave pulses with a frequency matching the Larmor frequency for the nucleus (ω_0) at a set magnetic field as follows:

$$v_0 = \frac{\gamma B_0}{2\pi}$$

$$\omega_0 = \gamma B_0$$

It is these NMR principles that allow MRI experiments to probe and visualize the biological properties of soft tissues through the study of nuclei.

The biological studies in this thesis rely on hydrogen NMR experiments. As discussed, quantum theory tells us that the hydrogen nuclei exist experimentally in quantized energy levels. Hydrogen nuclei are protons with two possible energy levels, known as spin up and spin down. When hydrogen nuclei are placed into an applied external magnetic field (B_0) of an MRI scanner, they line up with this external magnetic field in either a parallel or anti-parallel manner. The relative

numbers of nuclei with each alignment will be determined by the Boltzmann distribution:

$$\frac{N_2}{N_1} = exp\left[\frac{-(E_2 - E_1)}{kT}\right]$$

where *k* is the Boltzmann constant and *T* is the absolute temperature. The parallel orientation for hydrogen is a slightly lower energy state and is therefore thermodynamically more favorable, thus an excess of nuclei lie parallel with B_0. This establishes a net magnetization M_0 along B_0 in the equilibrium state. The amplitude of M_0 is dependent on the density of mobile spinning nuclei in the sample, also known as 'proton density' when describing hydrogen.

1.1.2 Relaxation

To generate a signal for magnetic resonance imaging or spectroscopy, an RF pulse is directed towards the sample by the transmission RF coil of the scanner. Before the RF pulse, nuclei in the sample are in the equilibrium energy state and are spinning out of phase, thus there is no net transverse magnetization in the *xy*-plane. The RF pulse moves the net magnetization vector *M* away from the longitudinal *z* direction (equilibrium, M_0) momentarily. This is because the introduction of the applied oscillating magnetic field of the RF pulse, B_1, causes spinning nuclei to be excited and to precess in phase. Excitation brings a balance between the parallel and anti-parallel energy states. This, combined with phase coherence, creates the net transverse magnetization. After the RF pulse, *M* returns to equilibrium in an oscillating manner through the processes of 'relaxation'.

The flip angle between M_0 and M_1 is dependent upon the frequency, duration, and therefore the energy of the RF pulse. After the RF pulse, *M* recovers towards equilibrium and the coherent precessing transverse magnetization induces electrical signal in the receiver solenoid. Based on the Cartesian coordinates system, Figure 1 depicts this process for a 90° RF pulse in the rotating frame of reference.

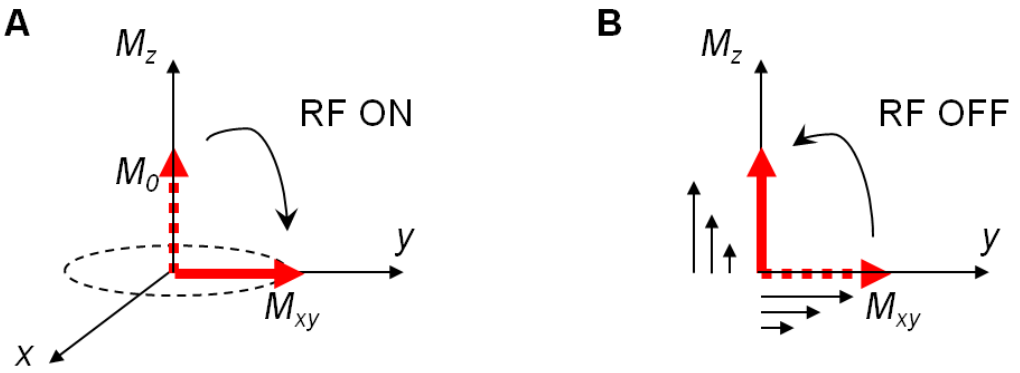

Figure 1. Nuclear magnetization response to a 90° radiofrequency (RF) pulse in the rotating frame of reference. **A**. During an applied RF pulse, the longitudinal magnetization vector (*M*) is flipped into the *xy*-plane. **B**. After the RF pulse, the transverse component of the magnetization vector (M_{xy}) relaxes by T_2 processes and the longitudinal component (M_z) begins to recover by T_1 processes. Figure adapted from Hashemi et al. 2004 in MRI: The Basics, Lippincott Williams and Wilkins, Second Edition.

The processes through which *M* recovers to its equilibrium position M_0 after RF irradiation are called relaxation. The rate of recovery of the M_z component is characterized as longitudinal T_1 relaxation, often termed restoring 'thermal equilibrium'. The rate of loss of the M_{xy} component is characterized as transverse T_2 relaxation, or loss of phase coherence. These are described by the Bloch equations (Bloch 1994):

$$\frac{dM_z}{dt} = \frac{M_0 - M_z}{T_1}$$

$$\frac{dM_{xy}}{dt} = -\frac{M_{xy}}{T_2}$$

T_1 relaxation and T_2 relaxation occur through independent processes with different relaxation rates in a given MRI voxel in a given tissue sample. Relaxation rates are dependent upon the biochemical setting of the nuclei under NMR study. This is because relaxation processes are affected by many factors, including dipole-dipole coupling, interactions through chemical bonds (*J* coupling), differences in magnetic susceptibility, intermolecular interactions, pH, temperature, and many other chemical and physical conditions embracing the nuclei.

T_1 relaxation occurs through spin-lattice interactions, whereby energy is transferred from the oscillating nuclei to the surrounding environment. This environment is termed 'the lattice' because it refers to molecular groups on close neighboring structures that are not the focus of study during the NMR experiment. The distribution of motional frequencies of a nucleus is influenced by its own oscillations and those of proximal structures, thus it is dependent on the physical and chemical environment within the tissue. Therefore, each relaxation parameter sensitizes the NMR measurement to certain biological processes by providing a window over small distributions of motional frequencies and timescales. The general T_1 tissue characteristics vary by tissue type according to Table 1. T_1 relaxation can be mathematically described through the spectral density function *J(ω)*:

$$J(\omega) \propto \frac{\tau_c}{1 + \omega^2 \tau_c^2}$$

where τ_c is the time required for a molecule to rotate one radian. For dipole-dipole interactions, T_1 depends on the oscillations of the neighboring molecules and can be described as follows:

$$\frac{1}{T_1} \propto \frac{\tau_c}{1 + \omega^2 \tau_c^2} + \frac{4\tau_c}{1 + 4\omega_0^2 \tau_0^2}$$

This demonstrates that the most efficient energy transfer to the lattice, hence the shortest T_1 time, occurs when the processes are resonating at the Larmor frequency. This is when $\tau_c = 1/\omega_0$.

T_2 relaxation occurs when the spinning nuclei dephase. Dephasing occurs through the transfer of energy between the spinning nuclei under MR study, thus T_2 relaxation occurs through 'spin-spin' interactions. The degree of interactions is determined by the physical and chemical environment around the nuclei, which varies greatly between tissue types and tissue conditions. T_2 characteristics in some general tissue types are described in Table 1. Dephasing due to dipole-dipole interactions between spinning nuclei can be mathematically described as follows:

$$\frac{1}{T_{2,dip}} \propto 3\tau_c + \frac{5\tau_c}{1 + \omega^2 \tau_c^2} + \frac{2\tau_c}{1 + 4\omega_0^2 \tau_0^2}$$

yet T_2 relaxation also occurs through diffusion and exchange of protons:

$$\frac{1}{T_2} = \frac{1}{T_{2,dip}} + \frac{1}{T_{2,dif}} + \frac{1}{T_{2,exc}}$$

Rapid dephasing leads to fast T_2 relaxation and therefore short T_2 times in a voxel. Conversely, slow dephasing leads to slow relaxation and therefore longer T_2 times in a voxel.

Table 1. A summary of general relaxation properties by tissue type. The motional frequencies (ω) are described for T_1 and T_2 relaxation processes.

Tissue type	**T_1 properties**	**T_2 properties**
Free H_2O	$\omega(H_2O) >> \omega_0$ Weakest lattice interactions Longest T_1 time	Averaging of spin-spin interactions Slowest dephasing Longest T_2 time Fast motion, small τ_c
Solid	$\omega(solid) < \omega_0$ Intermediate lattice interactions Intermediate T_1 time	Most spin-spin interactions Fastest dephasing Shortest T_2 time Slow motion, large τ_c
Proteinaceous	$\omega(proteinaceous) \approx \omega_0$ Strong lattice interactions Short T_1 time	Protein size and content dependent Long or short T_2
Fat	$\omega(fat) \approx \omega_0$ Strongest lattice interactions Shortest T_1 time	Intermediate spin-spin interactions Intermediate dephasing Intermediate T_2 time

By tailoring our MRI contrast preparation and acquisition parameters to measure changes in one kind of relaxation, we can generate contrast in our images that is specific for a certain tissue type, tissue condition, or tissue process. For example, in conventional T_2 weighted imaging, the white matter of the brain appears dark as the

water protons within it experience fast T_2 relaxation processes (short T_2 time, reduced signal intensity, dark on image) compared to grey matter. Each scan is tailored (weighted) towards a contrast parameter type, so by running multiple scans, we have a very versatile and accurate method for specifically visualizing different tissue types and for measuring physiological processes.

1.1.3 Signal and image contrast generation

To create an image, we can exploit the NMR signals of hydrogen nuclei in water molecules. The nature of these signals depends on the chemical, physical and biological properties of the tissue environment, for example, the local quantity and mobility of water. Importantly, approximately 60% of an adult's body is water and much of this water resides in soft tissues. This feature of tissue composition provides a high signal density for MRI; high resolution images with high signal-to-noise ratios are therefore achievable. Typically, small animal MRI has a resolution in the order of 100 µm, which can be optimized to 30-50 µm using the most advanced hardware and measurement techniques plus extended scan times. This resolution is quite remarkable, especially when one considers that the thickness of the granule cell layer in the rat hippocampus is around 50-100 µm. Therefore, neurobiological changes in small subregions of the brain can lead to distinct, measurable changes in the black-white contrast captured within MR images.

As already described, the transmission coil generates RF pulses that excite a sample and allow us to gain NMR signals and measure relaxation processes. After an RF pulse, the spinning nuclei dephase and the net magnetization vector *M* precesses freely around the *xy*-plane as equilibrium becomes restored (Figure 1). The oscillating movement of the transverse magnetization generates electrical signal in a receiver coil, due to the principles of electromagnetism. The free precession of spins induces a signal in the receiver coil and the signal decays over time through relaxation processes, hence we detect NMR signal as 'free induction decay' (FID).

The FID signal waveforms contain frequency, phase and amplitude information that must be translated into signal location and signal intensity for each voxel of our MR images. Detected FIDs are decoded by Fourier transformation, which converts the signal from the time domain to the frequency domain. To spatially encode the signals, intentional, spatially varying perturbations in the external magnetic field

are made. The scanner creates three magnetic field gradients that help provide a three dimensional coordinate system for the spatial localization of signals. Together, the action of these gradients and the RF pulses are controlled by the 'pulse sequence', which is a computer program that controls the process of sequentially introducing gradient and RF pulses and acquiring signals in order to collect all the required information for image reconstruction.

Signal localization for MRI relies on the principle that the precession frequency of a nucleus linearly depends on magnetic field strength ($\omega = \gamma B_{eff}$). Spatial localization is achieved through selectively applying the scanner's linear magnetic field gradients across the sample in the *x*, *y* and *z* directions, where *z* is the direction of B_0. Each linear magnetic field gradient creates a location dependent field along one direction, thus ω becomes location-dependent, allowing for slice selection or volume selection within the sample. Oblique imaging planes are achieved through the sample by a linear combination of two or three gradients. Selective excitation RF pulses each have a specific carrier frequency and frequency bandwidth. Therefore, RF energy only transfers to nuclei with a resonance frequency matching the RF carrier frequency, or to those closely matching the frequency bandwidth. This way, a combination of a linear gradient and selective RF pulse flips only the spinning nuclei within a selected slice. Also, the slice thickness is governed by the pulse bandwidth and the slope of the applied magnetic field gradient. A larger gradient increases the field variation along its direction, leading to a thinner selected slice.

Having made a slice selection, spatial localization of the signal arising from within a slice must be made. This happens through frequency encoding and phase encoding of FIDs. For frequency encoding, a frequency (or readout) gradient is applied along the readout direction (*x*) as the signal is received. Along this applied gradient, the frequency of the precession changes in a spatially-dependent manner, such that across the selected slice the spinning nuclei experiencing a higher magnetic field from the frequency-encoding gradient will oscillate with higher frequency, and vice versa. Frequency and position have a one-to-one relationship and thus the frequency component of the FID can be decoded to provide positional information from the signal within the slice. For phase encoding, a gradient is applied along the phase encoding direction before readout. The magnetic field gradient induces a phase shift between nuclei within the slice, which is dependent on the local field strength applied. With these techniques, the nuclei from each position within the slice carry distinct frequency and distinct phase,

which are unique and allow for encoding as x and y coordinates within the imaged slice.

To generate images, a range of magnetic field gradient conditions are employed and many arising FIDs are collected. The first dimension can be encoded by the slice selection (*z*) direction. The waveform information is arranged into the k-space matrix, where one direction encodes for different phases and the other encoding direction corresponds to frequency. Two phase encoding directions can be used to generate three-dimensional datasets. The k-space size dictates the image resolution and there are numerous acquisition pulse sequences available to provide different methodologies for filling all points on the k-space, each leading to various acquisition speeds and accuracy. MR images are finally created by Fourier transformation of the complete k-space. Central k-space regions discern image contrast while the k-space edges discern the fine details (sharpness) within the image.

1.2 Magnetic resonance imaging of hemodynamic and vascular activity: Cerebral blood flow and cerebral blood volume

Magnetic resonance methods do not only provide structural and anatomical imaging by measuring T_1 and T_2 relaxation. MRI techniques are continually being developed in order to investigate brain functions. For example, the physiological activity of the cerebrovascular blood supply is now a widespread topic of MRI studies in both clinical and preclinical settings. MRI methods can be used to measure small, regional changes in cerebral blood flow (CBF) and cerebral blood volume (CBV) in both patients and animal models of disease. Accurate, non-invasive and thus repeatable quantification of hemodynamic changes is of great healthcare and research importance because healthy tissues require a healthy blood supply to meet metabolic demands. Various pathologies and drugs may disrupt the blood supply and/or metabolism, thus vascular imaging techniques are vital for pathological investigations. Also, in the healthy brain, the activity of certain brain regions is reflected by hemodynamic changes, so their measurements form the basis of functional MRI (fMRI) studies that are now routinely used for both medical research and psychology research.

1.2.1 Arterial spin labeling for absolute quantification of cerebral blood flow

Cerebral blood flow can be measured using the arterial spin labeling (ASL) perfusion MR technique. The MRI scanner's transmitter coil and gradient systems are used to manipulate the nuclear spin of protons of water molecules within the flowing bloodstream. This can be achieved by applying a magnetic field gradient and a 180º 'inversion' RF pulse directed at arterial blood upstream from the imaging slice of interest. After a carefully calibrated delay time, the labeled water in the bloodstream arrives in the slice of interest, which could be a section of the brain (Figure 2). In the slice of interest, the net magnetization amplitude is decreased proportionally to the rate of tissue perfusion due to inflowing blood at the capillary bed, by around 2% (Wintermark et al. 2005). The imaging slice is imaged by proton density weighted imaging (Zaharchuk 2007) and the resulting signal intensities are subtracted from those acquired with a control labeling scheme, whereby the bloodstream flows without inversion labeling. The perfusion rate is therefore mapped across the slice of interest and thus regional CBF can be quantified absolutely. An exogenous contrast agent is not required because perfusion imaging is dependent on endogenous magnetization changes induced within the bloodstream. However, the sensitivity and spatial resolution of this method are limited because the spin label is very short-lived, thus careful calibration is required. The contrast-to-noise ratio of ASL is relatively low, thus scan times must often be extended to repeat perfusion measurements and improve accuracy by mapping average flow values.

Arterial spin labeling in the rat brain was first described in 1992 by Williams and colleagues (Williams et al. 1992). The authors modified the Bloch equations to include the MR signal effects of blood flow, allowing quantification of regional CBF by making spin inversion, a control image, and a T_1 map from one image slice. Starting with the modified Bloch equations, the ASL theory as a function of time (t) is described as follows:

$$\frac{dM_b(t)}{dt} = \frac{M_b^0 - M_b(t)}{T_1} + fM_a(t) - \frac{f}{\lambda}M_b(t)$$

where M_b is the *z* magnetization per gram of brain tissue; $M^0{}_b$ is the value of M_b at equilibrium (fully relaxed conditions); M_a is the *z* magnetization per ml of arterial blood; *f* is the brain blood flow (ml/g/s); λ

is the brain/blood partition coefficient for water [(quantity of water/gram of brain tissue)/(quantity of water/ml of blood)]; T_1 provides the spin-lattice relaxation time of brain water in the absence of flow or exchange between the blood and brain. Note that fM_a and fM_b/λ represent the magnetization of the incoming and outgoing water in the bloodstream of the brain, respectively. Our model carries some assumptions, such as the notion that a well-mixed compartment exists so the magnetization of spinning nuclei in the venous outflow is equal to that in the brain tissue ($fM_v = fM_b/\lambda$, where M_v is the *z* magnetization per ml of venous blood. At equilibrium, inflowing and outflowing magnetization are equal for the brain water and arterial blood, thus

$$fM_a^0 = fM_b^0/\lambda$$

We can assume that arterial spinning nuclei are continuously inverted, thus $M_a(t) = -M^0{}_a$ throughout. In addition, $-fM^0{}_b/\lambda$ can be substituted for fM_a, thus the time dependence of M_b can be solved:

$$M_b(t) = \frac{M_b^0}{1 + \frac{fT_1}{\lambda}} \times \left[\left(1 - \frac{fT_1}{\lambda}\right) + \frac{2fT_1}{\lambda} exp - t\left(\frac{1}{T_1} - \frac{f}{\lambda}\right)\right]$$

With continuous inversion of arterial spinning nuclei over varying time periods, then subsequent sampling of M_b, we see M_b decrease exponentially with the apparent time constant of T_{1app}:

$$\frac{1}{T_{1app}} = \frac{1}{T_1} + \frac{f}{\lambda}$$

Under steady state conditions, M_b can be denoted $M_b{}^{ss}$ as follows:

$$M_b^{ss} = M_b^0 \frac{\left(1 - \frac{fT_1}{\lambda}\right)}{\left(1 - \frac{fT_1}{\lambda}\right)}$$

allowing blood flow (*f*) to be solved for the basis of CBF quantification

$$f = \frac{\lambda}{T_{1app}} \cdot \frac{M_b^0 - M_b^{ss}}{2M_b^{ss}}$$

where T_{1app}, M^0_b and M^{ss}_b are measured by MRI. We can assume λ to be 0.9 (Herscovitch and Raichle 1985) in healthy brain tissue, which is used for the basis of CBF quantification in rats.

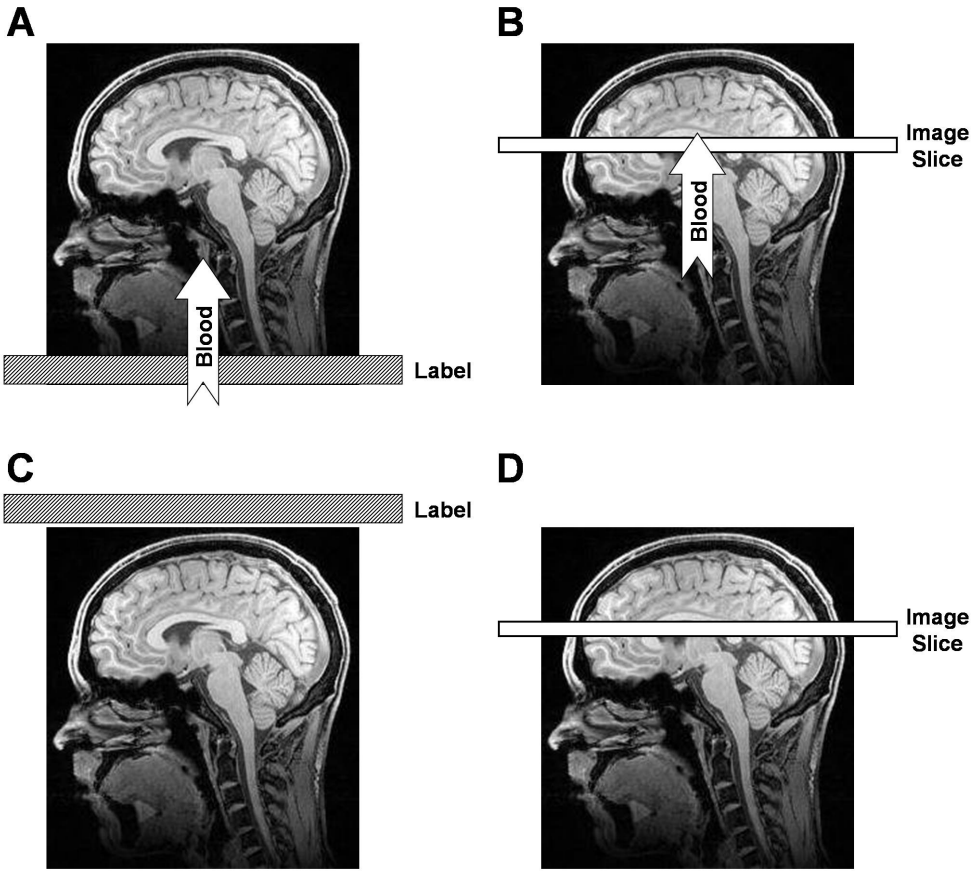

Figure 2. Arterial spin labeling (ASL) quantifies cerebral blood flow (CBF) by magnetic resonance imaging (MRI). **A**. The inversion labeling is applied at the neck of the patient and the magnetism of spinning nuclei in the inflowing blood becomes inverted. **B**. The labeled blood reaches the imaging slice of interest and proton density weighted imaging is performed. The whole process is then repeated without inversion labeling of inflowing blood. **C**. The inversion label is applied symmetrically outside of the brain to offset any magnetization transfer effects that the labeling RF pulse creates. **D**. Proton density weighted imaging of the same image slice of interest is made with unlabeled blood flowing. Subtraction of the image slice signal in **B** from that in **D** provides the basis of CBF quantification. Multiple pairs of labeled and control images may be averaged to construct a perfusion map of absolute CBF. A T_1 map is often made from the same image slice because T_1 values for each imaging voxel are required for the flow calculation. The sagittal background MR image of the head is not acquired during ASL yet can be acquired by anatomical imaging scans during the same MRI session. The background image is added for illustration purposes only (courtesy of Julian Bailes, PhD, University of London).

1.2.2 Dynamic susceptibility contrast methods for relative quantification of cerebral blood volume and cerebral blood flow

Dynamic susceptibility contrast (DSC) MRI is another MRI-based technique for perfusion measurement and it underpins most conventional perfusion weighted imaging (PWI) in clinics. It is also known as 'bolus tracking' because a bolus of intravenous contrast agent is injected and then sequentially imaged (tracked) rapidly within the capillary bloodstream during the contrast agent's first pass through the tissue region of interest. The MR signal change induced by the contrast agent is measured over time and the time-signal intensity plots allow analyses of tracer kinetics. These analyses provide quantification of hemodynamic parameters, including mean transit time (MTT), relative cerebral blood volume (CBV) and relative cerebral blood flow (CBF) (Figure 3).

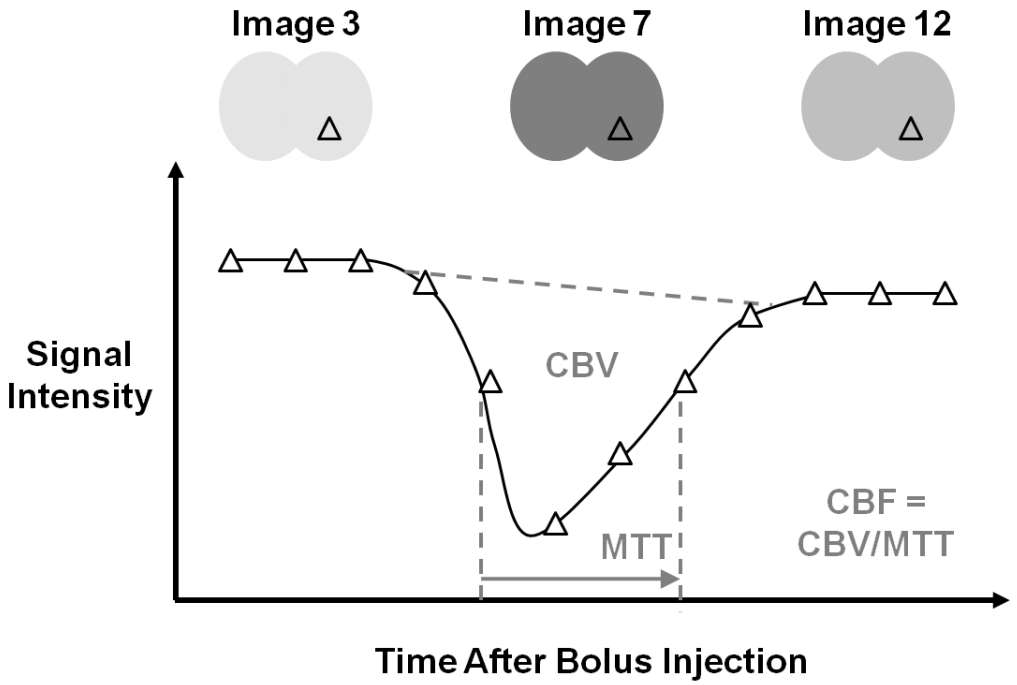

Figure 3. Dynamic susceptibility contrast (DSC) magnetic resonance imaging (MRI) for relative cerebral blood volume (CBV) and mean transit time (MTT) measurement. Each time point provides an image acquired rapidly during the first pass of the intravascular contrast agent. As the bolus permeates the region of interest (triangle point), the signal intensity decreases in a contrast agent concentration-dependent manner. Further data analysis provides a measurement for relative cerebral blood flow (CBF), which can be approximated as CBV divided by MTT.

Gadolinium chelates were among the first MRI contrast agents to be used to study perfusion because they are normally retained within the vascular lumen and have intrinsically high magnetic susceptibility (Zaharchuk 2007). As a gadolinium bolus passes through an MRI voxel, the MR signal intensity changes depending on the relaxation parameter measured. This is because gadolinium creates variations in the local magnetic field. These strong 'susceptibility gradients' lead to accelerated loss of phase coherence between spinning nuclei nearby. For gadolinium, this predominantly increases transverse relaxation rates (R_2) and thus results in signal loss in T_2 or T_2* weighted images. Most signal loss occurs when spinning nuclei have the opportunity to diffuse maximally within the susceptibility gradient during the course of the experiment, which corresponds to the echo time (TE). Longer TEs therefore allow for more dephasing and thus more T_2 weighted signal loss, yet the degree of relaxivity is complex and discerned by the vascular density and vessel size distribution (Ostergaard 2005). Still, it has been experimentally determined that DSC spin echo (T_2) measurements reflect vessel sizes comparable to the distance that water diffuses within the echo time (~10 μm) (Boxerman et al. 1995). Conversely, DSC gradient echo techniques (T_2*) are sensitive to all magnetic field inhomogeneities and all vessel sizes.

Measuring signal intensity reduction over time forms the basis of hemodynamic calculations:

$$\Delta R_2(t) \propto C_t(t)$$

where $C_t(t)$ is the concentration of contrast agent in the tissue at a given time. As already described, longitudinal (R_1) and transverse relaxation (R_2) occur with exponential decay and longitudinal relaxation happens slowly compared to transverse relaxation in most biological systems. Therefore, we can consider ΔR_2 while the signal contribution linked to R_1 remains small, to describe the signal (S) after a contrast agent bolus:

$$S(t) = S(t_0)(1 - exp^{-TR.R_1})exp^{-TE.\Delta R_2(t)}$$

where $S(t_0)$ is the baseline signal without contrast agent. Assuming that ΔR_2 is linearly proportional to C_t, tracer kinetics are determined by:

$$C_t(t) = -k \log\left(\frac{S(t)}{S(t_0)}\right)/TE$$

Cerebral blood volume (CBV) is calculated from $\int C_t(t)$, which is the area under the signal intensity-time curve, assuming a linear relationship between contrast agent concentration and ΔR_2 as described. To accurately calculate relative cerebral blood flow (CBF), the residue function *R(t)* must be analysed, which corresponds to the retention time of contrast agent within the tissue:

$$C_t(t) = CBF.C_a.R(t)$$

where C_a represents the arterial contrast agent concentration at $t = 0$. In reality, C_a is clearly proportional to the blood flow rate and also known as the arterial input function (AIF). It varies over time and can be expressed as the convolution of the residue function:

$$C_t(t) = CBF.C_a(t) \otimes R(t)$$

thus CBF is derived by deconvolution whereby *CBF.R(t)* is fitted from the experimentally determined signal variation over time. However, experimental noise can challenge the accuracy of this approach and the relationship between ΔR_2 and C_t may not be linear due to tissue pathology, thus relative CBF and CBV measurements are often mapped after DSC MRI, rather than absolute measures. In order to obtain sufficient temporal resolution during bolus tracking, ultrafast imaging such as echo planar imaging is used. DSC usually provides multislice mapping of hemodynamic parameters. A close variant of the DSC technique is known as steady-state contrast enchanced (ss-CE) MRI, which is based on the measurement of steady-state signal changes arising from a blood pool contrast agent with a long half life. CBV quantification is performed by imaging before and soon after contrast agent delivery, rather than by tracking the bolus first pass. While gadolinium is often used clinically, Dunn and colleagues (2004) have utilized monocrystalline iron oxide nanoparticles (MION) to monitor global changes in CBV by ss-CE in rats. MION particles have a maximum sensitivity to blood vessels of 5-8 μm in diameter (T_2 weighted imaging) and 8-12 μm in diameter when using gradient echo sequences for T_2* weighted imaging. This means that small CBV changes in microvasculature can be detected.

1.2.3 Other modalities for cerebral perfusion measurement

Magnetic resonance imaging is not the only neuroimaging modality to provide quantification of CBF and CBV. Brain hemodynamics can be studied in animals and patients using a variety of techniques, each with their own characteristics, which are summarized in Table 2. MRI based techniques provide non-invasive methods of choice for functional neuroimaging because subjects encounter no harmful radiation and can thus be safely imaged many times. This permits long-term, follow up studies in individuals. One should note that CBF may be measured using Doppler techniques and described as ‘cerebral blood flow velocity’ (cm/s) for one hemisphere, whereas data analysis for the non-invasive whole-brain imaging techniques may provide a measure of tissue perfusion (ml of blood flowing per 100 grams of tissue per minute: ml/100g/min). Doppler techniques may therefore be unsuitable for quantifying regional tissue perfusion changes and are often clinically suited to the investigation of blood flow velocity in major vessels.

Table 2. A summary of the characteristics of the common clinical and preclinical methods for cerebral blood flow (CBF) quantification. Note that values are a guide and may vary due to differences in hardware, software, tissue types, subjects, and systems variability between imaging centers. Abbreviations: ASL, arterial spin labeling; DSC, dynamic susceptibility contrast; MRI, magnetic resonance imaging; PCT, perfusion computed tomography; PET, positron emission tomography; SPECT, single photon emission computed tomography; XeCT, xenon-enhanced computed tomography. Sources: Austin et al. 1989, Kessler 2003, Lythgoe et al. 2003, Wintermark et al. 2005, Gallagher et al. 2007.

	Cerebral Blood Flow (CBF) Imaging Modality							
	ASL MRI	**DSC MRI**	**PET**	**SPECT**	**XeCT**	**PCT**	**Doppler**	**Autoradiography**
Subjects	Patients & animals	Patients & animals	Patients & animals	Patients & animals	Patients	Patients	Patients & animals	Animals
Invasive?	No	Minimally (i.v. contrast)	Minimally (i.v. contrast)	Minimally (i.v. contrast)	No	Minimally (i.v. contrast)	No	Yes (non-recovery)
Regional CBF?	Yes	Yes	Yes	Yes	Yes	Yes	No	Yes
Emergency room?	Emerging	Often	Rarely	Rarely	Often	Often	Yes	N/A
Radiation/study	None	None	0.5-2 mSv	3.5-12 mSv	3.5-10 mSv	2-3 mSv	None	N/A
Data acquisition	10 min	1 min	5-10 min	10-15 min	10 min	1 min	10 min	Much (hours)
Data processing	5 min	5 min	5-10 min	5 min	10 min	5 min	None	Much (hours)
Brain coverage	Usually 1 slice (2-10 mm)	Whole (multislice)	Whole	Whole	6 cm	5 cm	Hemispheric	Whole (multislice)
Experimental error	10%	10-15%	5%	10%	12%	10-15%	5%	10%
Spatial resolution	2 mm	2 mm	5-7 mm	10-14 mm	4 mm	2 mm	N/A	15-50 µm
Absolute CBF quantification?	Yes	Normally only relative	Yes	Yes (tracer used)	Yes	Yes	Yes	Yes

1.3 The value of preclinical magnetic resonance imaging and its clinical translation

Traditionally, MRI protocols have been pioneered and developed in experimental, preclinical studies using tissue samples or small animals. This is because the principles of NMR, and the hardware for MRI, are similar between preclinical and clinical settings. This also means that much of the testing and development of new MRI protocols can happen without taking time away from patients in hospitals. Also, hardware similarities mean that MRI innovations can often be readily transferred from the laboratory to the clinic and vice versa.

The translational nature of MRI techniques makes them especially appealing for experimental research because MRI-based preclinical findings can be similarly explored in people, i.e., with the same safe and non-invasive imaging approaches. This is not only of great value for exploring disease pathologies. It is also of paramount importance for therapeutic discovery and development. For example, preclinical MRI is accelerating the search for surrogate markers and biomarkers, which are indirect or direct indicators of normal biological processes, pathogenic processes, or pharmacological responses to a therapeutic intervention (Hayward et al. 2009).

The safety and efficacy of all new medicines must be explored before testing in man, thus follow-up studies by MRI can help assess efficacy and find side effects in the complete physiological setting that animals provide. In this regard, progress in both research and medicine require the development of physiologically relevant animal models of disease, which must closely resemble the pathological features of the clinical condition in order to provide valid comparisons between bench and bedside. Technically, *in vivo* MRI of animals provides more scientific freedom and model reproducibility than can be realistically achieved with patients. This is partly because animal models have been developed to provide a homogenous cohort of subjects for study, tissue for parallel histological studies, and partly because small animal MRI scanners have the higher field strengths which support MRI contrast developments.

As yet, neurobiology researchers are still reliant on the use of animals as there is no replacement for studying the whole brain *in vivo* or for detailed investigation of the systemic physiological responses to drugs over time. One may question the ethical boundaries of such research, although researchers strive to minimize the use of animals

wherever possible. In principle, MRI brings a great opportunity to minimize the number of animals used in biology because performing different scans during one imaging session allows multiple research questions to be asked from just one animal cohort. Also, MRI brings the opportunity for follow-up studies of a single cohort at multiple time points. This requires far fewer animals compared with studies where every research time point needs a new group of animals.

Although the value of small animal MRI is clear, it should be noted that NMR technique development can also be made using chemical 'phantom' samples or *ex vivo* samples. This is because NMR contrasts arise from endogenous molecular interactions, rather than an exogenous source such as the radioactive labels used for nuclear medicine and imaging. This is why NMR developments are often made even before animal studies commence. There are also recent examples where clinical MRI systems have provided 'patient ready' techniques and MRI developments ahead of preclinical systems, such as the advent of 'parallel imaging' to shorten MRI acquisition times or improve image quality.

2 REVIEW OF THE LITERATURE

2.1 Experimental traumatic brain injury

2.1.1 Traumatic brain injury

Traumatic brain injury (TBI) is a major cause of mortality and morbidity worldwide. It is estimated to be responsible for 1.5-2% of deaths and leads to permanent disability in around 2-3% of the developed population (Thurman et al. 1999, Pasco et al. 2007). TBI is the leading cause of death in Westerners under age forty and is therefore considered to be a silent epidemic of the 21st century (Center for Disease Control and Prevention 2003). TBI can be classified as focal or diffuse, whereby the 'impact loading' of external forces leads to localized damage and a predominantly focal injury (Saatman et al. 2008). Diffuse injury tends to arise from rotational forces due to 'inertial loading', which cause the brain to move within the skull and inflict remote damage. However, often both mechanisms can occur together and injuries may or may not penetrate the skull.

Chronically after TBI, the development of epilepsy by epileptogenesis may depend on the type and severity of the injury. Around 15% of all TBI patients develop epilepsy and 80% of those who develop epilepsy within 5 years present seizures within 2 years (Haltiner et al. 1997). As well as the risk of post-traumatic epilepsy, a spectrum of cognitive and functional impairments often results from TBI. The consequences for each patient are dictated by the injury mechanism, the brain regions affected and any confounding factors such as alcohol or drug abuse. All of these factors contribute to the heterogeneity of TBI among patients, which is a major hurdle for their clinical management and for the search for effective treatment interventions (Doppenberg et al. 2004). It is clear that structural plasticity underpins both epileptogenesis and functional recovery and the two progress within the same time scale in patients. Similarly, motor and cognitive recovery processes occur in parallel with epileptogenesis in animal models of TBI (Thompson et al. 2005, Kharatishvili et al. 2006, Pitkänen et al. 2009). However, the recovery extent and timeline vary greatly among subjects (Hammond et al. 2004), which emphasizes the need for researchers and clinicians to identify acute and chronic markers that predict outcomes after TBI. One goal is to help identify individuals that benefit from treatments most, while another goal is to predict the efficacy of neuroprotective treatments of the future.

To better understand the pathology of TBI, it has been classified into primary injury and secondary injury. Primary injury occurs as the result of the mechanical forces acting on the brain. Secondary injury is due to the molecular and physiological processes that progress once triggered by primary injury (Greve and Zink 2009). Secondary injury involves complex interplay between neuronal, glial and vascular factors (DeWitt and Prough 2003, Karhunen et al. 2005, Kharatishvili et al. 2006). Unfortunately, at least twenty-five new pharmaceuticals for secondary injury have failed to prove efficacy in clinical trials (Narayan et al. 2002), even though these innovations were based upon knowledge derived from animal models. It is therefore clear that further investigations of the physiological changes and the mechanisms underlying injury responses are essential to support the continuing search for novel treatments (Ghajar 2009). Thus, experimental traumatic brain injury remains a valuable area of medical research activity.

2.1.2 Magnetic resonance imaging of experimental traumatic brain injury in rodents

Vasogenic brain edema was long accepted as the main type of edema resulting from TBI. However, rodent TBI models such as lateral fluid-percussion injury (LFPI) and controlled cortical impact (CCI) injury have been examined by MRI to reveal that cytotoxic edema is of critical pathological significance first (Unterberg et al. 2004). In fact, cytotoxic edema emerges acutely and may resolve concurrently with sub-acute vasogenic edema, which resolves even later (Immonen et al. 2008, Lescot et al. 2010). The combination of MRI and animal models clearly provides the opportunity to study pathological changes over time in a relatively homogenous subject group.

MRI has also been used to study the temporal progression of hemorrhage after fluid percussion in rats, which has been shown to occur soon after TBI and become resolved by 3 months (Iwamoto et al. 1997). The regions of contusions and hemorrhage were gradually cleared and replaced by cerebrospinal fluid (CSF). Prolonged injury-induced changes in regions remote from the lesion site, such as the thalamus, have also been studied by MRI in animal models of TBI. Remote regions have been shown to undergo sub-acute atrophy and neurodegeneration (Obenaus et al. 2007). We aimed to further charaterise regional acute, sub-acute and chronic hemodynamic and cerebrovascular changes after TBI, thus the literature concerning these topics will now be discussed.

2.1.3 Hemodynamic and cerebrovascular responses to traumatic brain injury

Cerebrovascular changes are crucially involved in the secondary damage processes that occur after TBI because normal brain function and tissue survival require adequate cerebral perfusion, which can be impaired following brain trauma (Golding 2002). By using computed tomography techniques, CBF has been shown to decline in patients acutely (6 hours) after severe traumatic brain injury (Bouma et al. 1991). The degree of this hypoperfusion correlates with motor deficit among survivors. Other studies have observed hypoperfusion in moderate and severely injured patients (Marion et al. 1991, Martin et al. 1997, Kelly et al. 1997) and the degree of TBI-induced CBF impairment can predict the severity of long-term neurological outcomes (Kelly et al. 1997). Although there can be much variability between individual TBI patients (Bonne et

al. 2003), a three phase temporal profile of their cortical CBF variations after moderate and severe injury has become evident. Initial hypoperfusion occurs acutely yet recovers due to reactive hyperemia at 1 to 3 days post TBI, then another hypoperfusion phase may later be observed during days 4-15 (Marion et al. 1991, Bouma et al. 1991, Kelly et al. 1997, Martin et al. 1997).

A clear temporal profile of CBF changes in patients has been established. However, very few studies have investigated the hemodynamic responses to TBI in animal models. Immediately after acceleration induced concussion in rats, brief cortical hyperperfusion was replaced by significant hypoperfusion as soon as 10 min after injury. The perfusion deficit tended to normalize by 40 min post injury, as observed using a ^{14}C-ethanol tracer (Nilsson and Nordstrom 1977). More recent studies often rely on the LFPI model for mixed focal and diffuse TBI in rats (model is comprehensively reviewed in Thompson et al. 2005). After LFPI, a gradual, ipsilateral cortical CBF decline over 1 hour has been recorded using autoradiography (Yuan et al. 1988). With similar methods, others confirmed that CBF throughout the brain was significantly decreased 15 minutes after LFPI. This perfusion deficit gradually normalized in regions distal from the impact site, yet CBF remained impaired in the left parietal cortex near the lesion for up to 2 hours post injury. The extent of CBF disruption correlates with the necrosis observed histologically at the lesion site 4 weeks later (Yamakami and McIntosh 1989, McIntosh et al. 1989).

Initial hypoperfusion in the ipsilateral cortex after TBI has been confirmed by laser Doppler flowmetry during the 1990s (Muir et al. 1992, Bryan et al. 1995, Nilsson et al. 1996, DeWitt et al. 1997). Doppler measurements have been combined with orthogonal spectral polarization (OSP) imaging to measure CBF, vascular diameter and red blood cell velocity over 48 hours after controlled cortical impact (CCI) in rats (Thomale et al. 2002), which is an established method for modeling focal injury to the brain (Dixon et al. 1991). In line with previous reports, pericontusional cortical perfusion was heavily impaired soon after injury (+4 hours) and CBF reduction was due to vasoconstriction (Thomale et al. 2002). Between 24 and 48 hours after TBI, the OSP technique observed hyperemia through vasodilation, coupled with a significant increase in CBF compared to control measures. The extent of hyperperfusion negatively correlated with the penetration depth of the CCI injury, that is, a less severe injury led to greater hyperperfusion from 24 hours after TBI (Thomale et al. 2002). However, it is clear that CBF

and CBV changes beyond the acute and sub-acute phases after TBI require further characterization in rodents.

As discussed, the cerebrovascular responses to TBI affect long-term functional recovery (Kelly et al. 1997, Golding 2002, Xiong et al. 2010) and may also play a role in epileptogenesis (Pitkänen and Lukusiak 2009). However, very few studies have analysed the contribution of long-term vascular changes to functional recovery as well as epileptogenesis after TBI. Studies conducted more than 2 months post-injury using SPECT in patients have reported widespread hypoperfusion in the cortex, thalamus and temporal lobe (Goldenberg et al. 1992, Ichise et al. 1994, Gray et al. 1992, Oder et al. 1992, Prayer et al. 1993, Jacobs et al. 1996, Abdel-Dayem et al. 1998, Umile et al. 2002, Mazzini et al. 2003). Goldenberg and colleagues (1992) reported an association between low thalamic perfusion and poor cognitive outcome, which was possibly related to diffuse axonal injury. Oder and coworkers (1992) showed that reduced CBF in the frontal lobe associates with disinhibited behavior. They also found that reduced thalamic blood flow correlated with the severity of cognitive impairment. In experimental TBI, there is only one prior study of chronic vascular responses (Kochanek et al. 2002). The researchers observed remarkable reduction in cortical and hippocampal CBF at 1 year after controlled cortical impact (CCI) injury in rats. However, no thalamic CBF abnormalities were found and the study lacked both a histological assessment of blood vessel changes and consideration of epileptogenesis. To date, there are no chronic studies in animal models where hemodynamic and cerebrovascular changes have been correlated with functional outcomes.

2.1.4 Magnetic resonance imaging studies of the hemodynamic and cerebrovascular responses to traumatic brain injury

Despite its clinical prognostic value, CBF is not routinely monitored in trauma patients. This may be partly due to the limited spatial resolution of Doppler based techniques (Table 2) or the x-ray/contrast agent dosage concerns associated with repeated perfusion CT scans (Mulvey et al. 2004). We therefore need to bring safe, non-invasive and thus repeatable CBF measurement techniques to the clinic. As discussed, MRI has the potential to fill the clinical and experimental need for safely repeatable hemodynamic measurements after TBI. The MRI techniques for quantification of CBF and CBV described earlier have begun to be used to investigate the cerebrovascular consequences of TBI (Pasco et

al. 2007, Shen et al. 2007, Kochanek et al. 2002). Hypoperfusion in both the ipsilateral and contralateral cortex up to 5 hours after LFPI in rats was shown by DSC MRI (Pasco et al. 2007), and ipsilateral hypoperfusion was more pronounced than that contralaterally. CBV was unchanged contralaterally but ipsilateral cortical CBV was significantly decreased in a manner similar to CBF. Normalization of these hemodynamic changes was observed by day 3 (Pasco et al. 2007).

Susceptibility weighted imaging (SWI) of TBI rats has been used to measure blood oxygenation changes attributed to CBF in the injured cortex after injury (Shen et al. 2007). CBF was reduced by 26% in the major veins and 28% in the dorsal medial cortex, 4 hours after injury. However, the subsequent recovery from injury was mixed between animals, with only half showing CBF recovery by 48 hours (Shen et al. 2007). SWI CBF measurements were validated using arterial spin labeling (ASL), which provides a more accurate measure of any relative hemodynamic changes derived from SWI.

Pericontusional hypoperfusion is seen in patients and animals acutely after TBI. Yet we understand that hemodynamic adaptations then occur days and even months later in patients. However, post-acute changes in animal models are not well described. Chronically, only the aforementioned CBF study 1 year after CCI in rats (Kochanek et al. 2002) used ASL MRI to find long-term cortical and hippocampal hypoperfusion. If researchers are to continue relying on experimental TBI to model secondary damage, and to test potential new medicines, we can use MRI to test the hypothesis that post-acute hemodynamic adaptations after TBI in rodents match those seen in patients.

2.2 Ischemic stroke and experimental focal ischemia

2.2.1 Ischemic stroke

Stroke creates a major international healthcare burden. Stroke is the second most common cause of death worldwide (Donnan et al. 2008) and a leading cause of adult onset disability in developed countries (Thom et al. 2006). The disease impact is likely to increase over time as the Western population ages. The disease can be classified as hemorrhagic or ischemic in reference to an etiology of blood vessel rupture or blood vessel blockage, respectively. Ischemic stroke is the most common type and it is responsible for around 73% of new strokes

in patients (Thrift et al. 2001). Once vessel blockage occurs, perhaps due to a thrombosis or embolism, the immediate territory nearby suffers a reduced oxygen supply and is said to be ischemic.

Researchers in the 1950s (Opitz and Schneider 1950) were the first to highlight the fact that impaired cerebral energy production results from a loss of oxygen supply to the brain parenchyma. Under mild hypoxia, the functional activity of the brain is impaired first. With greater or prolonged hypoxia, metabolic activity then becomes suppressed enough for cells within the ischemic core to lose their structural integrity, leading to infarction (cell death) by anoxic depolarization. In 1977, CBF measurements after focal ischemia in rats helped to define the two hypoxia thresholds; one that governs cellular functional integrity and another that governs structural integrity (Symon et al. 1977). This led to the revelation that neuronal evoked potentials become disturbed during a 40% reduction in blood flow but ion gradients across cell membranes, which are indicative of cell viability, are maintained even during an 80% reduction in CBF. With focal ischemia, the two thresholds translate to an ischemic core surrounded by an ischemic penumbra. The ischemic penumbra lies between the infarcted core tissue and healthy, unaffected brain tissue. The penumbra therefore comprises potentially salvageable regions (Hossmann 2006) that are functionally silent but structurally sound. In the 1990s, research efforts focused on understanding the mechanisms responsible for neuronal and glial death after stroke, elucidating excitotoxicity, oxidative stress and molecular mediators of necrosis and apoptosis (reviewed in Hertz 2008). Next came the application of neuroimaging to investigate the ischemic penumbra and stroke recovery processes in animals models and patients, for which MRI has become a great asset.

2.2.2 Magnetic resonance imaging development for clinical and experimental ischemia

The use of MRI for stroke assessment has rapidly gained momentum over the last twenty years. Before the advent of modern neuroimaging, many stroke patients may have only received conservative treatment upon arrival at the hospital. During the 1990s, MRI was proven to help evaluate the sub-acute pathophysiology of ischemic stroke. Specifically, during the first 12-24 hours after stroke onset, MRI was found to be more sensitive than CT for detecting lesions and conventional MRI techniques were beginning to be routinely used to measure the location and extent of an infarct. The clinical techniques were mostly structural

and included T_1, T_2 and proton density weighted imaging (Wintermark et al. 2005). MR angiography soon became used to study the vascular integrity of the intracranial and extracranial vasculature after stroke (Warach et al. 1992). However, it was first thought that structural MRI methods alone were unsuitable for evaluating stroke acutely, within the first few hours of onset.

Experimental studies over the 1990s helped reveal the clinical potential of structural imaging, diffusion weighted imaging (DWI) and perfusion weighted imaging (PWI) for acute stroke (thoroughly reviewed in Baird and Warach 1998). For example, Gröhn and coworkers discovered that irreversible acute tissue damage after focal ischemia in rats can be detected by an irreversible decrease in T_2 (Gröhn et al. 1998). Later, Calamante and colleagues (1999) showed that multimodal high-field (8.5 T) MRI could provide detailed pathological explanations for how the ischemic lesion develops acutely after focal ischemia in rats. The researchers monitored tissue T_1, T_2, diffusion and CBF in and around the ischemic lesion during the first six hours after permanent middle cerebral artery occlusion (MCAO). Two functional MRI findings were reported. First, a decrease in T_2 and an increase in T_1 both occurred within the first few minutes of ischemia. The swift early decrease in T_2 was thought to be associated with an increase in deoxyhemoglobin, while the early T_1 increase was attributed to many factors including flow effects, alterations in tissue oxygenation, and changes in the water environment. Such insights helped lead to the implementation of MRI for the management of acute ischemic stroke patients. Yet perhaps more importantly, the combination of perfusion imaging and diffusion imaging provided distinction between a ‘moderately affected area’ with reduced perfusion but normal diffusion, and a ‘severely affected area’ in which both perfusion and diffusion are significantly reduced (Moseley et al. 1991). Today, this diffusion-perfusion mismatch can be measured by PWI and DWI MRI techniques in order to identify the ischemic penumbra acutely.

As described, the ischemic penumbra is structurally sound and thus its functional capacity can potentially be rescued by the early restoration of blood flow. If no reperfusion occurs, the penumbra will progress to infarction (Hacke et al. 2008). An emergency CT scan helps select patients suitable for acute thrombolysis by recombinant tissue plasminogen activator (rtPA), then MRI can also be used to follow the penumbral response to reperfusion (Olivot and Marks 2010). Thus, it is clear that preclinical and clinical stroke MRI have become very important for both primary stroke research and for stroke therapy development.

2.2.3 Hemodynamic and cerebrovascular responses to ischemic stroke

By definition, cerebral ischemia requires at least a local 50% decrease in CBF before any hypoxia response can be detected. Subsequently, very low levels of CBF such as 10-20 ml/100g/min lead to impairment of cortical electrical function and then cell death by infarction (Lassen 1977). Infarct regions may not recover after stroke, but the restoration of a healthy blood supply is essential for the recovery of peri-infarct regions as discussed. Much research has focused on the study of peri-infarct hemodynamic and cerebrovascular disruption after ischemia acutely. These responses will depend on the success of reperfusion and whether ischemia is complete or incomplete, focal or global, and transient or permanent (Kulik et al. 2008). The ischemic location will also affect the brain's response (Ginsberg et al. 1976; Dijkhuizen et al. 1998).

The acute cerebrovascular and hemodynamic consequences in peri-infarct regions have been thoroughly reviewed previously (del Zoppo and Mabuchi 2003, Kulik et al. 2008). Due to the lack of oxygen, inflammation in the endothelial cell wall results in leukocyte adhesion and cytotoxic edema (Amantea et al. 2009). The inflammatory response of leukocyte adhesion also promotes the breakdown of the blood-brain barrier (BBB) and subsequent vasogenic edema. This happens first in the venules and later in larger vessels (Kulik et al. 2008). Breakdown of the BBB allows entry of inflammatory cytokines that promote secondary damage in the brain parenchyma (Nagahiro et al. 1998). Excessive edema results in increased intracranial pressure that can invoke prolonged vasoconstriction and secondary blood flow reduction in nearby capillaries (Hossmann 2006). As well as the initial ischemic injury, reperfusion that occurs afterwards can trigger a similar series of destructive events in the brain, also known as 'reperfusion injury'. As blood returns to the hypoxic vasculature, oxidative stress is induced in the endothelium, which promotes further leukocyte adhesion, platelet activation, and downstream intravascular obstruction due to blood coagulation (del Zoppo and Mabuchi 2003). The focal hemodynamic consequence may be 'no-reflow' in peri-infarct regions. This, combined with edema-induced vasoconstriction, means that secondary hypoperfusion after ischemia is likely to be prolonged.

Although the early cerebrovascular and hemodynamic responses to ischemia are becoming well characterized, clinicians are less sure of such responses in the chronic phase. Chronic perfusion abnormalities play a long-term role in stroke recovery and may even increase the risk of dementia (del la Torre 2006). A greater knowledge of how the

cerebral blood supply adapts weeks after ischemic injury may aid our understanding of brain recovery processes (Pantano et al. 2008). Rodent models of focal ischemia provide the opportunity to study secondary brain damage after stroke (reviewed in Carmichael 2005). Most rodent studies of post-ischemia hemodynamics focus on the acute period, thus comparatively few studies have looked beyond the first 3 days after injury. However, a prolonged reduction in cerebral blood flow (CBF) after permanent MCAO has been shown by autoradiography in rats (Bolander et al. 1989). Specifically, CBF in the ipsilateral caudate putamen and peri-infarct cortex was decreased up to 7 days when compared to contralateral CBF. This hypoperfusion resolved by 28 days after ischemia, which may be due to the establishment of collateral blood supply.

More recently, laser Doppler flowmetry has been used to measure the long-term hemodynamic response to ischemia in rats and mice (Ulrich et al. 1998, Borlongan et al. 2004, Eve et al. 2009, Li et al. 2007). Ulrich and colleagues noted some recovery of cortical CBF over six weeks although it still remained decreased compared to controls at the end of this period (Ulrich et al. 1998). In a similar permanent MCAO model, Eve and colleagues (2009) noted that ipsilateral cortical CBF did not normalize to basal measures even by 10 weeks after MCAO. Prolonged cortical hypoperfusion has also been shown to prevail for at least 21 days after permanent MCAO in mice (Li et al. 2007). Even after transient MCAO, Doppler measures in striatal penumbra regions showed prolonged hypoperfusion for 2 weeks in rats (Borlongan et al. 2004). As already discussed, long-term follow up studies of hemodynamic changes in animal models can benefit from MRI techniques because the same rats can be investigated consecutively. For this aim, the chronic hemodynamic responses to focal ischemia have begun to become characterized by MRI.

2.2.4 Magnetic resonance imaging studies of the long-term hemodynamic and cerebrovascular response to focal ischemia in rodents

Long-term hemodynamic studies of focal ischemia in rats have also employed MRI techniques to measure perfusion, including dynamic susceptibility contrast (DSC) (Rudin et al. 2001, Lin et al. 2002) and arterial spin labeling (ASL) (Jiang et al. 1998). Both techniques have been evaluated and validated in rodent models of ischemia (Bratane et al. 2010). After permanent MCAO in rats, DSC showed that

hypoperfusion prevails for at least 3 days in the ipsilateral striatum (Rudin et al. 2001) and may continue for 14 days in the ipsilateral cortex (Lin et al. 2002). After transient MCAO in rats, ASL was used to follow CBF over 7 days in the ischemic striatum, where acute hypoperfusion normalized by 3 hours after reperfusion (Jiang et al. 1998).

These few prior MRI studies of long-term CBF fluctuations after MCAO only focus on the brain's striatal and cortical regions. However, as different brain regions respond differently to ischemia (Ginsberg et al. 1976, Dijkhuizen et al. 1998, Block et al. 2005, Lin et al. 2008), there is a need to investigate regional CBF variations because stroke severity and stroke recovery depend on the ischemia location. ASL MRI provides absolute regional quantification of blood flow with sufficient resolution to discern small substructures in the rat brain. ASL also provides the promising opportunity to make detailed regional CBF measurements non-invasively. Of note, the majority of the hemodynamic findings described here arose from permanent MCAO models. The ischemia severity and the brain's response are known to be different after transient MCAO in rats (Hossmann 2009, Bratane et al. 2010), thus further hemodynamic and cerebrovascular research after transient MCAO is necessary to further understand the chronic regional pathology of transient ischemic stroke.

2.3 Status epilepticus and experimental epilepsy

2.3.1 Epilepsy and status epilepticus

Around 0.8% of the global population has epilepsy, which is the second most common neurological disorder after stroke (Porter 1993). Rather than a single disorder, epilepsy is a syndrome with varying etiologies, characterized by spontaneous recurrent seizures due to uncontrolled electrical activity in the brain (Fisher et al. 2005). In around 30% of epilepsy patients, there is an identifiable precursor that invokes an injury to the brain that triggers epilepsy development through epileptogenesis (symptomatic epilepsies) (Hauser 1997). Conversely, 30% of patients have 'presumed symptomatic epilepsy' (previously known as 'cryptogenic epilepsy') in which a brain pathology is presumed to cause epilepsy but it has not been identified using current neuroimaging and neurophysiological recording techniques (Engel 2006).

As discussed earlier, TBI can be a trigger for epileptogenesis, which is the period when many neurobiological events take place and subsequently lead to the appearance of spontaneous recurrent seizures. Other triggers for epileptogenesis may include a stroke, tumor, cortical dysplasia and status epilepticus (SE), which is a condition defined as the existence of a prolonged seizure or a series of seizures during which the patient does not completely recover consciousness (Dupont and Crespel 2009). The duration of clinical SE is under debate, although the traditional viewpoint defines SE with a duration of 30 minutes or more. Although SE is a relatively rare cause of epilepsy in adults and often occurs together with other insults, such as TBI and stroke (Pitkänen and Lukasiuk 2009), the induction of SE in rodents by pilocarpine, kainate or electrical stimulation has allowed researchers to investigate the temporal profile of molecular and cellular alterations during the epileptogenic process (Pitkänen et al. 2007).

2.3.2 Magnetic resonance imaging studies of the hemodynamic and cerebrovascular responses to epileptogenesis

Structural MRI has been of great benefit for epileptogenesis studies in animals because non-invasive imaging allows researchers to visualize and measure ongoing neurobiological processes, through follow-up studies (reviewed in Grohn and Pitkänen 2007, Hayward et al. 2009). However, very few studies have considered using functional imaging to investigate the cerebrovascular consequences of SE, or to follow cerebrovascular activity during epileptogenesis. Fabene and co-workers (2003) performed DSC MRI 12 hours after pilocarpine induced SE in rats and found that hyperperfusion continues in the post-ictal phase. Later in epileptogenesis, ASL MRI has provided emerging evidence that hyperperfusion may be prolonged in the hippocampus for up to 7 days (Choy et al. 2010) or even 2 weeks (Ndode-Ekane et al. 2010) after pilocarpine-induced SE in rats. This seems surprising because prior neuroimaging studies report globally decreased glucose metabolism during epileptogenesis in the same model (Guo et al. 2009, Goffin et al. 2009). It is therefore plausible that prolonged hyperperfusion could serve as a marker for vascular reorganization (Marcon et al. 2009, Ndode-Ekane et al. 2010), rather than increased metabolic activity. However, further characterization of hemodynamic and vascular changes in relation to other hallmarks of the epileptogenic process are necessary to validate this claim.

3 HYPOTHESES AND AIMS

The studies within this thesis aimed to investigate the cerebrovascular pathology of traumatic brain injury, cerebral ischemia and status epilepticus in rat models of each disease. Whereas prior animal studies typically focus on the acute phases of these conditions, the present work used MRI to sequentially study sub-acute and chronic changes in cerebral hemodynamics. All MRI studies were supported with immunohistochemistry to investigate processes linked to vascular reorganization, such as angiogenesis, which may underlie any hemodynamic alterations in each disease model.

The specific hypotheses and aims for each study were as follows:

I. We hypothesized that post-acute hemodynamic responses to TBI in rodents match those of patients. This study aimed to quantify absolute regional CBF and relative regional CBV by MRI over 14 days after LFPI. In addition, we aimed to measure the corresponding regional blood vessel density changes in order to evaluate the contribution of vascular changes to any CBF and CBV disruption after TBI.

II. We hypothesized that neurovascularization has an important role in long-term, chronic, functional recovery after TBI in rats. We aimed to assess motor and cognitive recovery, seizure susceptibility, regional CBF, and eventually blood vessel density over 9 months after LFPI.

III. We hypothesized that long term hemodynamic and cerebrovascular changes occur in the thalamus of rats after transient focal cerebral ischemia, and these associate with ongoing neurodegenerative processes. We aimed to quantify thalamic CBF at baseline and sequentially over 3 months after cerebral ischemia. In the same animals, we aimed to correlate thalamic blood flow with sensorimotor recovery and angiogenesis during the follow-up.

IV. Knowing that the amygdala is often damaged after status epilepticus and can serve as a seizure focus in epilepsy patients (Pitkänen et al. 1998), it is surprising that no prior imaging studies

of epileptogenesis have considered amygdaloid vascular changes beyond the first day after SE. We therefore hypothesized that tissue reorganization in the rat amygdaloid complex includes hemodynamic changes and vascular reorganization after SE. We aimed to quantify CBF and CBV changes in the amygdala and cerebral cortex over 2 weeks after pilocarpine-induced SE in rats, which is when rats are undergoing epileptogenesis. We aimed to measure vascular density changes in the amygdala at the end of the study by immunohistochemistry.

4 MATERIALS AND METHODS

4.1 Animal models

Animal models of neurodegenerative diseases are essential for researching neuropathological mechanisms and also for trialing the latest therapies preclinically. Both tasks require the complete physiological setting of whole animal investigations. For MRI studies, animals provide a relatively homogenous subject group that can be studied repeatedly over many time points. Animals also provide the opportunity for histological validation of MRI findings. All studies in this thesis used either adult male Sprague Dawley (**I**, **II**, **IV**) or Wistar rats (**III**) (Harlan Netherlands B.V., Horst, Netherlands). All efforts were made to minimise the number of rats and their suffering, and to maximise the volume of appropriate data acquired from each rat. Rats were housed individually under controlled conditions (12 h light/dark cycle, temperature 22±1 °C, humidity 50-60%, *ad libitum* access to food and water). All animal procedures were approved by the Animal Ethics Committee of the Provincial Government of Southern Finland (ESLH-2009-07538/Ym-23), and conducted in accordance with the guidelines set by the European Community Council Directives 86/609/EEC.

*4.1.1 Lateral fluid-percussion induced traumatic brain injury (**I**, **II**)*

Traumatic brain injury was induced by lateral fluid-percussion injury (LFPI). The LFPI models mixed focal and diffuse brain injury that resembles mixed-type non-penetrating head injury in patients (Thompson et al. 2005). LFPI was conducted as described previously

(Kharatishvili et al. 2006, McIntosh et al. 1989). Briefly, rats were anesthetized by an injection cocktail (6 ml/kg, i.p.) containing sodium pentobarbital (58 mg/kg), chloral hydrate (60 mg/kg), magnesium sulfate (127.2 mg/kg), propylene glycol (42.8%), and absolute ethanol (11.6%). A 5 mm diameter hole was drilled between the bregma and lambda on the left convexity (anterior edge 2.0 mm posterior to the bregma; lateral edge adjacent to the left lateral ridge). Severe LFPI was induced by a transient (21-23 ms) fluid pulse impact against the exposed dura by using a fluid-percussion device (AmScien Instruments, Richmond, VA, USA). The impact pressure was measured by an extracranial transducer and controlled to a pressure of 3.2-3.4 atmospheres. After impact, the dura was checked to ensure it had remained intact. Sham operated control animals received all surgical procedures except the fluid-percussion impact. Animals that did not survive the first 72 hours after injury were pre-determined to be excluded from the study (Pitkänen and McIntosh 2006).

*4.1.2 Focal ischemia by transient middle cerebral artery occlusion (**III**)*

Transient middle cerebral artery occlusion (MCAO) was used to subject rats to focal ischemia. This is a well established model for ischemic stroke (Laing et al. 1993, Braeuninger and Kleinschnitz 2009). MCAO was made using the intraluminal filament technique (Longa et al. 1989). Anesthesia was induced in a chamber using 5% isoflurane in 30% O_2/70% N_2O. A surgical depth of anesthesia was maintained throughout the operation with 0.5 to 1% isoflurane delivered through a nose cone. To occlude blood flow to the right middle cerebral artery (MCA) territory, a heparinized nylon filament (∅ 0.25 mm, rounded tip) was advanced 1.9 to 2.1 cm into the internal common carotid artery until resistance was felt. The filament was held in place by tightening a suture around the internal common carotid artery and placing a microvascular clip around the artery. Body temperature was monitored and maintained at 37ºC using a heating pad connected to a rectal probe. After 90 min of MCAO, the filament was removed and the external carotid artery was permanently closed by electrocoagulation. To relieve postoperative pain**,** rats were treated with 0.03 mg/kg of buprenorfin (i.p.). In addition, postoperative care of MCAO rats included supplemental 0.9% NaCl (i.p.) and softened food pellets to prevent weight loss.

*4.1.3 Pilocarpine induced status epilepticus (**IV**)*

Pilocarpine is a muscarinic receptor agonist that, with correct dosage, can induce status epilepticus (SE) in rats. In this study, rats first received a subcutaneous injection of scopolamine (1 mg/kg; # S-8502, Sigma-Aldrich, Helsinki, Finland) to counteract the adverse effects of pilocarpine on the peripheral nervous system. Thirty minutes later, SE was triggered by intraperitoneal administration of pilocarpine (320 mg/kg, #P-6503, Sigma-Aldrich, Helsinki, Finland). The development and severity of generalized SE were monitored visually and the behavioral severity of the seizures during SE was scored according to the Racine scale (Racine 1972). Next, intraperitoneal diazepam (20 mg/kg, Stesolid Novum, Dumex-Alpharma, Antwerp, Belgium) was administered 120 min after the induction of SE in order to reduce mortality among the group. For this study, nine rats were injected with pilocarpine and five control rats received 0.9% NaCl instead of pilocarpine.

4.2 Magnetic resonance imaging

MRI was performed for all studies in this thesis using a 4.7 T magnet (Magnex, Oxford, UK) interfaced with a Varian Inova console (Varian Inc., Palo Alto, CA, USA) with an actively decoupled linear volume transmission coil (length = 80 mm) and quadrature surface receiver coil pair (Rapid Biomedical, Columbus, OH, USA), which provided imaging coverage of the whole brain.

4.2.1 Anesthesia

An isoflurane based anesthesia protocol was used for all MRI procedures. Rats were anesthetized under isoflurane in a carrier gas mixture of either 70% N_2O (**I**, **III**) or N_2 (**II**, **IV**) with 30% O_2. Rats were secured in a purpose built holder (Rapid Biomedical, Columbus, OH, USA) using ear bars and a bite bar, while anesthesia was delivered through a nose cone. Breath rate was continually measured throughout imaging via a pressure probe between the rat and the holder. The breathing rate was kept between 62 and 68 breaths per minute by adjusting the anesthesia concentration to 0.7-1.7%. The holder was electronically heated to sustain a temperature of 37 °C throughout imaging.

4.2.2 Anatomical imaging

Anatomical images were made in all studies to allow regions of interest to be drawn and structural abnormalities to be investigated. All studies utilized T_2 weighted images, which were acquired using a spin echo sequence whereby the time to echo = 70 ms, repetition time = 2500 ms, and field of view = 4 x 4 cm covered with 128 x 256 points. Datasets comprised of 15 stacked slices (thickness = 1 mm each). The center of the stack was positioned at -3.6 mm (**I**, **II**, **IV**) or -3.2 mm (**III**) from the bregma with the help of axial pilot images and with the aid of a rat brain atlas (Paxinos and Watson 1998). The estimated slice positioning error between repeated scans is <50% of the slice thickness. The total anatomical imaging time was 10.5 minutes for each rat.

T_1 relaxation changes were measured in all rats studied at 8 months after TBI (**II**). Images providing data for T_1 map calculations were made using a single coronal slice, inversion recovery fast spin echo sequence where the repetition time = 4 s, echo spacing = 13 ms, 4-8 echoes/excitation, field of view = 2.56 x 2.56 cm with 128 x 256 points, slice thickness 0.75 mm and incremented inversion times of 10, 400, 1000, and 1600 ms. The single T_1 map slice was at the same position as the central T_2 weighted imaging slice. T_1 weighted 3D images were also collected using a gradient echo sequence (time to echo = 2.7 ms, repetition time = 1200 ms). A volume of 3.5 x 3.5 x 2.5 cm^3 was covered with 270 x 270 x 193 points, resulting in 0.13 mm coronal slice thickness, with 2 averages per phase encoding step.

4.2.3 Cerebral blood flow

For all studies, absolute CBF was quantified in one coronal slice using continuous arterial spin labeling as described previously (Williams et al. 1992), with a fast spin echo read out with a field of view = 4 x 4 cm, 128 x 128 points, slice thickness = 2 mm, repetition time = 6 s, echo spacing = 7 ms, and number of echoes = 16. The duration and amplitude of the square labeling pulse causing flow driven adiabatic inversion were 3 s and 0.1 G, respectively, with a post labeling delay of 800 ms. The labeling pulse was positioned on the neck 2 cm from the imaging slice and the control image was acquired with an identical radiofrequency pulse positioned symmetrically opposite the imaging slice. Subtraction images from six pairs of label and control images were averaged, and used to provide a CBF map from one hippocampal slice, which was equivalent to the center of the T_2 weighted image stack.

As CBF measured by ASL is influenced by T_1 variations in tissue, T_1 was mapped in the same coronal slice as CBF using an inversion recovery fast spin echo sequence (**I**, **III**, **IV**) (repetition time = 4 s, echo spacing = 13 ms, 4-8 echoes/excitation, field of view = 4 x 4 cm with 64 x 64 points, slice thickness = 2 mm, incremented inversion times = 5, 300, 600, 1000, and 1500 ms). The total ASL imaging time was 25 minutes for each rat. For study **II**, the anatomical T_1 maps were used for CBF calculations.

4.2.4 Cerebral blood volume

Cerebral blood volume (**I**, **IV**) was studied in the same regions as CBF through an intravenous contrast agent approach. Prior to imaging, one catheter was inserted into the femoral vein for contrast agent delivery, and another into the femoral artery for blood sampling and subsequent blood testing. The first blood sample was taken approximately halfway through imaging before contrast agent administration. The second blood sample was made around 45 minutes later, once post contrast imaging was completed. Samples were analyzed immediately for pH, pO_2, pCO_2 and O_2 saturation percentage.

After CBF and anatomical T_2 weighted imaging, a bolus of Sinerem monocrystalline iron oxide nanoparticles (MION) contrast agent (6 mg/kg rat mass, Geurbet, Villepinte, France) was administered intravenously. Although this is iron oxide based, the contrast agent induces local magnetic field variations in the blood stream, much as described for gadolinium agents in section *1.2.2*. Three minutes later, the T_2 weighted imaging was repeated, allowing ΔR_2 to be calculated for each dataset ($R_2 = 1/T_2$) and ΔR_2 to be mapped or all slices. ΔR_2 was assumed to be directly proportional to CBV as described (Boxerman et al. 1995, Dunn et al. 2004).

4.2.5 MRI data analyses

All analytical tools were provided by our in-house software (Aedes, http://aedes.uku.fi/, Kuopio, Finland) written in Matlab 7.1 (MathWorks, Natick, MA, USA). The outlines of regions of interest (ROIs) were defined according to the rat brain atlas of (Paxinos and Watson 1998). Then ROIs were drawn manually on the anatomical T_2 weighted images

from each imaging session and copied to the T_1, CBF, and CBV maps in Aedes.

T_1 maps were calculated from the inversion recovery MRI data using a standard two-parameter fitting, and then used for CBF calculation (Barbier et al. 2001). ROI based analyses of CBF and CBV maps provided the quantitative CBF and CBV data, respectively. Coupling between CBF and CBV was investigated by testing the relationship $CBV = 0.5 \times CBF^{0.5}$ in a regional manner (van Zijl et al. 1998) (**I**).

4.3 Behaviorology

Behavioral testing was performed in the chronic studies in order to evaluate the rats' functional recovery to TBI (**II**) and focal ischemia (**III**) over the long-term study periods.

4.3.1 Composite neuroscore after traumatic brain injury

Neurological motor function was assessed through a variety of motor function tasks to provide a composite neuroscore at 2 days, 7 days, 2 weeks, 1 month, 2 months, 4 months and 6 months after TBI or sham-operation (**II**). The composite neuroscore included left and right forelimb flexion tests, left and right hindlimb flexion tests, left and right lateral propulsion tests and an angle board stability test. The approaches that comprise our composite neuroscore have been described in detail previously (Zhang et al. 2005, McIntosh et al. 1987, 1989).

4.3.2 Morris water maze after traumatic brain injury

The hippocampus-dependent learning and memory abilities as well as the motor skills of all rats were assessed using the Morris water maze at 7 months after TBI (**II**). The testing protocol was adapted from that described by Karhunen et al. 2003. Briefly, testing took place in a black pool of water (150 cm diameter, water at 20±2 °C) surrounded by visual cues to allow the rats to orientate themselves. The pool was divided into four quadrants. A platform (10 cm x 10 cm) was located 1.5 cm below the water surface in the middle of the northeast quadrant. Each swim was recorded using a video camera positioned above the pool and

connected to a computerized image analysis system (HVS image, Imaging Research Inc., St. Catherine's, Canada). Four parameters were measured: (a) latency to the platform (maximum 60 s), (b) length of the swimming path during the trial (cm), (c) mean swimming speed (cm/s), and (d) percent total time spent in each of the four quadrants of the pool. Latency and path length were used to assess achievement in the water-maze task. Swimming speed (path length/escape latency) was used for motor activity assessment in this task. The rats were tested on two consecutive days (5 trials per day). The swimming start position was altered for each trial. If a rat failed to find the platform within 60 s, it was manually guided to its target. After each trial, the rat was allowed to remain on the platform for 10 s. Thereafter, it rested in the cage for 30 s (after trials 1, 2, and 4) or 1 min (after trials 3 and 5). On a third testing day, a probe trial was performed without the platform to assess the rat's aptitude for memorizing the location of the platform (Karhunen et al. 2003).

4.3.3 Behavioral outcome measures after focal ischemia

The behavioral tests for study **III** were employed to detect long-term impairment in sensorimotor functions due to focal ischemia. The rats were tested before operation and on postoperative days 7, 14, 21, 30 and at 3 months.

Sensorimotor functions of hindlimbs were tested using a tapered/ledged beam (Zhao et al. 2005). The rats were pretrained for 3 days to traverse the beam before ischemia induction. The beam-walking apparatus consists of a tapered beam with underhanging ledges on each side to permit foot faults without falling. The end of the beam is connected to a black box (20.5 x 25 x 25 cm) with a platform at the starting point. A bright light is placed above the start point to motivate the rats to traverse the beam. Each rat's performance was videotaped and later analyzed by calculating the slip ratio for the impaired (contralateral to lesion) forelimb and hindlimb. The more slips indicates a greater degree of impairment. Steps onto the ledge were scored as a full slip and a half slip was given if the limb touched the side of the beam (slip ratio % = [(number of full slips + 0.5 *x* number of half slips)/(number of total steps)] *x* 100). The mean of three trials was used for the statistical analysis.

A cylinder test was used to assess imbalances between the impaired and non-impaired forelimb use (Karhunen et al. 2003). For the

test, the rat was placed in a transparent cylinder (ø 20 cm) and videotaped during the light part of the light/dark cycle. A mirror was placed at a 45º angle beneath the cylinder so that behavior could be filmed from below the cylinder. Exploratory activity for 1 to 3 minutes was analyzed by using a video recorder with slow motion capabilities. The number of contacts by both forelimbs and by either the impaired or unimpaired forelimb was counted. A cylinder score for impaired forelimb was calculated as: [(impaired forelimb)/(total contacts)] *x* 100%.

4.4 Chronic seizure susceptibility after traumatic brain injury

4.4.1 Video-electroencephalography (EEG) recording

To detect the possible development of spontaneous seizures after TBI, continuous video-electroencephalography (EEG) monitoring for all rats was performed for 2 weeks after all MRI had been completed (**II**). Electrode implantation was performed according to the methods described previously (Immonen et al. 2008). In brief, rats were anesthetized by a single i.p. Injection (6 ml/kg) of a mixture containing sodium pentobarbital (58 mg/kg), chloral hydrate (60 mg/kg), magnesium sulfate (127.2 mg/kg), propylene glycol (42.8%), and absolute ethanol (11.6%). The head of the rat was secured in a stereotaxic apparatus (lambda and bregma on the same horizontal level) and the skull exposed by a midline skin incision. Two cortical screw electrodes (E363/20 Plastics One Inc., Roanoke, VA, USA) were placed over the parietal cortex, one rostral to the injury site and the other contralateral to the center of the craniotomy. Two additional screw electrodes were inserted into the skull over the cerebellum bilaterally (10.3 mm caudal to the bregma, 2 mm lateral to the midline) and served as ground and indifferent electrodes. All electrode pins were inserted into the plastic pedestal and the entire assembly was cemented to the calvarium with dental acrylic.

The long-term video-EEG monitoring was performed as described previously (Nissinen et al. 2000). Briefly, electrical brain activity from the motor cortex was monitored with the Nervus EEG Recording System connected to a Nervus magnus 32/8 amplifier (Taugagreining, Iceland), and filtered with high-pass 0.3 Hz and low-pass 100 Hz cutoff. The behavior of the animals was recorded using the WV-BP330/GE video camera (Panasonic, Tokyo, Japan) that was positioned above the cages and connected to a SVT-N72P time lapse VCR and a PVM-145E video

monitor (Sony, Tokyo, Japan) to allow simultaneous videotaping of 8 animals.

4.4.2 Pentylenetetrazol test

To investigate whether TBI led to a reduced seizure threshold in rats, we administered a single dose of pentylenetetrazol (1,5-pentamethylenetetrazole, 98%, Sigma-Aldrich, Helsinki, Finland) (PTZ) 9 months after injury or sham-operation (**II**). Rats were followed by video-EEG (see previously) for 60 min after the PTZ dose (25 mg/kg). Analysis of the video-EEG data was performed according to the protocols established previously (Kharatishvili et al. 2006). In summary, each electrographic seizure was defined as a 45 s duration high-amplitude rhythmic discharge with clear onset, temporal evolution in wave morphology and amplitude, and offset. An electrographic interictal epileptiform discharge (ED) was defined as a high-amplitude rhythmic discharge containing a burst of slow waves, spike-wave and/or polyspike-wave components and lasting at least 55 s. A spike corresponded to a high amplitude (twice baseline), sharply contoured waveform with a duration of 20-70 ms. Latency to the first spike, total number of spikes and total number of epileptiform discharges were calculated during 60 min after PTZ administration.

4.5 Histological approaches

4.5.1 Tissue fixation and processing

Rats from all studies were transcardially perfused for histology in order to provide histological investigations of brain tissue that might complement our MRI findings. For studies **I**, **III** and **IV**, perfusion was made according to a paraformaldehyde fixation protocol described previously (Kharatishvili et al. 2007). Rats from study **II** were transcardially perfused according to the Timm fixation protocol (Sloviter 1982). The brains were postfixed in 4% paraformaldehyde for 4 h and then cryoprotected for 24 h in a solution containing 20% glycerol in 0.02 M (0.01 M, **III**) potassium phosphate buffered saline (KPBS, pH 7.4), frozen on dry ice, and stored at -70 °C. The frozen sections were cut in the coronal plane with a sliding microtome (thickness of 30 µm, 1-in-5 series) and stored in tissue collecting solution (30% ethylene glycol, 25% glycerol in 0.05 M sodium phosphate buffer) at -20 °C.

4.5.2 Nissl staining

In all studies, one series of sections for each brain was stained for thionin in order to identify the cytoarchitectonic borders of regions of interest, and to visually assess neuronal damage and gliosis in sections corresponding to the MRI slice.

4.5.3 RECA-1 immunohistochemistry after traumatic brain injury or status epilepticus

To assess the distribution and carry out quantitative analysis of vascular changes in the animal models of TBI (**I**, **II**) and SE (**IV**), one series of free-floating sections (1-in-5, 150 μm apart from each other) was stained with an antibody raised against rat endothelial cell antigen-1 (rat anti-RECA-1, 1:5000; #MCA970R, Serotec, Oslo, Norway). RECA-1 is a cell surface antigen specific for rat endothelial cell located both on the luminal and abluminal surface (Duijvestijn et al. 1992). The sections were washed in 0.02 M KPBS (pH 7.4), incubated with 1% H_2O_2 for 15 min to remove endogenous peroxidase, and blocked in a solution containing 10% normal horse serum (NHS) and 0.4% Triton X-100 in 0.02 M KPBS (pH 7.4) for 2 h at room temperature. Thereafter, sections were incubated with primary antibody overnight at 4 °C. They were subsequently washed in 2% NHS in 0.02 M KPBS (3 times 10 min each), and incubated for 2 h with biotinylated horse anti-mouse IgG (1:200; #BA-2000, Vector Laboratories, Burlingame, CA, USA). After three washes (10 min each) in 0.02 M KPBS, sections were incubated for 1 h in avidin-biotin-peroxidase complex (ABC) according to instructions provided by the manufacturer (Standard ABC kit; #PK-4000, Vector Laboratories). The sections were then recycled into secondary antibody solution for 45 min. After two 10 min washes in KPBS, they were recycled in the avidin-biotin-complex solution for 30 min and again washed in KPBS three times (10 min each time). The peroxidase activity was visualized by incubating sections for 4 min in a solution containing 0.05% 3',3'-diaminobenzidine (DAB) (Pierce Chemical Company, Rockford, IL, USA) and 0.04% H_2O_2 in 0.2 M KPBS. Following three washes in phosphate buffered saline (PBS; Lonza, Basel, Switzerland), sections were mounted on gelatin-coated slides, dried over night at 37 °C and intensified with osmium tetraoxide [(OsO_4) #19130, Electron Microscopy Sciences, Hatfield, PA, USA] and thiocarbohydrazide (#21900, Electron Microscopy Sciences) according to the method of Lewis et al. (1986). Sections were cover-slipped with DePeX (BDH Laboratory Supplies, Poole, UK) and left to dry overnight.

To assess the number and density of blood vessels, three consecutive RECA-1 immunostained sections were analyzed (150 µm apart from each other, slice thickness 450 µm) corresponding to the slices used to measure CBF with MRI from the same animals. The vessel counting was done in the perilesional cortex, septal hippocampus, amygdala (**IV**), and thalamus, both ipsilaterally and contralaterally. ROIs were drawn and vessel counting performed using Stereo Investigator software (MBF Bioscience, Williston, VT, USA) connected to an Olympus BX50 microscope (Olympus, Tokyo, Japan) using systematic random sampling. Firstly, an ROI was outlined and a sampling grid was laid on the section (cortex, 150 x 150 µm; amygdala, 250 x 250 µm; hippocampus, 250 x 250 µm; thalamus, 320 x 320 µm). Then, the number of hit points (Q) was recorded using a counting frame (cortex, 50 x 50 µm; amygdala, 60 x 60 µm; hippocampus, 70 x 70 µm; thalamus, 70 x 70 µm). Because of calcifications in the thalamus in study **II**, vessel density was calculated in five regions within and around the calcifications (in the center and to the north, east, south, and west of the calcifications; see **II**, Fig. 6). For each region, vessel density (D) was calculated in each section using a formula $D = \sum Q \cdot 1/asf$, where asf is the area sampling fraction (the area of counting frame divided by area of sampling grid). For statistical analyses, a mean density from the three sections for each region for each rat was calculated.

4.5.4 RECA-1 immunohistochemistry after focal ischemia

Three months after MCAO or sham-operation, sections from rats of study **III** were investigated for angiogenesis through immunohistochemistry. Double immunostaining for endothelial cell antibody (RECA-1) and neuron-specific nuclear protein (NeuN) was applied as a marker for blood vessels and to visualize loss of neurons in the thalamus, respectively. The sections were washed in 0.1 M PBS, pH 7.4 three times and blocked in 5% normal goat serum (NGS) after which the sections were transferred to a solution containing the primary antibody (NeuN at 1:4000, Millipore, Billerica, MA, USA) and tris-buffered saline with 5% NGS and 0.5% Triton X-100 (TBS-T). Following 18 hours of incubation in this solution on a shaker table at room temperature (20 ºC) in the dark, the sections were rinsed three times with TBS-T and transferred to a solution containing the secondary antibody (goat anti-mouse*biotin at 1:1000, Vector Laboratories, Peterborough, UK). After 2 h, the sections were rinsed three times with TBS-T and transferred to a solution containing mouse ExtrAvidin®

(Sigma-Aldrich, Helsinki, Finland) for 1 h and then rinsed in TBS-T and incubated for approximately 4-6 min with Ni-enhanced diaminobenzidine (Ni-DAB, blue). Then the staining protocol was repeated with an antibody for RECA-1 (1:2000, Serotec, Oslo, Norway). Immunostaining for RECA-1 was visualized with DAB (brown).

A point counting method was implemented to estimate the density of blood vessels in the RECA-1 and NeuN double stained sections. Sections were systematically sampled with a 150 µm interval from a 1-in-5 series using a fixed starting point. The part of the thalamus that corresponds to the MRI region of interest was included in the analysis. Brain sections were examined under a light microscope (Olympus BX50, Tokyo, Japan) fitted with the stereological image analysis system, equipped with a motorized stage controller and a camera (Hitachi HVC20A, Tokyo, Japan). The analysis was done with the aid of the Stereo Investigator software (Version 2006, MicroBrightField Inc., Williston, VT, USA). The instrumentation was calibrated before each series of measurements.

Briefly, the area of the ipsi- and contralateral thalamus was outlined under low magnification (x 2.5), and the outlined region was measured with a systematic random design of dissector counting frames. A sampling grid of 400 x 400 µm was laid on the section. A three-dimensional probe consisting of the counting frame of 65 x 65 µm (an “optical dissector”) with height (z-axis) of 10 µm was focused through a known depth of the section to estimate the total number of vascular branch hit points. Counting was performed throughout the section depth, according to point counting rules described by West et al. (1991). A 40 x PlanApo oil immersion objective having a 1.4 numerical aperture was used in the analyses. The total number of braching points was estimated using the formula: $N_{tot} = \sum Q \times 1/ssf \times 1/asf \times 1/tsf$, where section sampling fraction (ssf) is 1/5, area sampling fraction (asf, the area of counting frame, 4225.00 divided by area of sampling grid, 160000) 0.03, and tissue sampling fraction (tsf) 1.76. For statistical analysis, the branch point counts per ipsi- and contralateral thalamus sides from all sections from each subject were combined with the help of the Stereo Investigator system (Version 2006, MicroBrightField Inc., Williston, VT, USA). In order to obtain an estimate of the branching point density in the thalamus, the following formula was used:

$$N_V = \frac{N_{tot}}{V_{SN}}$$

Here, N_V is the numerical density and V_{SN} is the volume of the analyzed tissue. The variability within groups was assessed via the coefficient of error.

4.5.5 Quantifying blood-brain barrier leakage after focal ischemia

Immunoglobulin G (IgG) leakage into the brain was assessed as a marker of the BBB integrity during study **III**. Rats were perfused transcardially at 2 days, 7 days, 30 days and 3 months after surgery as described. A series of sections was washed in 0.1 M PBS three times and then incubated in 1% hydrogen peroxide for 15 min. Then the sections were blocked in 2% NGS. This was followed by incubation with biotinylated sheep anti-rat IgG (1:200, AbD Serotech, Oslo, Norway) for 48 h at 4 ^{o}C. The sections were washed with TBS-T and transferred to a solution containing mouse ExtrAvidin® (1:1000, Sigma-Aldrich, Helsinki, Finland) for 1 h and then incubated for approximately 4-6 min with DAB.

Images (x 1.25 magnification) of the ipsilateral and contalateral thalamus were acquired using an Olympus BX40 microscope (Olympus, Tokyo, Japan) with a digital camera DP50-CU and image acquisition software Viewfinder (Pixera Corporation, San Jose, CA, USA). ImageJ software (NIH, Bethesda, MD, USA) was used for image analysis. All images were converted to gray scale and then the thalamus was outlined to provide a mean gray scale value for statistical analysis.

4.6 Molecular biology techniques

It has been previously shown that expression of several cadherin superfamily members peaks during perinatal vascular development, but then gradually declines and disappears by adulthood (Krishna-K and Redies 2009). In study **III**, we hypothesized that some of these adhesion molecules begin to be re-expressed during angiogenesis after MCAO. Expression levels of cadherin-7, protocadherin-1 (PCDH1), protocadherin-17 (PCDH17) and vascular-endothelial cadherin (VE-cadherin) in addition to vascular endothelial growth factor (VEGF) were examined in the ipsilateral and contralateral thalami of rats at 2 days, 7

days, 30 days and 3 months post-MCAO by Western blotting. To achieve this, the ipsilateral and contralateral thalami were dissected and frozen immediately on dry ice and stored in -70 ºC. Samples were mechanically homogenized in cold PBS. Total protein contents were extracted in tissue extraction buffer containing protease and phosphatase inhibitors, and the protein concentrations were determined by using a protein assay kit (Pierce, Rockford, IL, USA). Forty µg of proteins were subjected to 4-12% Bis-Tris polyacrylamide gel electrophoresis (PAGE, Life Technologies, Carlsbad, CA, USA) under reducing conditions and blotted on polyvinylidene fluoride membranes. The membranes were blocked in 5% non-fat dry milk in Tris-buffered saline (TBS), pH 7.4, containing 0.1% Tween-20 (TBST) for one hour and incubated overnight at 4 ºC with the following antibodies: Rabbit anti-cadherin-7 (1:200; Santa Cruz Biotechnology Inc., Santa Cruz, CA, USA); mouse anti-PCDH1 (1:1000; Santa Cruz); rabbit anti-PCDH17 (1:200; Santa Cruz); VE-cadherin (1:200; Santa Cruz); and rabbit anti-VEGF (1:1000; Abcam, Cambridge, UK). Appropriate horseradish peroxidase-conjugated secondary antibodies and enhanced chemiluminescence were used to visualize the proteins using an ImageQuant reverse transcription electrochemiluminescence (RT ECL) imager (GE Healthcare, Helsinki, Finland).

Western blot images were quantified using Quantity One software (Bio-Rad, Helsinki, Finland). The levels of each protein were normalized to the levels of transferrin receptor in the same samples. The data are shown as expression levels of each protein in the ipsilateral thalamus as a % of the levels in contralateral thalamus.

4.7 Statistics

In all studies, data were analyzed using the SPSS software for Windows (v. 14, Chicago, IL, USA) and the level of significance was $p<0.05$ throughout. In study **I**, MRI measurements were made over many time points, thus differences between groups were tested using the Kruskal-Wallis test followed by Mann-Whitney U testing. Differences within groups were tested using Freidman's test with *post hoc* Wilcoxon's tests corrected for any multiple comparisons (Bonferroni). All values are given as mean ± the standard error of the mean (SEM).

In study **II**, the differences in MRI, PTZ test data, and vessel density between the TBI and sham groups were compared using the

Mann-Whitney U test. ANOVA for repeated measures was used to assess the differences in the temporal profile of neuroscore between the TBI and sham groups, as these data were suitable for parametric testing due to their proximity to the normal distribution. *Post hoc* analysis of differences at individual time points was performed using an unpaired Student's t-test. Morris water maze data were analyzed with ANCOVA using the swim speed as a covariate. All correlations are presented as Pearson's correlations.

For study **III**, all data were suitable for parametric testing. CBF, beam-walking, and cylinder data were analyzed for the overall group effect using ANOVA for repeated measures. Comparisons between groups or ipsilateral and contralateral regions were then made using unpaired or paired Student's t-tests, respectively. The number of blood vessel branching points was compared between ipsilateral and contralateral sides of the thalamus using a paired Student's t-test. For blood-brain barrier (BBB) breakdown studies by IgG immunoreactivity, ANOVA followed by *post hoc* multiple comparisons (Bonferroni) were used to find differences over time. For gene expression data, one-way ANOVA was used to find differences between groups followed by *post hoc* multiple comparisons (Newman-Keuls test) for differences between the ipsilateral and contralateral thalamus. All correlations are presented as Pearson's correlations.

Within study **IV**, the small datasets were more suited to non-parametric statistical testing. Analyses between 2 days and 14 days for each group were made using Wilcoxon's test for related samples. Analyses between groups at 2 days and at 14 days were made using the Mann-Whitney U test for independent samples.

5 RESULTS

5.1 Prolonged hemodynamic disruption after traumatic brain injury

Between 6 hours and 2 weeks after severe TBI in rats (**I**), successive ASL MRI showed that CBF varied over time ($p<0.001$). Although each brain region had a slightly different hemodynamic response to injury, three phases of temporal changes were evident ipsilaterally. These were acute hypoperfusion followed by sub-acute recovery, and then secondary hypoperfusion later. For example, in the perilesional cortex, CBF was reduced to only 54% of that in controls ($p<0.01$) at 6 hours post-injury (**I**, Fig. 3). This deficit recovered by 24 hours post-injury, being 15% above the control mean ($p<0.05$). However, during the next two weeks the perilesional cortex became hypoperfused again as the CBF reduced to only 75% of the control mean by two weeks ($p<0.05$). Within the TBI group, the recovery of perilesional hypoperfusion between 6 hours and 24 hours, and subsequent CBF decrease between 24 hours and 2 weeks, were significant (overall $p<0.01$). This temporal pattern of changes was similar in the septal hippocampus and thalamus over the same period in the same animals (**I**, Fig. 3).

Contralaterally after severe TBI, the three-phase temporal pattern of CBF fluctuations was similar but each change was milder than that seen ipsilaterally. CBF varied over time in the contralateral cortex and septal hippocampus ($p<0.01$) but not in the contralateral thalamus. For example, in the contralateral cortex of injured rats, CBF was decreased to 72% of that in controls at 6 hours ($p<0.01$, **I**, Fig. 3B). The hypoperfusion continued until 48 hours post-injury (CBF was 79% of controls, $p<0.05$). Within the TBI group, CBF increased between 6 hours and 1 week after injury ($p<0.05$). Thereafter, no differences compared to controls or over time were found, showing that secondary hypoperfusion was less prominent contralaterally than on the ipsilateral side. Although we detected clear changes in CBF in this study, DSC (ssCE) MRI showed no significant variations in CBV in any region at either 2 days or 2 weeks after TBI (**I**).

Chronically in the same model (**II**), the regional differences in CBF were striking when assessed 8 months after injury by ASL MRI. Hypoperfusion was found in the perilesional cortex, where CBF was markedly decreased to only 46% of that in controls ($p<0.01$, **II**, Fig. 4A).

The ipsilateral and contralateral septal hippocampus were also hypoperfused (**II**, Fig. 5A), but to a lesser extent than the perilesional cortex. In the ipsilateral hippocampus, CBF was decreased to 87% ($p<0.05$) and contralaterally to 80% of the control mean ($p<0.01$).

The thalamus has received very little TBI research attention compared to the hippocampus and cerebral cortex. Surprisingly, the thalamus showed a very different hemodynamic response to these other regions. Ipsilaterally, CBF was chronically increased to 134% of the control mean at 8 months after TBI ($p<0.01$, **II**, Fig. 6A). The discovery of chronic thalamic hyperperfusion after TBI is discussed later (section *6.1.4*). Importantly, it led us to investigate regional sub-acute and chronic CBF responses after a different kind of brain injury caused by cerebral ischemia in rats (**III**).

5.2 Vascular reorganization after traumatic brain injury

In each study, we used immunohistochemistry to investigate changes in blood vessel density in each animal model. Either regional vessel densities (**I**, **II**, **IV**) or regional vessel branching point numbers (**III**) were quantified from histological sections sampled from the coronal positions corresponding to the MRI slices from which CBF and CBV were analyzed. Vascular loss or recovery may partly explain the hemodynamic disruption in each neurological condition. Contralaterally after TBI, the vessel density in injured rats did not differ from that in controls in any regions studied at any time (**I**, **II**). Ipsilaterally, there was much evidence of vascular reorganization after TBI.

Six hours after TBI in rats (**I**), the vessel density in the perilesional cortex tended to become reduced to around 90% of that in controls ($p>0.05$, **I**, Fig. 5B, G). By 2 weeks post-injury, vessel density was 120% of that measured at 6 hours ($p<0.01$). This suggests that vessels in the perilesional cortex are acutely lost and later recovered, perhaps through angiogenesis. Although we did not study angiogenic markers after TBI, the density of blood vessels in the perilesional cortex was further increased to 128% of the control mean at 8 months after TBI ($p<0.01$, **II**, Fig. 4B, C). Chronically, there was also a negative correlation between CBF and vessel density in the perilesional cortex, meaning that a higher blood vessel density corresponded to lower CBF ($p<0.01$, **II**, Fig. 4E).

When the density of vessels was quantified from the ipsilateral septal hippocampus, no difference to controls was observed at the acute and sub-acute time points. However, looking closely at the sections revealed an acute vessel loss in the ipsilateral CA1 subfield. Vessel density measures from the stratum oriens of CA1 revealed that only 80% of vessels were remaining at 6 hours after TBI as compared to controls ($p<0.01$, **I**, Fig. 5E, H). These measures correlated positively with ipsilateral hippocampal CBF ($r=0.753$, $p<0.05$, **I**, Fig. 5I), thus more vessels implied increased blood flow. Vessel density in this region later returned to the control level by 2 weeks and was 112% of that measured at 6 hours ($p<0.05$, **I**, Fig. 5F, H). Chronically (**II**), there were no hippocampal blood vessel changes or clear correlations with CBF.

In the ipsilateral thalamus, vessel density changes were only seen at 8 months after TBI (**II**). In RECA-1 stained histological sections from this study, calcifications were present in all rats with TBI. In T_2 weighted MRI, 5/8 rats had a clear signal decrease at the location of calcifications seen in corresponding histology sections (**II**, Fig. 2D). Vessel density was therefore measured with respect to the calcification locations (regions outlined in **II**, Fig. 6). On average, thalamic blood vessel density was increased to 178% of that in controls and was as much as 2-fold higher in some thalamic regions ($p<0.01$, **II**, Fig. 6B). An increase in ipsilateral blood vessel density was observed in all regions except region 4 ($p<0.01$, **II**, Fig. 6B). In the contralateral thalamus, CBF and the density of blood vessels were comparable to the control means (**II**, Fig. 6). Unlike in the perilesional cortex, there was no association between the CBF and density of blood vessels in the thalamus.

5.3 Long-term functional consequences of traumatic brain injury

During the acute and sub-acute period after severe TBI (**I**), we did not perform behavioral investigations of cognitive and motor impairment, as this may have been impaired by the intensive imaging protocols. During the chronic study of TBI (**II**), motor impairment, hippocampus-dependent spatial memory and finally seizure susceptibility were assessed over the 9 month follow-up period. Over the first 6 months after TBI, the mean motor neuroscore remained lower than that of controls throughout ($p<0.01$, **II**, Fig. 7A). In line with neuroscore, the swimming speed in the Morris water maze was also decreased in injured animals when assessed 7 months post-TBI ($p<0.05$, **II**, Fig. 7B). In this model of TBI, complete motor recovery was never reached during our study. However,

some motor recovery did occur between day 2 and 1 month ($p<0.001$). Consequently, we calculated a recovery rate for each rat as the gradient of a line drawn between the neuroscores at day 2 and at 1 month. This assumed a linear recovery rate during this period. This rate was used to test correlations with other study parameters in the search for surrogate markers for neurological improvement. Unfortunately, we found no correlation between recovery rate and either CBF or vascular density in the perilesional cortex. Also, no correlations were found between the recovery rate and ipsilateral thalamic CBF or vascular density in our study.

The Morris water maze was used to investigate the hippocampus-dependent learning and memory performance at 7 months after TBI. The swimming latency time profile over 2 days was different between the TBI group and sham group ($p<0.05$, **II**, Fig. 8A). In particular, latency was prolonged in the TBI group compared to controls on day 1 by 27 ± 10 s ($p<0.05$) and on day 2 by 35 ± 13 s ($p<0.001$). In the probe trial without the platform, the average percentage time a rat spent swimming in the correct quadrant was lower in TBI rats compared to controls (reduction of 8% ± 6%, $p<0.05$, **II**, Fig. 8B). Unfortunately, we found no association between the water maze performance and hippocampal CBF or vessel density.

As TBI is a trigger for epileptogenesis, we investigated the possibility of increased seizure susceptibility long after TBI in rats (**II**). Firstly, we performed a 2-week continuous video-EEG session at 9 months after TBI or sham-operation, but no spontaneous seizures were observed in any of the rats. Consequently, seizure susceptibility was assessed using the PTZ test under continuous video-EEG. The latency to the first EEG spike in rats with TBI (168 ± 255 s, median 81 s) was reduced as compared to controls (646 ± 540, median 534 s, $p<0.05$, **II**, Fig. 9A). Also, 50% of rats with TBI had an abnormally high number of epileptiform discharges (control mean + 1SD). These markers of increased seizure susceptibility were then correlated with CBF and vessel density in the cortex, hippocampus, and thalamus. This led to some important correlations that suggest that the cerebrovascular responses to TBI are associated with the seizure threshold long after injury. For example, we found that the lower the CBF in the ipsilateral hippocampus, the shorter the latency to the first spike after PTZ administration ($r=0.78$, $p<0.05$, **II**, Fig. 9B). In addition, the higher the CBF in the ipsilateral thalamus, the shorter the latency to the first EEG spike ($r=0.69$, $p<0.05$, **II**, Fig. 9C). Also, the greater the vessel density in

the ipsilateral thalamus, the higher the number of seizures during the first hour after PTZ administration (r=0.71, p<0.05, **II**, Fig. 9D).

Lastly, we researched whether indicators of enhanced seizure susceptibility associate with functional performance. Of note, a greater neuroscore recovery rate correlated with a higher number of electrographic seizures during the first hour after PTZ administration (r=0.64, p<0.05, **II**, Fig. 9E). Furthermore, greater impairment in the water maze was associated with shorter latency to the first epileptiform spike after PTZ administration (r=0.56, p<0.05, **II**, Fig. 9F).

5.4 Prolonged cerebral blood flow disruption after cerebral ischemia

For study **III**, we used ASL MRI to investigate CBF at baseline, 2 days, 7 days, 30 days and 3 months after transient focal ischemia (MCAO) in rats. The analysis showed that CBF varied over time and between hemispheres (p<0.05) particularly in the thalamus (**III**, Fig. 2A). Two days after ischemia, CBF was decreased compared to respective values in sham-operated rats in the ipsilateral (73% of sham mean, p<0.001) and contralateral (64% of sham mean, p<0.001) thalamus. Surprisingly, the sub-acute ipsilateral CBF in MCAO rats was greater than that contralaterally (120% of contralateral mean, p<0.01), when one might expect ipsilateral regions to respond more severely. Partial recovery of thalamic CBF occurred by day 7 but hypoperfusion remained ipsilaterally (88% of sham mean, p<0.05) and contralaterally (77% of sham mean, p<0.01). Greater ipsilateral perfusion compared to contralateral perfusion in MCAO rats still prevailed at day 7 (116% of contralateral mean, p<0.001). Considering the chronic time points, 30 days and 3 months after ischemia, the ipsilateral thalamus was hyperperfused compared to its contralateral side in MCAO animals at day 30 (117% of contralateral mean, p<0.001) and at 3 months (118% of contralateral mean, p<0.001), much like we found in chronic TBI (**II**).

Cortical CBF also varied over time, between groups, and between the ipsilateral and contralateral cortex (**III**, Fig. 2B). Specifically, bilateral hypoperfusion was observed at 2 days after MCAO, as compared to shams (73-80% of sham mean, p<0.01). Close to the lesion, the ipsilateral cortex was variably affected between MCAO rats yet remained hypoperfused for the study duration on average. However, the

CBF of the contralateral cortex recovered by day 7 and subsequently remained comparable to control measures thereafter.

5.5 Vascular reorganization after cerebral ischemia

We searched for evidence of thalamic angiogenesis after focal cerebral ischemia (MCAO) in rats by RECA-1 immunohistochemistry at the end of the study (**III**). Unlike in the TBI studies, vessel branching points were counted by advanced stereology in order to provide a measure for vascular growth (**III**, Fig. 3). Quantitative analysis showed that the number of vessel branching points in MCAO rats was significantly higher in the ipsilateral thalamus compared to the contralateral thalamus (141% of contralateral mean, $p<0.001$, **III**, Fig. 3B). There was no such difference in sham-operated animals. Specifically, this increase occurred throughout the mediodorsal, submedial, ventrolateral, ventromedial and very often the paracentral and oval paracentral thalamic nuclei (**III**, Fig. 3E, G). The number of vessel branching points in the ipsilateral thalamus of MCAO rats did not correlate with the infarct lesion size assessed at the end of the follow-up, nor with the ipsilateral CBF assessed at 2 days after ischemia.

It is possible that vascular damage could influence CBF measures in animal models of brain injury, and reperfusion injury is of concern in models of transient cerebral ischemia. In study **III**, we investigated blood-brain barrier (BBB) damage by staining sections from additional MCAO rats for IgG immunoreactivity (**III**, Fig. 4). Semiquantitative analysis showed a slight, diffuse pattern of IgG immunoreactivity in the ipsilateral thalamus at 2 days after MCAO, which was not present at later time points. This may be related to reperfusion damage and is in line with the BBB leakage in this model (Belayev et al. 1996).

In study **III**, we chose to further investigate thalamic angiogenesis through molecular biology techniques. Cadherin adhesion molecules are likely required for angiogenesis because it is known that their expression peaks during perinatal vascular development, but then gradually declines and disappears by adulthood (Krishna-K and Redies 2009). Thus, expression levels of cadherin-7, protocadherin-1 (PCDH1), protocadherin-17 (PCDH17), and vascular endothelial growth factor (VEGF) were examined in the ipsilateral and contralateral thalamus over 3 months after MCAO by Western blotting. Cadherin-7, PCDH1 and PCDH17 were expressed in both the ipsilateral and contralateral

thalamus after MCAO (**III**, Fig. 6). The levels of cadherin-7 peaked at 2 days after MCAO and returned to contralateral levels by 3 months after MCAO. In contrast to cadherin-7, PCDH1 and PCDH17 levels were never significantly different between hemispheres. Vascular endothelial growth factor (VEGF) is well known to help initiate angiogenesis. We detected a 70% decrease in VEGF levels at 7 days after MCAO in the ipsilateral thalamus as compared to the contralateral thalamus (**III**, Fig. 6).

5.6 Long-term functional consequences of cerebral ischemia

The motor performance of rats subjected to cerebral ischemia was investigated repeatedly over the first 3 months following surgery, in order to evaluate the contribution of hemodynamic and cerebrovascular responses to functional recovery (**III**). Forelimb function was assessed using a cylinder test and hindlimb function was measured using a beam-walking test. Sham-operated rats and MCAO rats performed similarly in the cylinder test before their operation (**III**, Fig. 5A). Over 3 months after MCAO, rats were more impaired than sham-operated rats ($p<0.001$). There was also a significant 'group by day' interaction ($p<0.01$), showing that the initial severe forelimb deficit on day 2 recovered by day 14 after MCAO. Early hindlimb impairment was similarly severe ($p<0.001$) and did not recover during our study. On all post-operative days, the beam-walking performance of MCAO rats correlated with the volume of the infarct lesion (**III**, Table 1). This shows that the ischemic lesion size determines the degree of hindlimb motor impairment.

5.7 Prolonged hyperperfusion and increased blood vessel density after status epilepticus

Hemodynamic changes in the cerebral cortex and amygdala were quantified by ASL and DSC (ss-CE) MRI at both 2 days and 14 days after SE in rats (**IV**, Fig. 1). In the cortex, we found no hemodynamic changes after SE because CBF and CBV values were comparable between the groups and between the two time points. Instead we observed prolonged hyperperfusion in the amygdala during epileptogenesis. Here, CBF was increased and recorded as 116% of that in controls at 2 days after SE ($p<0.05$, **IV**, Fig. 1G). At 14 days, CBF was 129% of the control value ($p<0.01$, **IV**, Fig. 1E, G). In contrast, CBV

did not significantly differ between the groups at either 2 days or 14 days (**IV**, Fig. 1F) yet it tended to be increased at 14 days after SE (119% of the control value, p=0.08, **IV**, Fig. 1H). This CBV trend matches the pattern of CBF increase after SE, even though there was no significant linear correlation between CBF and CBV in individual rats.

The blood vessel density in the amygdala increased in a similar manner to CBF. In the SE group, vessel density was 127% of that in the control group ($p<0.05$) at 14 days after SE (**IV**, Fig. 1I, J, K). We found no clear correlation between hemodynamic measures and vascular density in the amygdala, possibly due to the small number of rats included in this study.

6 DISCUSSION AND CONCLUSIONS

6.1 Cerebrovascular responses to traumatic brain injury

For study **I**, we achieved detailed characterization of CBF at five time points over two weeks following severe TBI in rats by MRI. To our knowledge, this is the first time that hemodynamic profiles for several subregions of the brain have been investigated both during and beyond the acute phase of TBI in rats.

6.1.1 Severe traumatic brain injury disrupts acute contralateral cerebral blood flow

Hypoperfusion was recorded in the contralateral cortex at 6 hours and again at 48 hours after TBI. Hypoperfusion also occurred after 48 hours in the contralateral hippocampus. These findings are consistent with very early widespread hypoperfusion seen in TBI patients (Yoshino et al. 1985, Bouma et al. 1991, Martin et al. 1997, Coles 2004) and in animal TBI models (Yuan et al. 1988, Yamakami and McIntosh 1989, Muir et al. 1992, Cherian et al. 1994, Bryan et al. 1995, Nilsson et al. 1996, Dietrich et al. 1998, Pasco et al. 2007). However, unlike in the present work, some studies in rats noted recovery of contralateral CBF to control values within 6 hours. In one study, initial contralateral hypoperfusion seen 1 hour after moderate LFPI recovered by 2 hours (Yamakami and McIntosh 1989) and this difference may be due to the less severe injury than that of our study. After CCI, which inflicts a more focal insult than LFPI, the impaired contralateral CBF may normalize by 4 hours after injury (Bryan et al. 1995). Yet other studies describe a more prolonged initial decrease in CBF. Ishige and colleagues (1987) observed extensive hypoperfusion in contralateral regions at 24 hours after TBI. This may be because their model employed a 5 atm temporal fluid-percussion impact, which is different to CCI and to the 3.2-3.4 atm impact inflicted laterally to the brain midline in our study.

The variation in the temporal profile of CBF between studies is likely due to the range of impact severities and the variety of injury models available (LFPI, CCI, weight drop, etc). The hypoperfusion in the contralateral regions in our study normalized by 1 week after TBI and thereafter, CBF values were comparable to control measures. To our

knowledge, there are no similar studies available to support this finding in animal models.

6.1.2 Acute and sub-acute hemodynamic changes in ipsilateral regions match those of patients

We observed acute hypoperfusion in the perilesional cortex and ipsilateral hippocampus after TBI. Early focal hypoperfusion has been seen previously in a range of TBI studies in rats (Yuan et al. 1988, Yamakami and McIntosh 1989, Bryan et al. 1995, Nilsson et al. 1996, DeWitt et al. 1997, Dietrich et al. 1998, Robertson et al. 2000, Thomale et al. 2002, Pasco et al. 2007) and in patients (Bouma et al. 1991, Martin et al. 1997, Coles 2004). As in our study, acute ipsilateral hypoperfusion after TBI in rats is normally more severe than that contralaterally (Yamakami and McIntosh 1989, Bryan et al. 1995, Nilsson et al. 1996, Dietrich et al. 1998, Pasco et al. 2007) and may recover less readily (Yamakami and McIntosh 1989, Bryan et al. 1995).

By 24 hours after TBI, CBF in the ipsilateral regions had recovered in our study. A recent study of CCI in rats (Thomale et al. 2002) also demonstrated CBF normalization in and around the damaged cortex at 24 hours. After 48 hours in our study, a second phase of hypoperfusion was observed in the ipsilateral hippocampus, which is previously undocumented to our knowledge. One might expect the neighboring perilesional cortex to show a similar hemodynamic profile, yet a second phase of hypoperfusion in this region is not apparent until 2 weeks after TBI. Yet after 1 week, CBF in the ipsilateral hippocampus has fully recovered. The fact that the ipsilateral hippocampus makes a late CBF recovery in our study implies that it is less severely affected by secondary damage after TBI compared to the perilesional cortex, which may not recover in this model. We note that under healthy conditions, CBF and CBV are coupled by vascular autoregulation and are dependent upon cerebral perfusion pressure (CPP), which is controlled by dynamic actions of arterial vessel walls. We found no significant changes in CBV when CBF was clearly disrupted, thus it is possible that hemodynamic coupling is lost both acutely and sub-acutely after TBI.

Although our ipsilateral regions had a slightly different time course of CBF alterations, the three phases of hemodynamic unrest match the general hemodynamic pattern observed in TBI patients. This pattern includes acute hypoperfusion, CBF recovery at days 1-3 and then secondary hypoperfusion over the next 2 weeks (Marion et al. 1991,

Bouma et al. 1991, Kelly et al. 1997, Martin et al. 1997). In conclusion, our data suggest that the LFPI model for TBI in rats induces hemodynamic events in ipsilateral areas that resemble those seen in patients. However, one must always consider that hemodynamic variations after TBI in rats (Nilsson et al. 1996, Forbes et al. 1997, Shen et al. 2007) and patients (Golding 2002, Bonne et al. 2003) can be highly variable due to the mixed nature of the injury and due to much physiological variation between subjects.

6.1.3 Vascular reorganization only partly explains hemodynamic changes

We report an acute loss of blood vessel density and subsequent increase between 6 hours and 2 weeks after TBI in the stratum oriens and perilesional cortex. In the perilesional cortex, CBF measures did not correlate with vessel density and it is possible that newly formed vessels may not be fully functional 2 weeks after TBI. A recent immunohistochemistry study by Park and colleagues (2009) demonstrated cortical blood vessel loss 24 hours after LFPI, which recovered by 2 weeks in moderately injured rats but not in severely injured rats. Vessel loss and recovery may give some explanation to the hemodynamic uncoupling we observed. However, we observed hypoperfusion in regions without significant vessel loss, such as the thalamus, thus vessel reorganization may only partly explain our hemodynamic findings.

6.1.4 Chronic cerebrovascular responses to traumatic brain injury are region specific

Our study made at 8-9 months after TBI (**II**) shows that chronic cerebrovascular changes are different between brain regions. In the perilesional cortex, chronic hypoperfusion was associated with increased vascular density. In the ipsilateral hippocampus, mild hypoperfusion was not associated with any blood vessel changes. Differently again, hyperperfusion in the ipsilateral thalamus was linked with a considerably increased vascular density. Although regional CBF has long been suggested to correlate positively with regional blood vessel density (Gross et al. 1986), our correlations indicated very few links between CBF and vascular reorganization. In contrast, we found that the lower the CBF in the perilesional cortex, the higher the vascular density. This implies that cortical angiogenesis after TBI may not provide

sufficient new blood vessels or sufficient vascular integrity to recover the chronic perfusion deficit.

There is remarkably little prior literature that describes chronic cerebrovascular responses to TBI in either patients or animal models. It is therefore difficult to suggest possible mechanisms for our regionally specific results. One factor that could explain the regional differences is increased volume of cerebrospinal fluid (CSF) and hydrocephalus, which was seen in all rats at 8-9 months after TBI. Reduced CBF in the perilesional cortex and ipsilateral hippocampus could be because these brain areas are close to the ventricles, thus they are most exposed to hydrocephalus-induced compression due to elevated intracranial pressure (ICP). This mechanism has been proposed by Dombrowski and colleagues (2008) in a model of chronic hydrocephalus. Increased ICP can impede CBF and over time this may trigger the hypoxic conditions that could promote angiogenesis, particularly around the cortical lesion (Dombrowski et al. 2008, Chen et al. 2009, Madri 2009). Although we did not measure ICP after TBI in our study, there is already evidence that ICP remains elevated beyond the acute phase in experimental TBI (Ghabriel et al. 2010).

Vascular density and CBF in the thalamus were markedly increased, which is a combination different from that of other regions. This could be because our thalamic results relate to nuclei that are not at the thalamic surface, thus they could remain less susceptible to chronic hydrocephalus. Furthermore, the thalamus is known to have unique pathological hallmarks that are in contrast with other regions after TBI, including diffuse white matter damage and chronic calcifications (Bramlett et al. 1997, Pierce et al. 1998, Graham et al. 2000, Osteen et al. 2001, Rodriguez-Paez et al. 2005). This links in with our observation that angiogenesis was most abundant around calcified thalamic regions. Taken together, the variable pattern of changes in vascular function and structure in the cortex, hippocampus, and thalamus many months after TBI warrant further studies to understand whether they reflect differences in exposure to hydrocephalus or whether they serve as surrogate markers for delayed secondary damage and calcifications.

6.1.5 Traumatic brain injury and epileptogenesis

The risk of epilepsy development is a major clinical concern after TBI. The chance of TBI patients presenting with epilepsy later in life is 16%

after moderate brain injury and may be as high as 53% after ballistics or blast injuries (Lowenstein 2009). In study **II**, one of our aims was to assess the association between chronic vascular integrity and seizure susceptibility after TBI. TBI in rodents often results in epileptogenesis (Kharatishvili and Pitkänen 2010) yet LFPI did not result in spontaneous seizures during a relatively short period of 2-wk video-EEG monitoring. However, rats showed enhanced seizure susceptibility in the PTZ test.

Although the perilesional cortex may generate ictal activity after LFPI (D'Ambrosio et al. 2004, 2005, Kharatishvili et al. 2006), we found no association between the hypoperfusion or increased vascular density in the perilesional cortex and seizure susceptibility. This might be because injury to more caudal cortical areas associates with hyperexcitability, rather than the cortical regions close to the lesion (Kharatishvili and Pitkänen 2010). More importantly, circuitry alterations and cerebrovascular responses in the hippocampus are common in experimental epilepsy and patients (Pitkänen and Lukasiuk 2009, Ndode-Ekane et al. 2010) and electrographic activity during spontaneous seizures after TBI involves the ipsilateral hippocampus (Kharatishvili et al. 2006). We saw that a reduction in the ipsilateral hippocampal CBF at 8 months after TBI was associated with increased seizure susceptibility at 9 months such that the lower the CBF, the higher the seizure susceptibility. In line with this, it is already feasible to delineate the ictogenic zone with ASL and other neuroimaging techniques (Rougier et al. 1999, Lim et al. 2008). Further studies are needed to discern whether chronic hippocampal hypoperfusion after TBI can be used as a surrogate marker for epileptogenesis.

The thalamus is often damaged in moderate and severely injured TBI patients as well as in animal models (Pierce et al. 1998, Maxwell et al. 2004, 2006, Tollard et al. 2009, Little et al. 2010). However, the role of the thalamus in epileptogenesis after acquired etiologies like TBI is poorly understood (Bonilha et al. 2004, Blumenfeld et al. 2009). Here we found that a high vessel density in the thalamus was associated with enhanced seizure susceptibility in injured rats. This is in line with a previous clinical report in which increased thalamic CBF was recorded during secondary generalization of focal onset seizures (Blumenfeld et al. 2009). Yet because we did not detect any spontaneous seizures during 2 weeks of video-EEG monitoring, we concluded that markedly increased thalamic CBF after LFP injury was not associated with ictal activity. In general, one must be cautious with the interpretation of such clinical and preclinical correlations. Animal physiology is so complex that associations do not confer causation, thus links between merely two

biological phenomena that occur together within just one study must be discussed modestly. Only by performing many detailed mechanistic studies can we provide evidence to suggest that cerebrovascular sequelae are either the cause or consequence of, for example, either epileptogenesis or functional recovery after brain injury.

6.2 Cerebrovascular responses to cerebral ischemia

6.2.1 Thalamic hypoperfusion and delayed hyperperfusion after cerebral ischemia

In study **III**, we observed sub-acute bilateral hypoperfusion in the thalamus after MCAO, followed by ipsilateral hyperperfusion chronically. To our knowledge, this is the first time that long-term blood flow changes in the thalamus have been studied after focal ischemia in rats. Chronic thalamic hyperperfusion associated with increased vessel density was also seen after TBI (**II**), suggesting shared pathology between these two conditions (section *6.3.2*).

Most rodent studies of hemodynamics after ischemia focus on the acute period. However, a prolonged reduction in cerebral blood flow (CBF) after permanent MCAO in rats has been shown by autoradiography (Bolander et al. 1989). Specifically, CBF in the ipsilateral caudate putamen and peri-infarct cortex was decreased up to 7 days when compared to contralateral values. This hypoperfusion resolved by 28 days after ischemia, which may be due to the establishment of collateral blood supply. More recently, laser Doppler flowmetry has been used to measure the long-term hemodynamic response to ischemia in rats (Ulrich et al. 1998, Borlongan et al. 2004, Eve et al. 2009). After permanent MCAO, Ulrich and colleagues (1998) noted incomplete recovery of cortical CBF over six weeks, and Eve and colleagues (2009) noted that ipsilateral cortical CBF did not normalize to basal measures even by 10 weeks after ischemia. Prolonged cortical hypoperfusion has also been shown to prevail for at least 21 days after permanent MCAO in mice (Li et al. 2007). Also after transient MCAO, Doppler measures in striatal penumbra regions showed prolonged hypoperfusion for 2 weeks in rats (Borlongan et al. 2004).

As in the present work, long-term hemodynamic studies of focal ischemia have also employed magnetic resonance techniques to measure perfusion, including DSC MRI (Rudin et al. 2001, Lin et al.

2002) and ASL (Jiang et al. 2008). After permanent MCAO in rats, DSC showed that hypoperfusion prevails for at least 3 days in the ipsilateral striatum (Rudin et al. 2001) and up to 14 days in the ipsilateral cortex (Lin et al. 2002). After transient MCAO in rats, ASL was used to follow CBF for 7 days and acute hypoperfusion was found in the ischemic striatum, yet this normalized within 3 hours (Jiang et al. 1998), which contrasts with our cortical and thalamic findings. However, these prior studies do not specifically focus on the hemodynamic response of the thalamus, which could be different to prior findings because different brain regions respond differently to ischemia (Ginsberg et al. 1976, Block et al. 2005, Dijkhuizen et al. 1998, Lin et al. 2008). Also, the majority of described hemodynamic findings arise from permanent MCAO models, which may have different pathological consequences to those of transient MCAO (Hossmann 2006, Bratane et al. 2010). Overall, the proposal of chronic hyperperfusion in the thalamus after ischemic stroke is, to our knowledge, entirely new.

6.2.2 Thalamic hyperperfusion is likely due to angiogenesis

We observed angiogenesis in the ipsilateral thalamus chronically after transient focal ischemia. This matches a recent study by Ling and colleagues (2009), who found ipsilateral thalamic angiogenesis at 14 days after permanent MCAO in stroke-prone hypertensive rats. The present work suggests that chronically increased thalamic blood flow is at least partly due to angiogenesis, which has previously been suggested for the cortex over 2 weeks after permanent ischemia in rats (Lin et al. 2002). Angiogenesis can be considered as a mechanism to bring an oxygen and nutrient supply to peri-infarct regions after stroke (Beck and Plate 2009), and indeed, angiogenesis in the ischemic border begins 3-4 days after stroke and correlates with patient survival (Krupinski et al. 1994). This suggests that angiogenesis is a prolonged, natural recovery process in peri-infarct regions. Our observation of ipsilateral thalamic hyperperfusion at day 30 implies that the newly formed vasculature may then be functional.

Our ischemia study cannot confirm precisely when thalamic angiogenesis begins. However, we did find upregulated expression of cadherin-7 in the ipsilateral thalamus after MCAO. Also of angiogenic interest, we observed elevated ipsilateral VEGF in the thalamus at 2 days after MCAO. In line with our study, Hayashi and colleagues (2003) observed endothelial cell proliferation from day 1 after transient MCAO

in mice, leading to increased vessel density in the cortex and caudate putamen already at day 3. Angiogenesis may continue for many days as vessel density continued to increase in both regions for at least 21 days after ischemia. The researchers used gene expression studies to show that angiogenesis is initiated just hours after ischemic insult. This was noted due to elevated mRNA levels from 42 genes implicated in angiogenesis, including VEGF. More recently, the expression of cadherin adhesion molecules during brain vascular development in ferrets has been reported (Krishna-K and Redies 2009) but their expression was no longer detectable in the adult brain. In conclusion, these results suggest that certain cadherin adhesion molecules that are normally only expressed during brain development are re-expressed in the thalamus of rats after MCAO, particularly ipsilaterally. Further, the peak in expression levels precedes the chronic angiogenesis and hyperperfusion we observed. Lastly, we note the possibility that the prolonged sub-acute hypoperfusion that we measure could have promoted angiogenesis after MCAO, as shown previously (Hermann and Zechariah 2009, Beck and Plate 2009).

6.3 The cerebrovascular sequalae of traumatic brain injury and ischemic stroke may share common neurobiological mechanisms

Numerous physiological events occur sub-acutely and chronically after TBI and cerebral ischemia, thus the mechanisms that underpin the cerebrovascular responses to these brain injuries are complex and remain poorly understood (Golding 2002, Udomphorn et al. 2008, Park et al. 2009). However, the literature supporting our studies suggests that some possible pathological mechanisms that may affect cerebrovascular responses are common to both conditions. Indeed, many similarities between the pathological consequences of TBI and ischemia have recently been reviewed (Bramlett and Dietrich 2004).

6.3.1 Early shared mechanisms

The cerebral blood supply and metabolism are normally tightly coupled such that CBF is dependent on the metabolic demands of the tissue it serves (Reivich 1974). Soon after TBI in rats, metabolic uncoupling can occur, whereby regional CBF decreases when regional cerebral glucose utilization increases (Ginsberg et al. 1997, Richards et al. 2001). This

means that interpreting the role of CBF in the context of the metabolic demands of secondary brain damage is difficult. However, it is understood that as early as 6 hours after TBI in rats, a period of depressed oxidative metabolism with reduced CBF may occur (Hovda et al. 1995), much as we observed (**I**). Similarly, sub-acute hypoperfusion in the thalamus after TBI and ischemia may be due to depressed metabolic activity, as this has been shown in remote brain regions within one week after cerebral ischemia in rats (Watanabe et al. 1998, Barbelivien et al. 2002). Thalamic hypometabolism after ischemic stroke has been shown in patients and is thought to result from depressed synaptic activity (diaschisis) due to acute structural damage in the infarcted cortex nearby (Binkofski et al. 1996). It is thus feasible that diaschisis could also be partly responsible for the widespread hemodynamic changes that occur early after TBI.

As well as metabolic concerns, both molecular factors and mechanical factors can simultaneuously influence the cerebrovascular responses to brain injury (Graham et al. 2000) and many such processes occur during secondary brain damage. Therefore, many possible secondary damage processes could be linked to early regional CBF reduction after TBI or ischemic stroke. For example, increased ICP is commonly observed acutely and sub-acutely in TBI patients. This is often due to a hematoma exerting mechanical force on the brain parenchyma, which induces vasoconstriction, decreases CPP, and thus blood flow becomes restricted (Yuan et al. 1988). ICP is also raised by the prolonged cytotoxic edema and vasogenic edema that develop acutely and sub-acutely after TBI (Pasco et al. 2007, Greve and Zink 2009). Cytotoxic edema arises when acutely reduced perfusion impairs metabolic substrate delivery and causes a loss of ionic gradients and subsequent depolarization of glia and neurons. Voltage gated Ca^{2+} channels then open and release excitatory amino acids (EAAs) into the extracellular space. One EAA is glutamate, which activates glutamate receptors and causes an influx of Ca^{2+} into the cells, leading to an efflux of K^+ and cell swelling occurs due to passive retention of water, Cl^- and Na^+ (Liang et al. 2007). Both acutely and sub-acutely, vasogenic edema occurs after TBI due to disruptions in the endothelial wall (blood-brain barrier, BBB) (Graham et al. 2000). BBB openings allow inflammatory intravascular proteins and fluid to be released into the extracellular space of the brain parenchyma. Cytotoxic edema, vasogenic edema, and BBB breakdown also occur after cerebral ischemia (Pantano et al. 2008). Specifically, these events occur together from 2 days after cerebral ischemia in rats (Lin et al. 2002). Likewise, we observed much edema and slight BBB breakdown in the ipsilateral thalamus at 2 days

after cerebral ischemia, which coincided with decreased CBF. Thus, sub-acute hypoperfusion in the thalamus could be due to BBB breakdown and edema, which have been described in other brain regions after ischemia (Nordborg et al. 1994). As in that study, we also observed brain midline shift after cerebral ischemia by anatomical MRI at day 2, which resolved by day 7. This further supports the notion that extensive edema causes increased ICP and promotes the widespread sub-acute hypoperfusion we observed. In conclusion, edema could be responsible for the early reductions in CBF that we observed after both TBI and ischemic stroke.

As discussed, secondary brain damage after TBI and ischemia involves vasogenic edema due to BBB damage. BBB damage may also be the cause of platelet activation and microthrombi formation, which have been recorded after TBI in patients (Huber 1993) and also in rat models of ischemia (Obrenovitch and Hallenbeck 1985, Stagliano et al. 1997). Microthrombi formation may be a natural defense mechanism to prevent the occurrence of hemorrhages after the primary brain insult (Dietrich et al. 1998), but this process may impede blood flow to nearby tissues. A decrease in CBF may also be due to vasoactive signaling that occurs during secondary damage to the brain (Nilsson et al. 1996, Park et al. 2009). The endothelium controls vasoconstriction through releasing a range of endothelium-derived contracting factors (EDCFs) that moderate the luminal diameter in response to vasoactive substances, stretch and pressure. EDCFs include endothelin and arachidonic acid metabolites and these may actively promote vasoconstriction, and thus CBF reduction, after brain injury (reviewed in Golding 2002). However, such vasoactive signaling may not function reliably after the BBB becomes damaged. During and soon after ischemia, damage to the endothelium leads to leukocyte adhesion and non-reversible intravascular injury (Kulik et al. 2008). CBF may therefore decline passively, when the damaged endothelium is unable to coordinate vasoactive adjustments to suit metabolic demands (Forbes et al. 1997).

In all ipsilateral regions, we saw a recovery of CBF around 24 hours after severe TBI. Again, an explanation for precisely why this happens is unclear, especially because there are so many ongoing degenerative processes that instead reduce CBF through vasoconstriction. The CBF increase at 24 hours could be due to reactive hyperemia within the brain as an attempt to restore ionic gradients and rescue regions that were damaged acutely (Kelly et al. 1997, Martin et al. 1997), perhaps driven by vasodilation through nitric oxide (NO)

signaling (Hlatky et al. 2003). CBF recovery could also be due to prolonged inflammation or increased metabolic demands. Specifically, gliosis has been shown to begin 24 hours after TBI (Gehrmann et al. 1995, Graham et al. 2000), which is the consequence of inflammation and is energetically demanding. Although gliosis is a prolonged response to brain injury (Hiltunen et al. 2009), it may at least be partly responsible for the transient CBF recovery observed in ipsilateral regions at 24 hours after TBI.

In summary, there are many overlapping physiological processes that occur after both TBI and ischemic stroke. Although there is much commonality between these conditions (Bramlett and Dietrich 2004), there are a few mechanistic differences during the immediate phase of these neurotrauma etiologies. As examples, contusions, axotomy, and membrane shearing arise due to the mechanical impact of TBI, but these are absent during ischemia. Regardless, the acute and sub-acute pathophysiological sequelae after the initial brain insult are remarkably similar. Overall though, many further studies of each disease are still required in order to ascertain the exact nature and timing of the mechanisms responsible for acute and sub-acute hypoperfusion or recovery after brain injury.

6.3.2 Chronic shared mechanisms of thalamic cerebrovascular responses

After both TBI and cerebral ischemia, we found chronic hyperperfusion associated with markedly increased blood vessel density in the ipsilateral thalamus. It is likely that the increased CBF is due to the increased vascularity, as the two are known to correlate (Gross et al. 1986). The importance of angiogenesis has been discussed for each study (TBI, section *6.1.3*; ischemia, section *6.2.2*). During long-term neurodegeneration in general, there is also evidence that angiogenesis occurs in chronic demyelinating diseases such as multiple sclerosis, and this was associated with ongoing inflammation (Holley et al. 2010). We observed chronic thalamic calcifications after both TBI and cerebral ischemia, which is evidence for prolonged inflammation in the brain due to secondary damage. Indeed, calcifications were recently found to result from impaired Ca^{2+} homeostasis and co-occur with both chronic amyloid precursor protein (APP) processing and chronic angiogenesis after cerebral ischemia (Hiltunen et al. 2009). After TBI in rats, axonal injury in the thalamus is also associated with chronic APP accumulation, which leads to enhanced amyloid beta ($A\beta$) levels and expression of

enzymes that process APP (Pierce et al. 1996, Bramlett et al. 1997, Johnson et al. 2010). Thalamic axonal damage continues for up to 12 months after LFPI (Rodriguez-Paez et al. 2005) thus is likely linked to our chronic cerebrovascular changes. Only further research may ascertain whether chronic axonal damage, APP processing, and calcifications trigger the maintenance of a chronic angiogenic response in the thalamus after TBI or cerebral ischemia.

Chronic thalamic hyperperfusion may also be the result of vasoactive signaling through agents such as NO or adenosine. These arise from the endothelium and glia (Iadecola and Nedergaard 2007) and promote CBF increase to serve cellular processes with high energy demands. Such chronic processes may include the aforementioned APP processing or gliosis after ischemia (Hiltunen et al. 2009) and TBI (Pekny and Nilsson 2005). In conclusion, only a with more complete understanding of pathologies behind chronic TBI and cerebral ischemia can we clarify the delayed mechanisms of neurodegeneration and recovery, in order to find effective therapeutic targets and potential biomarkers for disease progression.

6.4 Cerebrovascular responses to status epilepticus

Studies in epilepsy patients have revealed that the amygdaloid complex is damaged in around 30% of those with seizures of temporal lobe origin (Pitkänen et al. 1998). Unfortunately, very little is known about the complex formation of an amygdaloid focus. In study **IV**, we investigated the lateral, basal, and accessory basal nuclei, and the periamygdaloid cortex after SE in rats. These regions undergo neurodegeneration in both animal models of epilepsy and in patients (Pitkänen et al. 1998). We aimed to test a hypothesis that post-SE tissue reorganization in the rat amygdaloid complex includes hemodynamic changes and vascular reorganization. After SE, amygdaloid hyperperfusion prevailed at 2 days and 14 days and was associated with increased blood vessel density at 14 days. We believe that this is the first report of long-term hemodynamic and cerebrovascular changes in the amygdala after SE.

There are no clinical studies and very few preclinical studies that have investigated cerebrovascular changes in the amygdala during epileptogenesis. The only one we could find is that published by Fabene and co-workers (2003), who used DSC MRI to find hyperperfusion in the amygdala at 12 hours after pilocarpine-induced SE. Our study suggests

that amygdaloid hyperperfusion may continue beyond this sub-acute phase and for up to 2 weeks, which is similar to the pattern we recently reported for the hippocampus (Ndode-Ekane et al. 2010). Long-term amygdaloid hyperperfusion is likely to be at least partly due to the parallel increase in blood vessel density (Gross et al. 1986) over 2 weeks after SE, yet we did not find any clear correlation between amygdaloid vessel density and CBF, which may be due to the small size of the study group. We believe that the increase in vessel density is due to angiogenesis over the study period because we found proliferating endothelial cells in the amygdala at 2 days and 14 days post-SE (Ndode-Ekane and Pitkänen, unpublished results). In line with this, angiogenesis has previously been documented in the rat amygdala after SE, where a 30% increase in vessel density occurred at 1 week after pilocarpine-induced SE and coincided with elevated VEGF (Marcon et al. 2009). Also, Collumbet and colleagues (2007) found elevated VEGF expression in the amygdala at 3 days after SE.

In conclusion, our data show that vascular reorganization is associated with hyperperfusion during tissue remodeling in the amygdaloid complex during epileptogenesis. Angiogenesis and hyperperfusion may serve to support processes with high metabolic demands, such as gliosis (Pitkänen et al. 1998), axonal sprouting, or reorganization of extracellular matrix in the amygdala soon after SE (Pitkänen and Lukasiuk 2009).

6.5 Methodological considerations

6.5.1 Magnetic resonance imaging suits hemodynamic studies of brain disorders

Arterial spin labeling (ASL) MRI successfully provided completely non-invasive, absolute quantification of regional CBF in our animal models. This technique allows consecutive imaging of individual animals, thus longitudinal studies of regional hemodynamic changes in models of neurological disorders are feasible. The absolute measurement of CBF is an improvement over the relative measures of CBF provided by DSC (ss-CE) MRI. However, in addition to ASL, ss-CE has been an asset to two studies in this thesis by providing relative CBV quantification for a more complete hemodynamic investigation (**I**, **IV**). Both techniques have been well validated in rodent models before (Bratane et al. 2010, Zaharchuk et al. 2000). However, ss-CE unfortunately carries the added

complication of femoral catheter insertion and removal before and after imaging, which extends a rat's time spent under anesthesia, interferes with any subsequent behavioral testing, and brings added risks to animals that are already recovering from a brain injury. To alleviate these shortcomings and avoid follow-up complications, one could catheterize the tail vein instead of the femoral vein. In the clinic, catheter insertion is routine and the majority of patients tolerate MRI contrast agents well. Overall, as outlined in the Introduction and in Table 2, MRI techniques for cerebrovascular investigations generally bring many advantages over other technologies and will continue to develop as NMR research continues.

6.5.2 Anesthesia

Repetitive anesthesia is necessary for long-term MRI studies of animals. Inhalation anesthesia is easy to use and isoflurane is a commonly chosen anesthetic for rodent studies, yet there is emerging evidence that it can increase baseline blood flow (Iltis et al. 2005). Also, a dose of 1% isoflurane over only 10 minutes may be sufficient to invoke transient BBB opening (Tetrault et al. 2008). In our studies, the anesthesia dosage was consistently moderated to be as small as possible by measuring the breathing rate throughout imaging. Importantly, all results comparisons were made with sham-operated rats undergoing the same anesthesia and MRI procedures under the same setup. The measurement of arterial blood-derived physiological variables such as pH, pO_2, and pCO_2 was used to check each rats' physiological health during the longest imaging sessions (**I, IV**), and physiological normality was achieved without any additions to our experimental setup.

6.5.3 Functional recovery after TBI and cerebral ischemia

We hypothesized that enhanced cortical or thalamic vascular function would associate with better functional recovery after TBI or cerebral ischemia in rats. Hyperperfusion and angiogenesis in the thalamus were associated with recovery of forelimb function after cerebral ischemia (**III**). However, the hindlimb function remained impaired after ischemia and did not associate with our vascular measures. Similarly, neuroscore recovery after TBI was incomplete and not clearly associated with any vascular measures (**II**). Overall, it is not possible to compare the motor recovery profiles between these two animal models based on our studies because the motor test designs were so different. In particular,

we studied forelimb function independently from hindlimb function after ischemia, whereas different tasks with different timings were combined to measure neuroscores after TBI.

6.6 Future directions

The value of MRI in healthcare and research is already high and this should continue to grow in the future. The reliable, safe, non-invasive and therefore repeatable MRI methods that we can use to measure the cerebrovascular sequelae of secondary damage to the central nervous system (CNS) are of special interest, simply because neurological health relies on cerebrovascular health. As cerebrovascular MRI develops, researchers and clinicians may harness its potential to provide even more detailed studies of cerebrovascular events during secondary brain damage. New cerebrovascular findings must in turn become placed within the context of the other injury processes that together influence neurodegeneration and/or recovery. Such advanced understandings may help us achieve our ultimate long-term goals in neurobiological MRI as follows:

1. Generate successful novel treatments that reduce secondary damage, prevent epileptogenesis, or encourage functional recovery after CNS injury.

2. Accurately follow CNS injury progression by finding biomarkers or surrogate markers that carry the ability to predict both native outcomes and treatment responses in individual subjects.

However, only a with more thorough understanding of the pathologies of traumatic brain injury, cerebral ischemia and status epilepticus can we begin to clarify the intricate mechanisms that underlie neurodegeneration and recovery. For example, we must continue to try to delineate the processes of plasticity that lead to epilepsy from those that lead to brain recovery. This presents a great challenge to our long-term objectives because the pathology behind CNS injury is very complex, thus the relative importance of each pathological process that overlaps so many others is difficult to deduce. With many processes, such as hemodynamic fluctuations, we are not yet sure if they either beneficial or detrimental to the brain, or possibly even both.

Even though decades of research have led to dozens of clinical trials of direct medicinal interventions for secondary brain damage (Narayan 2002), none have yet been successful. These potential innovations were based upon knowledge derived from experimental animal models. One could therefore legitimately question the value of our animal studies. However, many new medicinal attempts to alleviate CNS injury may have sadly been ill-conceived. For example, if we are to promote hemodynamic recovery after TBI, what would be the therapeutic time window? When would hyperperfusion be beneficial, and for which brain regions? How can we carefully manage physiological heterogeneity among our study cohorts? Considering we are only just beginning to understand the temporal and regional profiles of the brain's natural responses to CNS injury, perhaps pharmaceutical research has taken too many steps forward too soon. Instead, a more detailed characterization of endogenous physiological changes and their mechanisms must be achieved at more time points in animal models, patients, and control groups, in order to provide the necessary foundations from which to launch therapeutic endeavors.

7 REFERENCES

Abdel-Dayem HM, Abu-Judeh H, Kumar M, Atay S, Naddaf S, El-Zeftawy H, Luo JQ (1998). SPECT brain perfusion abnormalities in mild or moderate traumatic brain injury. Clin Nucl Med 23 (5): 309-317.

Amantea D, Nappi G, Bernardi G, Bagetta G, Corasaniti MT (2009). Post-ischemic brain damage: pathophysiology and role of inflammatory mediators. FEBS J 276 (1): 13-26.

Austin RE,Jr, Hauck WW, Aldea GS, Flynn AE, Coggins DL, Hoffman JI (1989). Quantitating error in blood flow measurements with radioactive microspheres. Am J Physiol 257 (1 Pt 2): H280-8.

Baird AE and Warach S (1998). Magnetic resonance imaging of acute stroke. J Cereb Blood Flow Metab 18 (6): 583-609.

Barbelivien A, Jolkkonen J, Rutkauskaite E, Sirvio J, Sivenius J (2002). Differentially altered cerebral metabolism in ischemic rats by alpha2-adrenoceptor blockade and its relation to improved limb-placing reactions. Neuropharmacology 42 (1): 117-126.

Barbier EL, Lamalle L, Decorps M (2001). Methodology of brain perfusion imaging. J Magn Reson Imaging 13 (4): 496-520.

Beck H and Plate KH (2009). Angiogenesis after cerebral ischemia. Acta Neuropathol 117 (5): 481-496.

Belayev L, Busto R, Zhao W, Ginsberg MD (1996). Quantitative evaluation of blood-brain barrier permeability following middle cerebral artery occlusion in rats. Brain Res 739 (1-2): 88-96.

Binkofski F, Seitz RJ, Arnold S, Classen J, Benecke R, Freund HJ (1996). Thalamic metbolism and corticospinal tract integrity determine motor recovery in stroke. Ann Neurol 39 (4): 460-470.

Block F (1946). Nuclear induction. Physics Review 70: 460-473.

Block F, Dihne M, Loos M (2005). Inflammation in areas of remote changes following focal brain lesion. Prog Neurobiol 75 (5): 342-365.

Blumenfeld H, Varghese GI, Purcaro MJ, Motelow JE, Enev M, McNally KA, Levin AR, Hirsch LJ, Tikofsky R, Zubal IG, Paige AL, Spencer SS (2009). Cortical and subcortical networks in human secondarily generalized tonic-clonic seizures. Brain 132 (Pt 4): 999-1012.

Bolander HG, Persson L, Hillered L, d'Argy R, Ponten U, Olsson Y (1989). Regional cerebral blood flow and histopathologic changes after middle cerebral artery occlusion in rats. Stroke 20 (7): 930-937.

Bonilha L, Rorden C, Castellano G, Pereira F, Rio PA, Cendes F, Li LM (2004). Voxel-based morphometry reveals gray matter network atrophy in refractory medial temporal lobe epilepsy. Arch Neurol 61 (9): 1379-1384.

Bonne O, Gilboa A, Louzoun Y, Kempf-Sherf O, Katz M, Fishman Y, Ben-Nahum Z, Krausz Y, Bocher M, Lester H, Chisin R, Lerer B (2003). Cerebral blood flow in chronic symptomatic mild traumatic brain injury. Psychiatry Res 124 (3): 141-152.

Borlongan CV, Lind JG, Dillon-Carter O, Yu G, Hadman M, Cheng C, Carroll J, Hess DC (2004). Bone marrow grafts restore cerebral blood flow and blood-brain barrier in stroke rats. Brain Res 1010 (1-2): 108-116.

Bouma GJ, Muizelaar JP, Choi SC, Newlon PG, Young HF (1991). Cerebral circulation and metabolism after severe traumatic brain injury: the elusive role of ischemia. J Neurosurg 75 (5): 685-693.

Boxerman JL, Hamberg LM, Rosen BR, Weisskoff RM (1995). MR contrast due to intravascular magnetic susceptibility perturbations. Magn Reson Med 34 (4): 555-566.

Braeuninger S and Kleinschnitz C (2009). Rodent models of focal cerebral ischemia: procedural pitfalls and translational problems. Exp Transl Stroke Med 1: 8.

Bramlett HM, Kraydieh S, Green EJ, Dietrich WD (1997). Temporal and regional patterns of axonal damage following traumatic brain injury: a beta-amyloid precursor protein immunocytochemical study in rats. J Neuropathol Exp Neurol 56 (10): 1132-1141.

Bramlett HM and Dietrich WD (2004). Pathophysiology of cerebral ischemia and brain trauma: similarities and differences. J Cereb Blood Flow Metab 24 (2): 133-150.

Bratane BT, Walvick RP, Corot C, Lancelot E, Fisher M (2010). Characterization of gadolinium-based dynamic susceptibility contrast perfusion measurements in permanent and transient MCAO models with volumetric based validation by CASL. J Cereb Blood Flow Metab 30 (2): 336-342.

Bryan RM,Jr, Cherian L, Robertson C (1995). Regional cerebral blood flow after controlled cortical impact injury in rats. Anesth Analg 80 (4): 687-695.

Calamante F, Thomas DL, Pell GS, Wiersma J, Turner R (1999). Measuring cerebral blood flow using magnetic resonance imaging techniques. J Cereb Blood Flow Metab 19 (7): 701-735.

Carmichael ST (2005). Rodent models of focal stroke: size, mechanism, and purpose. NeuroRx 2 (3): 396-409.

Center for Disease Control and Prevention (CDC) (2003). Report to congress on mild traumatic brain injury in the United States: steps to prevent a serious public health problem.

Chen L, Endler A, Shibasaki F (2009). Hypoxia and angiogenesis: regulation of hypoxia-inducible factors via novel binding factors. Exp Mol Med 41 (12): 849-857.

Cherian L, Robertson CS, Contant CF,Jr, Bryan RM,Jr (1994). Lateral cortical impact injury in rats: cerebrovascular effects of varying depth of cortical deformation and impact velocity. J Neurotrauma 11 (5): 573-585.

Choy M, Cheung KK, Thomas DL, Gadian DG, Lythgoe MF, Scott RC (2010). Quantitative MRI predicts status epilepticus-induced hippocampal injury in the lithium-pilocarpine rat model. Epilepsy Res 88 (2-3): 221-230.

Coles JP (2004). Regional ischemia after head injury. Curr Opin Crit Care 10 (2): 120-125.

Collombet JM, Four E, Fauquette W, Burckhart MF, Masqueliez C, Bernabe D, Baubichon D, Lallement G (2007). Soman poisoning induces delayed astrogliotic scar and angiogenesis in damaged mouse brain areas. Neurotoxicology 28 (1): 38-48.

D'Ambrosio R, Fender JS, Fairbanks JP, Simon EA, Born DE, Doyle DL, Miller JW (2005). Progression from frontal-parietal to mesial-temporal epilepsy after fluid percussion injury in the rat. Brain 128 (Pt 1): 174-188.

D'Ambrosio R and Perucca E (2004). Epilepsy after head injury. Curr Opin Neurol 17 (6): 731-735.

de la Torre JC (2006). How do heart disease and stroke become risk factors for Alzheimer's disease? Neurol Res 28 (6): 637-644.

del Zoppo GJ and Mabuchi T (2003). Cerebral microvessel responses to focal ischemia. J Cereb Blood Flow Metab 23 (8): 879-894.

DeWitt DS and Prough DS (2003). Traumatic cerebral vascular injury: the effects of concussive brain injury on the cerebral vasculature. J Neurotrauma 20 (9): 795-825.

DeWitt DS, Smith TG, Deyo DJ, Miller KR, Uchida T, Prough DS (1997). L-arginine and superoxide dismutase prevent or reverse cerebral hypoperfusion after fluid-percussion traumatic brain injury. J Neurotrauma 14 (4): 223-233.

Dietrich WD, Alonso O, Busto R, Prado R, Zhao W, Dewanjee MK, Ginsberg MD (1998). Posttraumatic cerebral ischemia after fluid percussion brain injury: an autoradiographic and histopathological study in rats. Neurosurgery 43 (3): 585-93; discussion 593-4.

Dijkhuizen RM, Knollema S, van der Worp HB, Ter Horst GJ, De Wildt DJ, Berkelbach van der Sprenkel JW, Tulleken KA, Nicolay K (1998). Dynamics of cerebral tissue injury and perfusion after temporary hypoxia-ischemia in the rat: evidence for region-specific sensitivity and delayed damage. Stroke 29 (3): 695-704.

Dixon CE, Clifton GL, Lighthall JW, Yaghmai AA, Hayes RL (1991). A controlled cortical impact model of traumatic brain injury in the rat. J Neurosci Methods 39 (3): 253-262.

Dombrowski SM, Deshpande A, Dingwall C, Leichliter A, Leibson Z, Luciano MG (2008). Chronic hydrocephalus-induced hypoxia: increased expression of VEGFR-2+ and blood vessel density in hippocampus. Neuroscience 152 (2): 346-359.

Donnan GA, Fisher M, Macleod M, Davis SM (2008). Stroke. Lancet 371 (9624): 1612-1623.

Doppenberg EM, Choi SC, Bullock R (2004). Clinical trials in traumatic brain injury: lessons for the future. J Neurosurg Anesthesiol 16 (1): 87-94.

Duijvestijn AM, van Goor H, Klatter F, Majoor GD, van Bussel E, van Breda Vriesman PJ (1992). Antibodies defining rat endothelial cells: RECA-1, a pan-endothelial cell-specific monoclonal antibody. Lab Invest 66 (4): 459-466.

Dunn JF, Roche MA, Springett R, Abajian M, Merlis J, Daghlian CP, Lu SY, Makki M (2004). Monitoring angiogenesis in brain using steady-state quantification of DeltaR2 with MION infusion. Magn Reson Med 51 (1): 55-61.

Dupont S and Crespel A (2009). Satus epilepticus: epidemiology, definitions and classifications. Rev Neurol (Paris) 165 (4): 307-314.

Engel J,Jr (2006). Report of the ILAE classification core group. Epilepsia 47 (9): 1558-1568.

Eve DJ, Musso J,3rd, Park DH, Oliveira C, Pollock K, Hope A, Baradez MO, Sinden JD, Sanberg PR (2009). Methodological study investigating long term laser Doppler measured cerebral blood flow changes in a permanently occluded rat stroke model. J Neurosci Methods 180 (1): 52-56.

Fabene PF, Marzola P, Sbarbati A, Bentivoglio M (2003). Magnetic resonance imaging of changes elicited by status epilepticus in the rat brain: diffusion-weighted and T2-weighted images, regional blood volume maps, and direct correlation with tissue and cell damage. Neuroimage 18 (2): 375-389.

Fisher RS, van Emde Boas W, Blume W, Elger C, Genton P, Lee P, Engel J,Jr (2005). Epileptic seizures and epilepsy: definitions proposed by the International League Against Epilepsy (ILAE) and the International Bureau for Epilepsy (IBE). Epilepsia 46 (4): 470-472.

Forbes ML, Hendrich KS, Kochanek PM, Williams DS, Schiding JK, Wisniewski SR, Kelsey SF, DeKosky ST, Graham SH, Marion DW, Ho C (1997). Assessment of cerebral blood flow and CO2 reactivity after controlled cortical impact by perfusion magnetic resonance imaging using arterial spin-labeling in rats. J Cereb Blood Flow Metab 17 (8): 865-874.

Gallagher CN, Hutchinson PJ, Pickard JD (2007). Neuroimaging in trauma. Curr Opin Neurol 20 (4): 403-409.

Gehrmann J, Banati RB, Wiessner C, Hossmann KA, Kreutzberg GW (1995). Reactive microglia in cerebral ischaemia: an early mediator of tissue damage? Neuropathol Appl Neurobiol 21 (4): 277-289.

Ghabriel MN, Zdziarski IM, Leigh C, Vink R (2010). Changes in the blood-CSF barrier in experimental traumatic brain injury. Acta Neurochir Suppl 106: 239-245.

Ghajar J (2009). Essay: the future of traumatic brain injury. Mt Sinai J Med 76 (2): 190-193.

Ginsberg MD, Medoff R, Reivich M (1976). Heterogeneities of regional cerebral blood flow during hypoxia-ischemia in the rat. Stroke 7 (2): 132-134.

Ginsberg MD, Zhao W, Alonso OF, Loor-Estades JY, Dietrich WD, Busto R (1997). Uncoupling of local cerebral glucose metabolism and blood flow after acute fluid-percussion injury in rats. Am J Physiol 272 (6 Pt 2): H2859-68.

Goffin K, Nissinen J, Van Laere K, Pitkanen A (2007). Cyclicity of spontaneous recurrent seizures in pilocarpine model of temporal lobe epilepsy in rat. Exp Neurol 205 (2): 501-505.

Goldenberg G, Oder W, Spatt J, Podreka I (1992). Cerebral correlates of disturbed executive function and memory in survivors of severe closed head injury: a SPECT study. J Neurol Neurosurg Psychiatry 55 (5): 362-368.

Golding EM (2002). Sequelae following traumatic brain injury. The cerebrovascular perspective. Brain Res Brain Res Rev 38 (3): 377-388.

Graham DI, McIntosh TK, Maxwell WL, Nicoll JA (2000). Recent advances in neurotrauma. J Neuropathol Exp Neurol 59 (8): 641-651.

Gray BG, Ichise M, Chung DG, Kirsh JC, Franks W (1992). Technetium-99m-HMPAO SPECT in the evaluation of patients with a remote history of traumatic brain injury: a comparison with x-ray computed tomography. J Nucl Med 33 (1): 52-58.

Greve MW and Zink BJ (2009). Pathophysiology of traumatic brain injury. Mt Sinai J Med 76 (2): 97-104.

Grohn OH, Lukkarinen JA, Oja JM, van Zijl PC, Ulatowski JA, Traystman RJ, Kauppinen RA (1998). Noninvasive detection of cerebral hypoperfusion and reversible ischemia from reductions in the magnetic resonance imaging relaxation time, T2. J Cereb Blood Flow Metab 18 (8): 911-920.

Grohn O and Pitkanen A (2007). Magnetic resonance imaging in animal models of epilepsy-noninvasive detection of structural alterations. Epilepsia 48 Suppl 4: 3-10.

Gross PM, Sposito NM, Pettersen SE, Fenstermacher JD (1986). Differences in function and structure of the capillary endothelium in gray matter, white matter and a circumventricular organ of rat brain. Blood Vessels 23 (6): 261-270.

Guo Y, Gao F, Wang S, Ding Y, Zhang H, Wang J, Ding MP (2009). In vivo mapping of temporospatial changes in glucose utilization in rat brain during epileptogenesis: an 18F-fluorodeoxyglucose-small animal positron emission tomography study. Neuroscience 162 (4): 972-979.

Hacke W, Kaste M, Bluhmki E, Brozman M, Davalos A, Guidetti D, Larrue V, Lees KR, Medeghri Z, Machnig T, Schneider D, von Kummer R, Wahlgren N, Toni D, ECASS Investigators (2008). Thrombolysis with alteplase 3 to 4.5 hours after acute ischemic stroke. N Engl J Med 359 (13): 1317-1329.

Haltiner AM, Temkin NR, Dikmen SS (1997). Risk of seizure recurrence after the first late posttraumatic seizure. Arch Phys Med Rehabil 78 (8): 835-840.

Hammond FM, Hart T, Bushnik T, Corrigan JD, Sasser H (2004). Change and predictors of change in communication, cognition, and social function between 1 and 5 years after traumatic brain injury. J Head Trauma Rehabil 19 (4): 314-328.

Hashemi RHand Bradley WG (2004). MRI: The Basics. Second Edition edn. Lippincott Williams & Wilkins:

Hauser WA (1997). Incidence and prevalence, in: Engel Jr J, and Pedley TA (eds), Epilepsy: a comprehensive textbook, Philadelphia: Lippincott–Raven: pps. 47-57.

Hayashi T, Noshita N, Sugawara T, Chan PH (2003). Temporal profile of angiogenesis and expression of related genes in the brain after ischemia. J Cereb Blood Flow Metab 23 (2): 166-180.

Hayward NMEA, Kurkinen KMA, Gröhn O, Pitkänen A (2009). EPILEPTOGENESIS | Surrogate Markers for Epileptogenesis, in: Philip A. Schwartzkroin (ed), Encyclopedia of Basic Epilepsy Research, Academic Press: Oxford, pps. 259-265.

Herscovitch P and Raichle ME (1985). What is the correct value for the brain--blood partition coefficient for water? J Cereb Blood Flow Metab 5 (1): 65-69.

Hertz L (2008). Bioenergetics of cerebral ischemia: a cellular perspective. Neuropharmacology 55 (3): 289-309.

Hiltunen M, Makinen P, Peraniemi S, Sivenius J, van Groen T, Soininen H, Jolkkonen J (2009). Focal cerebral ischemia in rats alters APP processing and expression of Abeta peptide degrading enzymes in the thalamus. Neurobiol Dis 35 (1): 103-113.

Hlatky R, Lui H, Cherian L, Goodman JC, O'Brien WE, Contant CF, Robertson CS (2003). The role of endothelial nitric oxide synthase in the cerebral hemodynamics after controlled cortical impact injury in mice. J Neurotrauma 20 (10): 995-1006.

Holley JE, Newcombe J, Whatmore JL, Gutowski NJ (2010). Increased blood vessel density and endothelial cell proliferation in multiple sclerosis cerebral white matter. Neurosci Lett 470 (1): 65-70.

Hossmann KA (2009). Pathophysiological basis of translational stroke research. Folia Neuropathol 47 (3): 213-227.

Hossmann KA (2006). Pathophysiology and therapy of experimental stroke. Cell Mol Neurobiol 26 (7-8): 1057-1083.

Hovda DA, Lee SM, Smith ML, Von Stuck S, Bergsneider M, Kelly D, Shalmon E, Martin N, Caron M, Mazziotta J (1995). The neurochemical and metabolic cascade following brain injury: moving from animal models to man. J Neurotrauma 12 (5): 903-906.

Huber A, Dorn A, Witzmann A, Cervos-Navarro J (1993). Microthrombi formation after severe head trauma. Int J Legal Med 106 (3): 152-155.

Iadecola C and Nedergaard M (2007). Glial regulation of the cerebral microvasculature. Nat Neurosci 10 (11): 1369-1376.

Ichise M, Chung DG, Wang P, Wortzman G, Gray BG, Franks W (1994). Technetium-99m-HMPAO SPECT, CT and MRI in the evaluation of patients with chronic traumatic brain injury: a correlation with neuropsychological performance. J Nucl Med 35 (2): 217-226.

Iltis I, Kober F, Dalmasso C, Lan C, Cozzone PJ, Bernard M (2005). In vivo assessment of myocardial blood flow in rat heart using magnetic resonance imaging: effect of anesthesia. J Magn Reson Imaging 22 (2): 242-247.

Immonen RJ, Kharatishvili I, Niskanen JP, Grohn H, Pitkanen A, Grohn OH (2009). Distinct MRI pattern in lesional and perilesional area after traumatic brain injury in rat--11 months follow-up. Exp Neurol 215 (1): 29-40.

Immonen RJ, Kharatishvili I, Sierra A, Einula C, Pitkanen A, Grohn OH (2008). Manganese enhanced MRI detects mossy fiber sprouting rather than neurodegeneration, gliosis or seizure-activity in the epileptic rat hippocampus. Neuroimage 40 (4): 1718-1730.

Ishige N, Pitts LH, Berry I, Carlson SG, Nishimura MC, Moseley ME, Weinstein PR (1987). The effect of hypoxia on traumatic head injury in rats: alterations in neurologic function, brain edema, and cerebral blood flow. J Cereb Blood Flow Metab 7 (6): 759-767.

Iwamoto Y, Yamaki T, Murakami N, Umeda M, Tanaka C, Higuchi T, Aoki I, Naruse S, Ueda S (1997). Investigation of morphological change of lateral and midline fluid percussion injury in rats, using magnetic resonance imaging. Neurosurgery 40 (1): 163-167.

Jacobs A, Put E, Ingels M, Put T, Bossuyt A (1996). One-year follow-up of technetium-99m-HMPAO SPECT in mild head injury. J Nucl Med 37 (10): 1605-1609.

Jiang Q, Zhang RL, Zhang ZG, Ewing JR, Divine GW, Chopp M (1998). Diffusion-, T2-, and perfusion-weighted nuclear magnetic resonance imaging of middle cerebral artery embolic stroke and recombinant tissue plasminogen activator intervention in the rat. J Cereb Blood Flow Metab 18 (7): 758-767.

Johnson VE, Stewart W, Smith DH (2010). Traumatic brain injury and amyloid-beta pathology: a link to Alzheimer's disease? Nat Rev Neurosci

Karhunen H, Pitkanen A, Virtanen T, Gureviciene I, Pussinen R, Ylinen A, Sivenius J, Nissinen J, Jolkkonen J (2003). Long-term functional consequences of transient occlusion of the middle cerebral artery in rats: a 1-year follow-up of the development of epileptogenesis and memory impairment in relation to sensorimotor deficits. Epilepsy Res 54 (1): 1-10.

Kelly DF, Martin NA, Kordestani R, Counelis G, Hovda DA, Bergsneider M, McBride DQ, Shalmon E, Herman D, Becker DP (1997). Cerebral blood flow as a predictor of outcome following traumatic brain injury. J Neurosurg 86 (4): 633-641.

Kessler RM (2003). Imaging methods for evaluating brain function in man. Neurobiol Aging 24 Suppl 1: S21-35; discussion S37-9.

Kharatishvili I, Immonen R, Grohn O, Pitkanen A (2007). Quantitative diffusion MRI of hippocampus as a surrogate marker for post-traumatic epileptogenesis. Brain 130 (Pt 12): 3155-3168.

Kharatishvili I, Nissinen JP, McIntosh TK, Pitkanen A (2006). A model of posttraumatic epilepsy induced by lateral fluid-percussion brain injury in rats. Neuroscience 140 (2): 685-697.

Kharatishvili I and Pitkanen A (2010). Posttraumatic epilepsy. Curr Opin Neurol 23 (2): 183-188.

Kochanek PM, Hendrich KS, Dixon CE, Schiding JK, Williams DS, Ho C (2002). Cerebral blood flow at one year after controlled cortical impact in rats: assessment by magnetic resonance imaging. J Neurotrauma 19 (9): 1029-1037.

Krishna-K and Redies C (2009). Expression of cadherin superfamily genes in brain vascular development. J Cereb Blood Flow Metab 29 (2): 224-229.

Krupinski J, Kaluza J, Kumar P, Kumar S, Wang JM (1994). Role of angiogenesis in patients with cerebral ischemic stroke. Stroke 25 (9): 1794-1798.

Kulik T, Kusano Y, Aronhime S, Sandler AL, Winn HR (2008). Regulation of cerebral vasculature in normal and ischemic brain. Neuropharmacology 55 (3): 281-288.

Laing RJ, Jakubowski J, Laing RW (1993). Middle cerebral artery occlusion without craniectomy in rats. Which method works best? Stroke 24 (2): 294-7; discussion 297-8.

Lassen NA (1977). Cerebral ischaemia. Intensive Care Med 3 (4): 251-252.

Lescot T, Fulla-Oller L, Po C, Chen XR, Puybasset L, Gillet B, Plotkine M, Meric P, Marchand-Leroux C (2010). Temporal and regional changes after focal traumatic brain injury. J Neurotrauma 27 (1): 85-94.

Lewis DA, Campbell MJ, Morrison JH (1986). An immunohistochemical characterization of somatostatin-28 and somatostatin-281-12 in monkey prefrontal cortex. J Comp Neurol 248 (1): 1-18.

Li Y, Lu Z, Keogh CL, Yu SP, Wei L (2007). Erythropoietin-induced neurovascular protection, angiogenesis, and cerebral blood flow restoration after focal ischemia in mice. J Cereb Blood Flow Metab 27 (5): 1043-1054.

Liang D, Bhatta S, Gerzanich V, Simard JM (2007). Cytotoxic edema: mechanisms of pathological cell swelling. Neurosurg Focus 22 (5): E2.

Lim YM, Cho YW, Shamim S, Solomon J, Birn R, Luh WM, Gaillard WD, Ritzl EK, Theodore WH (2008). Usefulness of pulsed arterial spin labeling MR imaging in mesial temporal lobe epilepsy. Epilepsy Res 82 (2-3): 183-189.

Lin CY, Chang C, Cheung WM, Lin MH, Chen JJ, Hsu CY, Chen JH, Lin TN (2008). Dynamic changes in vascular permeability, cerebral blood volume, vascular density, and size after transient focal cerebral ischemia in rats: evaluation with contrast-enhanced magnetic resonance imaging. J Cereb Blood Flow Metab 28 (8): 1491-1501.

Lin TN, Sun SW, Cheung WM, Li F, Chang C (2002). Dynamic changes in cerebral blood flow and angiogenesis after transient focal cerebral ischemia in rats. Evaluation with serial magnetic resonance imaging. Stroke 33 (12): 2985-2991.

Ling L, Zeng J, Pei Z, Cheung RT, Hou Q, Xing S, Zhang S (2009). Neurogenesis and angiogenesis within the ipsilateral thalamus with secondary damage after focal cortical infarction in hypertensive rats. J Cereb Blood Flow Metab 29 (9): 1538-1546.

Little DM, Kraus MF, Joseph J, Geary EK, Susmaras T, Zhou XJ, Pliskin N, Gorelick PB (2010). Thalamic integrity underlies executive dysfunction in traumatic brain injury. Neurology 74 (7): 558-564.

Longa EZ, Weinstein PR, Carlson S, Cummins R (1989). Reversible middle cerebral artery occlusion without craniectomy in rats. Stroke 20 (1): 84-91.

Lowenstein DH (2009). Epilepsy after head injury: an overview. Epilepsia 50 Suppl 2: 4-9.

Lythgoe MF, Sibson NR, Harris NG (2003). Neuroimaging of animal models of brain disease. Br Med Bull 65: 235-257.

Madri JA (2009). Modeling the neurovascular niche: implications for recovery from CNS injury. J Physiol Pharmacol 60 Suppl 4: 95-104.

Marcon J, Gagliardi B, Balosso S, Maroso M, Noe F, Morin M, Lerner-Natoli M, Vezzani A, Ravizza T (2009). Age-dependent vascular changes induced by status epilepticus in rat forebrain: implications for epileptogenesis. Neurobiol Dis 34 (1): 121-132.

Marion DW, Darby J, Yonas H (1991). Acute regional cerebral blood flow changes caused by severe head injuries. J Neurosurg 74 (3): 407-414.

Martin NA, Patwardhan RV, Alexander MJ, Africk CZ, Lee JH, Shalmon E, Hovda DA, Becker DP (1997). Characterization of cerebral hemodynamic phases following severe head trauma: hypoperfusion, hyperemia, and vasospasm. J Neurosurg 87 (1): 9-19.

Maxwell WL, MacKinnon MA, Smith DH, McIntosh TK, Graham DI (2006). Thalamic nuclei after human blunt head injury. J Neuropathol Exp Neurol 65 (5): 478-488.

Maxwell WL, Pennington K, MacKinnon MA, Smith DH, McIntosh TK, Wilson JT, Graham DI (2004). Differential responses in three thalamic nuclei in moderately disabled, severely disabled and vegetative patients after blunt head injury. Brain 127 (Pt 11): 2470-2478.

Mazzini L, Campini R, Angelino E, Rognone F, Pastore I, Oliveri G (2003). Posttraumatic hydrocephalus: a clinical, neuroradiologic, and neuropsychologic assessment of long-term outcome. Arch Phys Med Rehabil 84 (11): 1637-1641.

McIntosh TK, Noble L, Andrews B, Faden AI (1987). Traumatic brain injury in the rat: characterization of a midline fluid-percussion model. Cent Nerv Syst Trauma 4 (2): 119-134.

McIntosh TK, Vink R, Noble L, Yamakami I, Fernyak S, Soares H, Faden AL (1989). Traumatic brain injury in the rat: characterization of a lateral fluid-percussion model. Neuroscience 28 (1): 233-244.

Moseley ME, Wendland MF, Kucharczyk J (1991). Magnetic resonance imaging of diffusion and perfusion. Top Magn Reson Imaging 3 (3): 50-67.

Muir JK, Boerschel M, Ellis EF (1992). Continuous monitoring of posttraumatic cerebral blood flow using laser-Doppler flowmetry. J Neurotrauma 9 (4): 355-362.

Mulvey JM, Dorsch NW, Mudaliar Y, Lang EW (2004). Multimodality monitoring in severe traumatic brain injury: the role of brain tissue oxygenation monitoring. Neurocrit Care 1 (3): 391-402.

Nagahiro S, Uno M, Sato K, Goto S, Morioka M, Ushio Y (1998). Pathophysiology and treatment of cerebral ischemia. J Med Invest 45 (1-4): 57-70.

Narayan RK, Michel ME, Ansell B, Baethmann A, Biegon A, Bracken MB, Bullock MR, Choi SC, Clifton GL, Contant CF, Coplin WM, Dietrich WD, Ghajar J, Grady SM, Grossman RG, Hall ED, Heetderks W, Hovda DA, Jallo J, Katz RL, Knoller N, Kochanek PM, Maas AI, Majde J, Marion DW, Marmarou A, Marshall LF, McIntosh TK, Miller E, Mohberg N, Muizelaar JP, Pitts LH, Quinn P, Riesenfeld G, Robertson CS, Strauss KI, Teasdale G, Temkin N, Tuma R, Wade C, Walker MD, Weinrich M, Whyte J, Wilberger J, Young AB, Yurkewicz L (2002). Clinical trials in head injury. J Neurotrauma 19 (5): 503-557.

Ndode-Ekane XE, Hayward N, Grohn O, Pitkanen A (2010). Vascular changes in epilepsy: functional consequences and association with network plasticity in pilocarpine-induced experimental epilepsy. Neuroscience 166 (1): 312-332.

Nilsson B and Nordstrom CH (1977). Experimental head injury in the rat. Part 3: Cerebral blood flow and oxygen consumption after concussive impact acceleration. J Neurosurg 47 (2): 262-273.

Nilsson P, Gazelius B, Carlson H, Hillered L (1996). Continuous measurement of changes in regional cerebral blood flow following cortical compression contusion trauma in the rat. J Neurotrauma 13 (4): 201-207.

Nissinen J, Halonen T, Koivisto E, Pitkanen A (2000). A new model of chronic temporal lobe epilepsy induced by electrical stimulation of the amygdala in rat. Epilepsy Res 38 (2-3): 177-205.

Nordborg C, Sokrab TE, Johansson BB (1994). Oedema-related tissue damage after temporary and permanent occlusion of the middle cerebral artery. Neuropathol Appl Neurobiol 20 (1): 56-65.

Obenaus A, Robbins M, Blanco G, Galloway NR, Snissarenko E, Gillard E, Lee S, Curras-Collazo M (2007). Multi-modal magnetic resonance imaging alterations in two rat models of mild neurotrauma. J Neurotrauma 24 (7): 1147-1160.

Obrenovitch TP and Hallenbeck JM (1985). Platelet accumulation in regions of low blood flow during the postischemic period. Stroke 16 (2): 224-234.

Oder W, Goldenberg G, Spatt J, Podreka I, Binder H, Deecke L (1992). Behavioural and psychosocial sequelae of severe closed head injury and regional cerebral blood flow: a SPECT study. J Neurol Neurosurg Psychiatry 55 (6): 475-480.

Olivot JM and Marks MP (2008). Magnetic resonance imaging in the evaluation of acute stroke. Top Magn Reson Imaging 19 (5): 225-230.

Opitz E and Schneider M (1950). Über die sauerstoffversorgung des gehirns und den mechanisms von mangelwirkungen. Ergebn Physiol 46: 126-260.

Osteen CL, Moore AH, Prins ML, Hovda DA (2001). Age-dependency of 45calcium accumulation following lateral fluid percussion: acute and delayed patterns. J Neurotrauma 18 (2): 141-162.

Ostergaard L (2005). Principles of cerebral perfusion imaging by bolus tracking. J Magn Reson Imaging 22 (6): 710-717.

Pantano P, Totaro P, Raz E (2008). Cerebrovascular diseases. Neurol Sci 29 Suppl 3: 314-318.

Park E, Bell JD, Siddiq IP, Baker AJ (2009). An analysis of regional microvascular loss and recovery following two grades of fluid percussion trauma: a role for hypoxia-inducible factors in traumatic brain injury. J Cereb Blood Flow Metab 29 (3): 575-584.

Pasco A, Lemaire L, Franconi F, Lefur Y, Noury F, Saint-Andre JP, Benoit JP, Cozzone PJ, Le Jeune JJ (2007). Perfusional deficit and the dynamics of cerebral edemas in experimental traumatic brain injury using perfusion and diffusion-weighted magnetic resonance imaging. J Neurotrauma 24 (8): 1321-1330.

Pekny M and Nilsson M (2005). Astrocyte activation and reactive gliosis. Glia 50 (4): 427-434.

Pierce JE, Smith DH, Trojanowski JQ, McIntosh TK (1998). Enduring cognitive, neurobehavioral and histopathological changes persist for up to one year following severe experimental brain injury in rats. Neuroscience 87 (2): 359-369.

Pitkanen A, Immonen RJ, Grohn OH, Kharatishvili I (2009). From traumatic brain injury to posttraumatic epilepsy: what animal models tell us about the process and treatment options. Epilepsia 50 Suppl 2: 21-29.

Pitkanen A, Kharatishvili I, Karhunen H, Lukasiuk K, Immonen R, Nairismagi J, Grohn O, Nissinen J (2007). Epileptogenesis in experimental models. Epilepsia 48 Suppl 2: 13-20.

Pitkanen A and Lukasiuk K (2009). Molecular and cellular basis of epileptogenesis in symptomatic epilepsy. Epilepsy Behav 14 Suppl 1: 16-25.

Pitkanen A and McIntosh TK (2006). Animal models of post-traumatic epilepsy. J Neurotrauma 23 (2): 241-261.

Pitkanen A, Tuunanen J, Kalviainen R, Partanen K, Salmenpera T (1998). Amygdala damage in experimental and human temporal lobe epilepsy. Epilepsy Res 32 (1-2): 233-253.

Porter RJ (1993). Classification of epileptic seizures and epileptic syndromes, in: Laidlaw J, Richens A and Chadwick D (eds), A textbook of epilepsy, New York: Churchill Livingstone:

Prayer L, Wimberger D, Oder W, Kramer J, Schindler E, Podreka I, Imhof H (1993). Cranial MR imaging and cerebral 99mTc HM-PAO-SPECT in patients with subacute or chronic severe closed head injury and normal CT examinations. Acta Radiol 34 (6): 593-599.

Racine RJ (1972). Modification of seizure activity by electrical stimulation. II. Motor seizure. Electroencephalogr Clin Neurophysiol 32 (3): 281-294.

Reivich M (1974). Blood flow metabolism couple in brain. Res Publ Assoc Res Nerv Ment Dis 53: 125-140.

Richards HK, Simac S, Piechnik S, Pickard JD (2001). Uncoupling of cerebral blood flow and metabolism after cerebral contusion in the rat. J Cereb Blood Flow Metab 21 (7): 779-781.

Robertson CL, Hendrich KS, Kochanek PM, Jackson EK, Melick JA, Graham SH, Marion DW, Williams DS, Ho C (2000). Assessment of 2-chloroadenosine treatment after experimental traumatic brain injury in the rat using arterial spin-labeled MRI: a preliminary report. Acta Neurochir Suppl 76: 187-189.

Rodriguez-Paez AC, Brunschwig JP, Bramlett HM (2005). Light and electron microscopic assessment of progressive atrophy following moderate traumatic brain injury in the rat. Acta Neuropathol 109 (6): 603-616.

Rougier A, Lurton D, El Bahh B, Lespinet V, Bidabe AM, Guillot M, Caille JM (1999). Bilateral decrease in interictal hippocampal blood flow in unilateral mesiotemporal epilepsy. J Neurosurg 90 (2): 282-288.

Rudin M, Baumann D, Ekatodramis D, Stirnimann R, McAllister KH, Sauter A (2001). MRI analysis of the changes in apparent water diffusion coefficient, T(2) relaxation time, and cerebral blood flow and volume in the temporal evolution of cerebral infarction following permanent middle cerebral artery occlusion in rats. Exp Neurol 169 (1): 56-63.

Saatman KE, Duhaime AC, Bullock R, Maas AI, Valadka A, Manley GT, Workshop Scientific Team and Advisory Panel Members (2008). Classification of traumatic brain injury for targeted therapies. J Neurotrauma 25 (7): 719-738.

Shen Y, Kou Z, Kreipke CW, Petrov T, Hu J, Haacke EM (2007). In vivo measurement of tissue damage, oxygen saturation changes and blood flow changes after experimental traumatic brain injury in rats using susceptibility weighted imaging. Magn Reson Imaging 25 (2): 219-227.

Sloviter RS (1982). A simplified Timm stain procedure compatible with formaldehyde fixation and routine paraffin embedding of rat brain. Brain Res Bull 8 (6): 771-774.

Stagliano NE, Zhao W, Prado R, Dewanjee MK, Ginsberg MD, Dietrich WD (1997). The effect of nitric oxide synthase inhibition on acute platelet accumulation and hemodynamic depression in a rat model of thromboembolic stroke. J Cereb Blood Flow Metab 17 (11): 1182-1190.

Symon L, Branston NM, Strong AJ, Hope TD (1977). The concepts of thresholds of ischaemia in relation to brain structure and function. J Clin Pathol Suppl (R Coll Pathol) 11: 149-154.

Tetrault S, Chever O, Sik A, Amzica F (2008). Opening of the blood-brain barrier during isoflurane anaesthesia. Eur J Neurosci 28 (7): 1330-1341.

Thom T, Haase N, Rosamond W, Howard VJ, Rumsfeld J, Manolio T, Zheng ZJ, Flegal K, O'Donnell C, Kittner S, Lloyd-Jones D, Goff DC,Jr, Hong Y, Adams R, Friday G, Furie K, Gorelick P, Kissela B, Marler J, Meigs J, Roger V, Sidney S, Sorlie P, Steinberger J, Wasserthiel-Smoller S, Wilson M, Wolf P, American Heart Association Statistics Committee and Stroke Statistics Subcommittee (2006). Heart disease and stroke statistics--2006 update: a report from the American Heart Association Statistics Committee and Stroke Statistics Subcommittee. Circulation 113 (6): e85-151.

Thomale UW, Kroppenstedt SN, Beyer TF, Schaser KD, Unterberg AW, Stover JF (2002). Temporal profile of cortical perfusion and microcirculation after controlled cortical impact injury in rats. J Neurotrauma 19 (4): 403-413.

Thompson HJ, Lifshitz J, Marklund N, Grady MS, Graham DI, Hovda DA, McIntosh TK (2005). Lateral fluid percussion brain injury: a 15-year review and evaluation. J Neurotrauma 22 (1): 42-75.

Thrift AG, Dewey HM, Macdonell RA, McNeil JJ, Donnan GA (2001). Incidence of the major stroke subtypes: initial findings from the North East Melbourne stroke incidence study (NEMESIS). Stroke 32 (8): 1732-1738.

Thurman DJ, Alverson C, Dunn KA, Guerrero J, Sniezek JE (1999). Traumatic brain injury in the United States: A public health perspective. J Head Trauma Rehabil 14 (6): 602-615.

Tollard E, Galanaud D, Perlbarg V, Sanchez-Pena P, Le Fur Y, Abdennour L, Cozzone P, Lehericy S, Chiras J, Puybasset L (2009). Experience of diffusion tensor imaging and 1H spectroscopy for outcome prediction in severe traumatic brain injury: Preliminary results. Crit Care Med 37 (4): 1448-1455.

Udomphorn Y, Armstead WM, Vavilala MS (2008). Cerebral blood flow and autoregulation after pediatric traumatic brain injury. Pediatr Neurol 38 (4): 225-234.

Ulrich PT, Kroppenstedt S, Heimann A, Kempski O (1998). Laser-Doppler scanning of local cerebral blood flow and reserve capacity and testing of motor and memory functions in a chronic 2-vessel occlusion model in rats. Stroke 29 (11): 2412-2420.

Umile EM, Sandel ME, Alavi A, Terry CM, Plotkin RC (2002). Dynamic imaging in mild traumatic brain injury: support for the theory of medial temporal vulnerability. Arch Phys Med Rehabil 83 (11): 1506-1513.

Unterberg AW, Stover J, Kress B, Kiening KL (2004). Edema and brain trauma. Neuroscience 129 (4): 1021-1029.

van Zijl PC, Eleff SM, Ulatowski JA, Oja JM, Ulug AM, Traystman RJ, Kauppinen RA (1998). Quantitative assessment of blood flow, blood volume and blood oxygenation effects in functional magnetic resonance imaging. Nat Med 4 (2): 159-167.

Warach S, Li W, Ronthal M, Edelman RR (1992). Acute cerebral ischemia: evaluation with dynamic contrast-enhanced MR imaging and MR angiography. Radiology 182 (1): 41-47.

Watanabe H, Kumon Y, Ohta S, Sakaki S, Matsuda S, Sakanaka M (1998). Changes in protein synthesis and calcium homeostasis in the thalamus of spontaneously hypertensive rats with focal cerebral ischemia. J Cereb Blood Flow Metab 18 (6): 686-696.

West MJ, Slomianka L, Gundersen HJ (1991). Unbiased stereological estimation of the total number of neurons in thesubdivisions of the rat hippocampus using the optical fractionator. Anat Rec 231 (4): 482-497.

Williams DS, Detre JA, Leigh JS, Koretsky AP (1992). Magnetic resonance imaging of perfusion using spin inversion of arterial water. Proc Natl Acad Sci U S A 89 (1): 212-216.

Wintermark M, Sesay M, Barbier E, Borbely K, Dillon WP, Eastwood JD, Glenn TC, Grandin CB, Pedraza S, Soustiel JF, Nariai T, Zaharchuk G, Caille JM, Dousset V, Yonas H (2005). Comparative overview of brain perfusion imaging techniques. Stroke 36 (9): e83-99.

Xiong Y, Mahmood A, Chopp M (2010). Angiogenesis, neurogenesis and brain recovery of function following injury. Curr Opin Investig Drugs 11 (3): 298-308.

Yamakami I and McIntosh TK (1989). Effects of traumatic brain injury on regional cerebral blood flow in rats as measured with radiolabeled microspheres. J Cereb Blood Flow Metab 9 (1): 117-124.

Yoshino E, Yamaki T, Higuchi T, Horikawa Y, Hirakawa K (1985). Acute brain edema in fatal head injury: analysis by dynamic CT scanning. J Neurosurg 63 (6): 830-839.

Yuan XQ, Prough DS, Smith TL, Dewitt DS (1988). The effects of traumatic brain injury on regional cerebral blood flow in rats. J Neurotrauma 5 (4): 289-301.

Zaharchuk G (2007). Theoretical basis of hemodynamic MR imaging techniques to measure cerebral blood volume, cerebral blood flow, and permeability. AJNR Am J Neuroradiol 28 (10): 1850-1858.

Zaharchuk G, Yamada M, Sasamata M, Jenkins BG, Moskowitz MA, Rosen BR (2000). Is all perfusion-weighted magnetic resonance imaging for stroke equal? The temporal evolution of multiple hemodynamic parameters after focal ischemia in rats correlated with evidence of infarction. J Cereb Blood Flow Metab 20 (9): 1341-1351.

Zhang C, Saatman KE, Royo NC, Soltesz KM, Millard M, Schouten JW, Motta M, Hoover RC, McMillan A, Watson DJ, Lee VM, Trojanowski JQ, McIntosh TK (2005). Delayed transplantation of human neurons following brain injury in rats: a long-term graft survival and behavior study. J Neurotrauma 22 (12): 1456-1474.

Nick Hayward

Magnetic Resonance Imaging of the Hemodynamic and Cerebrovascular Sequelae of Traumatic Brain Injury, Ischemic Stroke, and Status Epilepticus in Rats

Magnetic resonance imaging (MRI) provides a range of high resolution, safe, and non-invasive tools for in vivo visualization of soft tissue structures and functions. This thesis research explored the long-term cerebrovascular adjustments that occur after traumatic brain injury, ischemic stroke, and status epilepticus through MRI of rat models for each disease. Each study led to new understandings of the pathological processes that occur after different types of brain injury.

UNIVERSITY OF
EASTERN FINLAND

Publications of the University of Eastern Finland
Dissertations in Health Sciences

ISBN 978-952-61-0261-0